INTEGRATED HYDROLOGICAL MODELLING OF RIVER-GROUNDWATER INTERACTIONS IN THE BOTETI RIVER AREA, BOTSWANA

ALENE MITIKU
February, 2019

SUPERVISORS:
DR. M. W. Lubczynski
DR. B. H. P. Maathius

ADVISOR:
T.L. Masaka

INTEGRATED HYDROLOGICAL MODELLING OF RIVER-GROUNDWATER INTERACTIONS IN THE BOTETI RIVER AREA, BOTSWANA

ALENE MITIKU

Enschede, The Netherlands, February 2019

Thesis submitted to the Faculty of Geo-Information Science and Earth Observation of the University of Twente in partial fulfilment of the requirements for the degree of Master of Science in Geo-information Science and Earth Observation.
Specialization: Water Resources and Environmental Management

SUPERVISORS:
DR. M. W. Lubczynski
DR. B. H. P. Maathius

THESIS ASSESSMENT BOARD:
Dr. Ir. C. van der Tol (Chair)
Dr. P. Gurwin (External Examiner, University of Wraclow)

DISCLAIMER

This document describes work undertaken as part of a programme of study at the Faculty of Geo-Information Science and Earth Observation of the University of Twente. All views and opinions expressed therein remain the sole responsibility of the author, and do not necessarily represent those of the Faculty.

ABSTRACT

The Boteti River derives flow from Okavango Delta, the main contemporary river and surface water body within the Boteti District. The source of water for the Boteti River is mainly dependent on the inflow from the Okavango Delta. It is remarkable that the river stages are the highest in the peak dry season (because of flood arrival from Okavango Delta), i.e. from July to September.

The study area along the Boteti River is characterized by arid to semi-arid climate, low rainfall and high evapotranspiration. The low topographic gradient in conjunction with geology and lithology affected the Boteti River meanders, changing direction in several places. The Boteti-River-groundwater interaction is an important component of the hydrological cycle of the adjacent area.

To assess and characterize river-groundwater interactions of the Boteti River study area thereby to quantify and analyze the water balance of the modelled domain a 3D transient state, integrated hydrological model, MODFLOW-NWT coupled with UZF1 and SFR2 packages under ModelMuse graphical user interface was used. The modelling period was set to three years from the beginning of September 2016, to the end of August 2017. The calibration was carried out throughout the manual trial and error method.

The Inflow through the Boteti River from the northwest side of the modelled domain and the precipitation accounts for 64.96% and 33.65% of the total model input respectively. Seasonal and yearly variations of the groundwater fluxes was pronounced. The gross recharge which accounts for 85% of the total groundwater input and groundwater evapotranspiration for 81% of the total groundwater output, were the highest in the wet seasons.

The Boteti River-groundwater interactions and the related leakage transfers between the two hydrological domains depend on the relative position of the groundwater table with respect to river stages. The variation in groundwater level increases in river flow seasons from July to September. The total loss of water from the Boteti River to Kalahari aquifer system for 2016 and 2017 hydrological years was approximately 67 mm while the discharge from aquifer to the river was 99 mm which resulted in 32 mm net groundwater loss i.e. 16 $mmyr^{-1}$.

Keywords: Boteti River, Integrated hydrological modelling, River-groundwater interactions, water balance

ACKNOWLEDGEMENTS

First and foremost, glory to the Almighty God for his guidance and protection with full health to finish this work.

I would like to express my heartfelt thanks to the Netherlands Government for providing me the opportunity to study my Master of Science degree course through the Netherlands Fellowship Programme (NFP) scholarship at the faculty of Geo-information Science and Earth observation, ITC, University of Twente, The Netherlands.

I am deeply indebted to Dr. Maciek Lubczynski, my first supervisor, for his invaluable, endless and proper guidance and support during the whole study period. I am also very great full to Dr. B.H. Maathius my second supervisor for his support and encouragement with critical comments during the study.

I would like to thank also Mr. T. L. Masaka my advisor for his support during the study.

I would like to thank Dr. Ir. CM Mannaerts who provided me data for reference evapotranspiration with finer resolutions and his guidance during preprocessing.

I am very great full to Mr. Arno van Lieshout, course director for Department of Water Resources and Environmental Management for his guidance, encouragement, care and help with patience during the study.

Many thanks also go to all the staff members of the water resources department for all the guidance, technical support and encouragement given to me during the course study. To my friends and classmates at ITC, thank you for the journey we went through together as a family.

Last but not least my heartfelt gratitude goes to my family, colleagues and friends back home for all moral support and encouragement.

TABLE OF CONTENTS

LIST OF FIGURES

LIST OF TABLES

1. INTRODUCTION

1.1. Background

Botswana, a landlocked country located in the center of Southern Africa is covered by semi-arid and arid lands with average annual rainfall ranging from 250 mm in the southwest to 650 mm in the northeast (Swatuk, Motsholapheko, & Mazvimavi, 2011). As drought is common in the region, the rainfall received is highly unreliable and experiences high evapotranspiration rate. Consequently, the country has limited surface water resources and low groundwater recharge (VanderPost & McFarlane, 2007). On the other hand, a study by (Rahm, et al., 2006) shows that water demand in the Boteti River area will increase from 193.4 $Mm3yr^{-1}$ in 2000 to 335.2 $Mm3yr^{-1}$ by 2020. Gokmen et al., (2013) revealed that in such regions additional water source for supplementary water uses rely on groundwater resources. As a result, assessment and evaluation of the exchange between surface and groundwater resources is crucial for better water resources management.

Unlike surface water, groundwater is the major fresh water source for any hydrological system. Specially in arid and semi-arid regions like in Botswana, it is estimated that about 80% of the wellbeing of living things depends on groundwater acquired through drilled wells and boreholes (Rahm et al., 2006). This accounts most of water needs for supplementary uses i.e. for irrigation, industry and other uses.

Assessment and characterization of surface water and groundwater resources in the Boteti River area (BRA) focused on monitoring and evaluation of either surface or sub surface hydrological systems separately (Hu, et al., 2016 and VanderPost & McFarlane, 2007). However, most of biological and physical characteristics of any hydrological system which are considered as complex and interacting processes control the interaction of the two systems (Jutebring Sterte et al., 2018) and behave an inter-dependent manner. The interaction between surface and groundwater lies in complexities of the whole system due to system heterogeneity and unequal partitioning of water in all directions across time and space (Hassan, et al., 2014 and IDOWU, 2007). Thus, The authors indicated that having an insight about such a system is helpful even if it is challenging for accurate evaluation and characterization of the state or condition of those systems.

As postulated by (Hassan et al., 2014; Hu et al., 2016; Li, et al., 2016) an integrated hydrological modelling (IHM) opposed to stand alone models (models that simulate either surface water or groundwater separately) helps to understand and evaluate the dynamics of interactions between surface and groundwater more realistically. For instance, integrating MODFLOW NWT (Niswonger, et al., 2011) with packages such as unsaturated zone flow (UZF1), stream flow roughing (SFR2), Lake (LAK), and Reservoir package improves the capability of the MODFLOW to represent and simulate surface-groundwater interactions in an optimal way.

This research mainly focused on assessment and evaluation of the river-groundwater interactions there by analyzing the water balance of the BRA by developing a transient state IHM. The study used MODFLOW NWT code coupled with UZF1 and SFR2 packages under ModelMuse graphical user interface (Winston, 2009) which simulates water flow in surface, unsaturated and saturated zones of the system.

1.2. Problem Statement

In arid and semi-arid regions due to limited and highly variable rainfall and high evapotranspiration rate, fresh water resources are the most crucial for human wellbeing (Roussouw, et al., 2018). The Boteti River, outlet of the Okavango Delta running through the Boteti District, the semi-arid Botswana Kalahari have been an important factor for immigration and modern villages development around the area. However, since 1990s the Boteti River appeared to be 'failing', which resulted in concern over people's water supply and livelihoods (VanderPost & McFarlane, 2007). Historical data collected from hydrological stations indicated the river started flowing again since 2010 to date. Such a seasonal and fluctuating river is not a dependent water source for the wellbeing of the living community and wildlife. On the other hand, the study by (Rahm et al., 2006) showed water demand in the BRA increasing from time to time resulting in an increase of the over exploitation of groundwater resources. Investigation of groundwater resources using GIS tools was conducted by (VanderPost & McFarlane, 2007) and groundwater exploration through Airborne Electromagnetic Modelling (AEM) by (Sattel & Kgotlhang, 2004) was performed. However, the interaction between surface water and groundwater in the BRA has not been studied yet.

1.3. Research Settings

1.3.1. Relevance of the research

Results of the study helps to understand and describe: 1) The dynamics of river-groundwater interactions of the BRA; 2) The spatio-temporal variation of water balance components of the area in general and 3) can be used as a reference for managing water resources thereby beneficial to local stakeholders and government officials in planning and management of surface and groundwater resources in the BRA.

1.3.2. Research Objectives

Main objective

The overall aim of this research is to assess the dynamics of river-groundwater interactions in the BRA.

Specific objectives

- To develop a conceptual hydrogeological model of the BRA.
- To set up and calibrate transient state integrated hydrological model of the BRA.
- To analyze the water balance of the river-groundwater exchange at the BRA.

1.3.3. Research questions

Main research question

What is the spatio-temporal impact of Boteti River on groundwater balance components of the BRA?

Specific research questions

- What is the conceptual model of the BRA?
- What is an optimal way to evaluate river-groundwater interactions of the BRA?
- What is the spatio-temporal variation of groundwater balance components (fluxes) within the BRA?

1.3.4. Novelty of the study

The results of the study will give an insight about the state/condition of river groundwater interactions of the BRA having the following novelties:

- Using high-resolution satellite products of precipitation and potential evapotranspiration as an input for the integrated hydrological model of the BRA.
- Integrated hydrological modelling (IHM) to evaluate and characterize the river-groundwater interactions of the BRA for simulation period from the beginning of September 2014 to the end of August 2017 as no research has been conducted in the area through IHM.

1.3.5. Research Hypothesis

It is hypothesized that the balance of water exchange between Boteti River and aquifer is positive i.e. there is gain of groundwater storage.

1.3.6. Assumptions

- Groundwater within the modelled domain is not affected by salt water intrusion throughout the simulation period.
- It is assumed that there is hydraulic connection between river and modelled aquifer (Kalahari Aquifer) and eventual leakage across the bottom boundary of the Kalahari Aquifer has negligible impact on the fluxes.
- The surface water and groundwater abstraction rates have negligible impact on river-aquifer interactions and the water balance of the system.

1.4. Literature Review

1.4.1. Review of integrated hydrological simulations for surface-groundwater interaction studies

Surface water and groundwater are often interconnected and interdependent components of a hydrological system (Newman et al., 2006; Hassan et al., 2014; Hu et al., 2016). As a result, it is crucial to get an insight about the exchange of water, material and energy between the surface and subsurface components of the system there by not only possible to solve problems related to water supply and water quality but also maintain ecosystem diversity and functioning (Sophocleous, 2002). Numerous researchers entail that arid and semi-arid regions cover large portion of the earth's surface with fastest growing population and limited resources needs special attention and understanding about surface water and groundwater interactions for better water resources management (Newman, et al., 2006; Tian et al., 2015)

Three main methods can be used to investigate and characterize surface-groundwater interactions. These methods are: 1) Statistical analysis based on measured variables; for instance, monitoring data of groundwater levels and stream flows. Several Authors used the method to investigate surface-groundwater interactions. For example, (Newman, et al., 2006) reviewed different features of interactions in semi-arid drainages and drew their conculusion presenting series of conceptual models that describe surface-groundwater (river-aquifer) interactions as losing river, gaining river and disconnected river. In addition, (Hu et al., 2016) developed an integrated river-groundwater model, model that uses one dimensional open channel flow model and three dimensional saturated groundwater flow model and described the spatial and seasonal variability of river- groundewater relationships in response to river flows and groundwater uses. 2) (Kumar, et al., 2008) introduced the relationship between surface water (reservior, lake) and groundwater (springs) using environmental isotopes and geologic, hydrochemical and in situ physiochemical parameters and deduced that both systems are interdependent each other. 3) Numerical distributed model, the most widely used and common method to quantify the fluxes resulted due to interactions between surface water and groundwater (Hassan et al., 2014; El-Zehairy, et al., 2018; Lekula, et al., 2018).

A number of integrated hydrological models (simulators) have been developed for management of surface water and groundwater resources; Such as SWATMOD, MODHMS, HydroGeosphere and GSFLOW to mention some.

SWATMOD integrates the commonly applied Soil Water Assessment Tool (SWAT) (Arnold, et al., 1998) with 3D groundwater flow model, MODFLOW. SWAT model was developed to simulate and predict agricultural management impacts on long term (hundreds of years) erosion and sedimentation rates. However, SWAT does not simulate detailed event-based flood and sediment routing. In addition, it assumes the channel dimensions as static throughout the simulation period which is another limitation of SWAT.

MODHMS (Panday & Huyakorn, 2004) is MODFLOW based modelling system for surface/subsurface simulations of the water budget. It represents the subsurface by a three dimensional saturated-unsaturated flow equation and integrate with the 2D wave equation of surface water (overland flow).

HydroGeoSphere (HGS) (Brunner & Simmons, 2012) is capable to simulate water flow in a fully integrated, natural and physically based manner. It allows partitioning of precipitation (model input) into overland and stream flow, evaporation, transpiration, groundwater recharge and/or subsurface discharge into surface water bodies like rivers and lakes. In addition, the model is capable of simulating processes other than hydrologic cycles like variable density flow and transport, thermal energy transport, unsaturated flow and flow through fractures.

Groundwater-Surface water FLOW (GSFLOW) (Markstrom, et al., 2008) is an integration of the U.S. Geological Survey (USGS) Precipitation Runoff Modelling System (PRMS) and the USGS Modular Ground-Water Flow Model (MODFLOW). Three regions, namely: the upper region bounded between top

of canopy to bottom of the lower limit of the soil zone, the second region consisting all streams and lakes and the third region, the subsurface zone (beneath the soil zone) are simulated by GSFLOW. The hydrologic responses in the first region are simulated by PRMS whereas the hydrologic processes in the second and third region are simulated by MODFLOW.

To assess and characterize river-groundwater interactions of the BRA there by to quantify and analyse the water balance of the modelled domain a 3D transient state hydrological model, MODFLOW NWT (Niswonger, et al., 2011) coupled with UZF1 and SFR2 packages under ModelMuse graphical user interface was used for the present study.

1.4.2. Review of previous studies in BRA

In the Kalahari regions of Botswana, the region with arid and semi-arid climate, surface water resources are limited and groundwater recharge is low. Additional water source for supplementary water uses in such regions rely on groundwater resources. Researchers had interest in groundwater and studies have been done in the Kalahari region over the past years.

Groundwater recharge studies by de Vries, et al., (2000) using environmental tracers and groundwater flow models reveal that recharge is variable with rainfall and found to be 5 $mmyr^{-1}$ in the eastern fringe of the Kalahari which has annual rainfall of above 400 mm and 1 $mmyr^{-1}$ in the Central Kalahari with lower precipitation.

Sattel & Kgotlhang, (2004), mapped lithologies and structures for potential fresh groundwater using Airborne Electromagnetic (AEM) and ground data in the BRA (but for selected AEM survey areas). They discussed the correlation between AEM derived conductivity-depth profiles with borehole records and found that the Kalahari Sands are constituents of clay content, water saturation, and water salinity in the lower-lying areas. On the other hand, sandstones are the target aquifers on elevated terrains which are overlain and underlain by dry alluvium or basalts and mudstone respectively. The Authors also identified subsurface lithologies of the area based on conductivity depth, north-south cross section (not presented in this study) as Kalahari Sands, Stormberg Basalt, Ntane Sandstone, Mosolotsane Sandstone, Mosolotsane Mudstone and Ecca Group from top to bottom schematization respectively with their respective hydrogeological and geophysical properties.

Large and complex sedimentary aquifer systems of the Central Kalahari Basin which lays in the south and south western part from the study area was modelled by (Lekula, et al., 2018) through IHM. They schematized six hydro stratigraphic units with three aquifer flow systems, Lebung, Ecca and Ghanzi directed towards discharge area of Makgadikgadi Pans. The thick unsaturated and lower saturated part of Kalahari Sand unit was considered as first lithological layer of that study i.e. the overlying unconfined aquifer which is hydraulically connected with all three aquifers and redistribute annual average recharge of 1.87 $mmyr^{-1}$ sourced from rainfall.

Overall, to the Author's knowledge, no studies have been conducted to analyze the river-groundwater interactions of the BRA using integrated hydrological modelling.

2. STUDY AREA

2.1. Geographical location and monitoring network

Figure 2-1 shows base map of the Boteti River area and elevation range within the area. The BRA covers an area of about 19, 550 km² and bounded by coordinates between latitude 19°30' to 21°30'S by longitude 23°00' to 25°00'E.

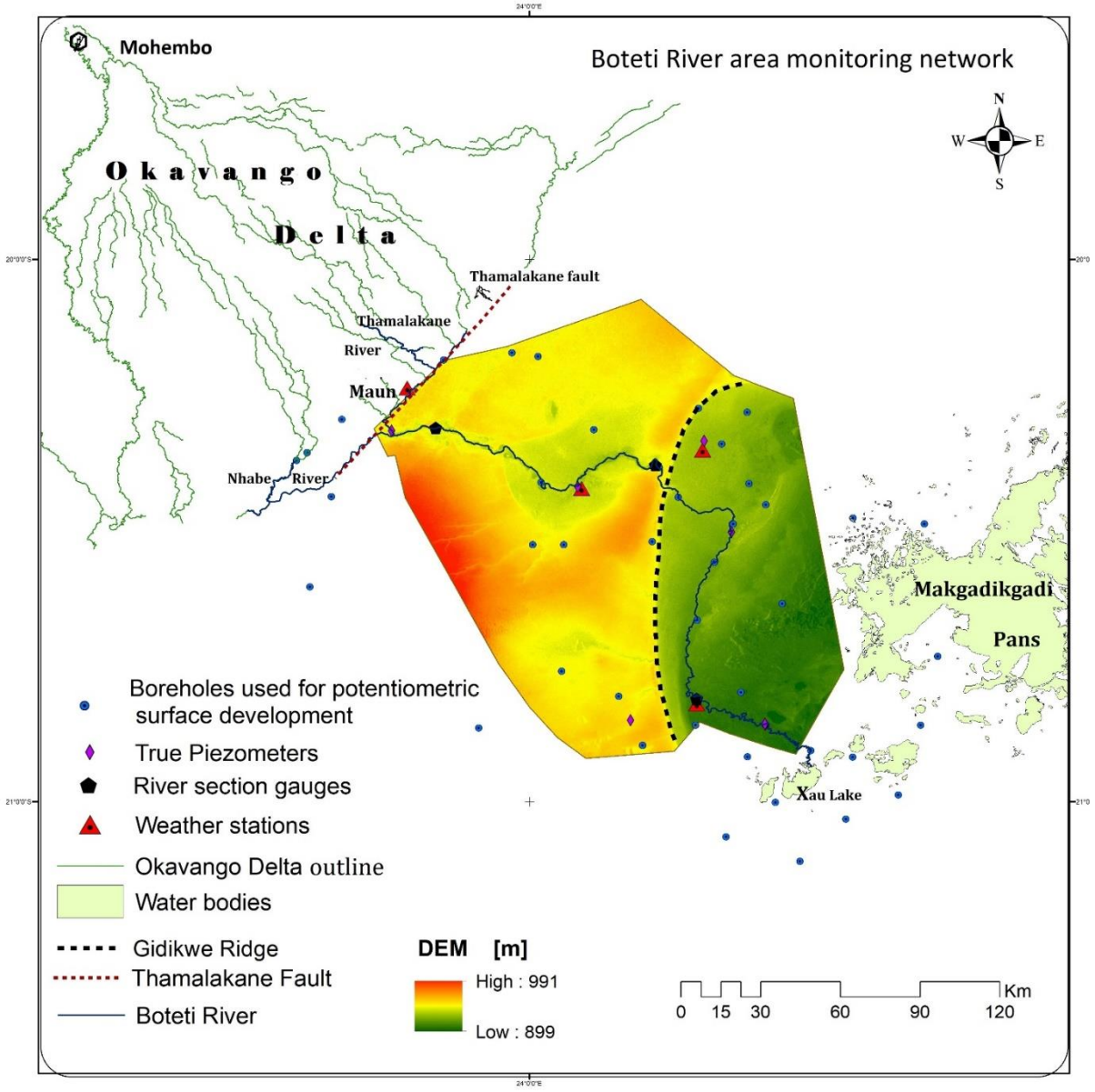

Figure 2-1 Base map of the Boteti River area

There are different hydrological and hydrogeological variables within the BRA. The time series data of rainfall, river discharge, river stage, temperature and relative humidity for stations Maun, Mareomaota, Phuduhudu and Rakops which were collected from different sources from the beginning of September 2014 to end of August 2017. There are four weather stations and three river discharge measuring gauges.

Table 2-1 Data sets and source of data

Required data	Temporal resolution	Source /Remark	Duration
Rainfall	Daily	Hydrological stations, Online sourced data and CHIRPS at 5 Km resolution from ILWIS ISOD Tool Box	September 2014 to August 2017
Potential evapotranspiration	Daily	US-based GMAO GOES-5 model at 20 Km resolution	September 2014 to August 2017
Maximum and minimum, temperature, sunshine hours, Relative humidity, Wind speed	Daily	Weather stations/SASSCAL Online weather data, http://www.sasscalweathernet.org/	September 2014 to August 2017
River discharge	Daily	River gauge stations	September 2014 to August 2017
Depth to groundwater	-	Field work (Measured)	-
Aquifer parameters	-	Literature (Lekula, 2018)	-
Interception	Daily	Derived	September 2014 to August 2017
Extinction depth	-	Derived	-
Infiltration rate	Daily	Derived	September 2014 to August 2017
Land cover map	-	https://www.esa-landcover-cci.org/	2016
Digital elevation model (SRTM 30 m DEM)	-	https://earthexplorer.usgs.gov/	-

2.2. Topography

The Boteti River, the main surface water body of the Boteti district drives flow from the distal Okavango Delta through Thamalakane River in Maun (north west of BRA) and continues running to the south easterly direction to Lake Xau with an irregular form through the mid Botswana Kalahari for more than 300 kilometers to terminate at Lake Xau (VanderPost & McFarlane, 2007). Thus, forms the main physiographic feature of the area. In addition, as it is presented on (Figure 2) of (McFarlane & Eckardt, 2006)) in conjunction with SRTM 30 m digital elevation model of the BRA (Figure 2-1) the Gidikwe Ridge south western to north easterly trending (as presented by dashed lines) forms the main topographic feature of the BRA. The elevation with in the area ranges from 884 m to 993 m a.s.l. The gradient is towards easterly direction i.e. to the Makgadikgadi Pan depressions (lowest regional topography).

2.3. Climate

The BRA experiences arid to semi-arid climate characterized by limited and highly variable convective type of rainfall (Lekula, et al., 2018) and high evapotranspiration rate. Ninety percent of the annual rainfall occurs in wet, hot and humid season, summer from November to March whereas in the cold and dry winter season from May to August, rainfall hardly occurs (MMEWR, 2006). There are several meteorological stations with in the BRA namely, Xhuemo, Mmadikola, Rakops, Phuduhudu, Moreomaoto, Motopi, Maun for recording hourly and daily meteorological variables. However, the complete meteorological data was not found from these stations instead the study relies on online sourced data like, GSOD (ISOD tool box, ILWIS) (see Table 2-1). Average annual rainfall ranges from 250 mm in the southwest to 650 mm in the northeast (Swatuk et al., 2011).

Figure 2-2 shows long term temporal variation of rainfall and temperature within the BRA.

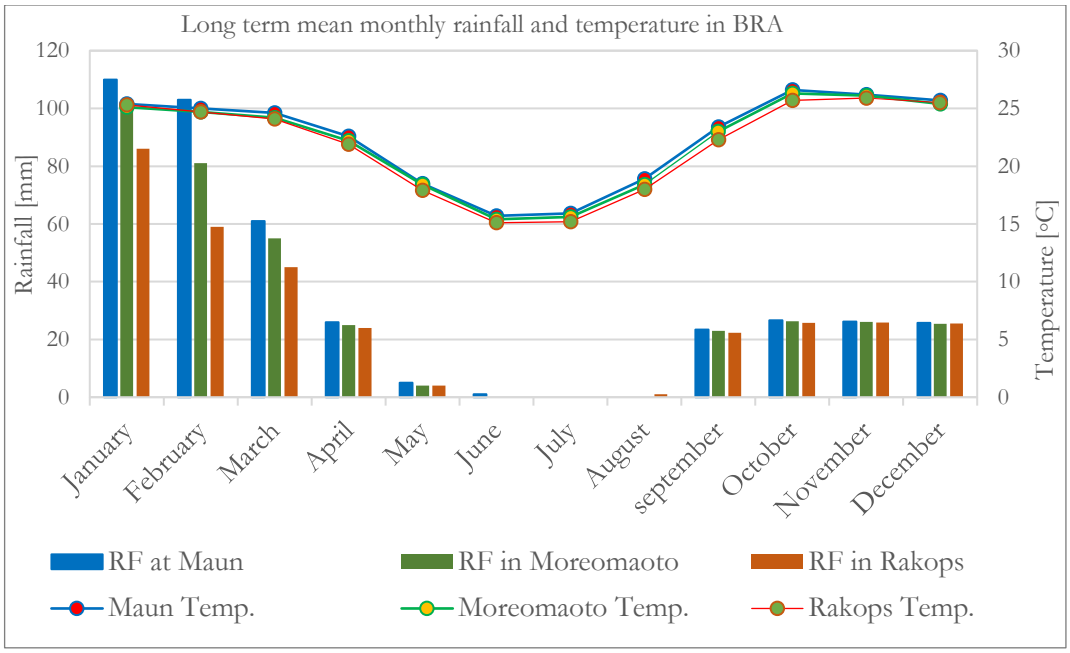

Figure 2-2 Long term monthly average rainfall (RF) and temperature (Temp.) in BRA (1982-2012) (Source: Climate-data.org); Locations of the meteorological stations are presented in Figure 2.1.

2.4. Soils and Vegetation

Figure 2-3 represents the soil types in the Boteti river area, (sourced from the department of Geological Surveys of Botswana). Arenosols, luvisols, calcisols and solonchaks are the dominant soil types in the BRA. Arenosols are deep sandy soils mainly found in the Kalahari Sandveld environment. These soil types are situated away from the Boteti River (MEWT, 2007) and characterized by very low moisture content. Luvisols have better moisture content than arenosols i.e. situated close to the Boteti River and are favored agriculturally. Calcisols, also known as Desert Soils and Takyrs are common in calcareous parent materials. These are soils with substantial secondary accumulation of lime. Another common soil types in the BRA are solonchaks, pale and grey soil types. These soil types are situated around poorly drained areas (conditions) for example, near the paleo lake, pans.

The land cover map of the BRA was downloaded from https://www.esa-landcover-cci.org/ with 20 m resolution and consists of trees, shrubs, grassland, bare areas, crop land, aquatic and regularly flooded vegetation, and lichen mosses. As cropland, aquatic and regularly flooded vegetation, and lichen mosses (sparse vegetation) covers negligible area compared to other land cover classes; those were later reclassified as grassland. Thus, the BRA land cover map reclassified into shrubs (woody vegetation), naturally occurring savannah grassland, acacia species trees and bare land. The reclassification process and calculation of percentage area of each land cover classes were carried out in ArcGIS environment. later, this map was resampled to 1 km^2 spatial resolution via nearest neighbor resampling method and further used for interception loss and extinction depth calculations.

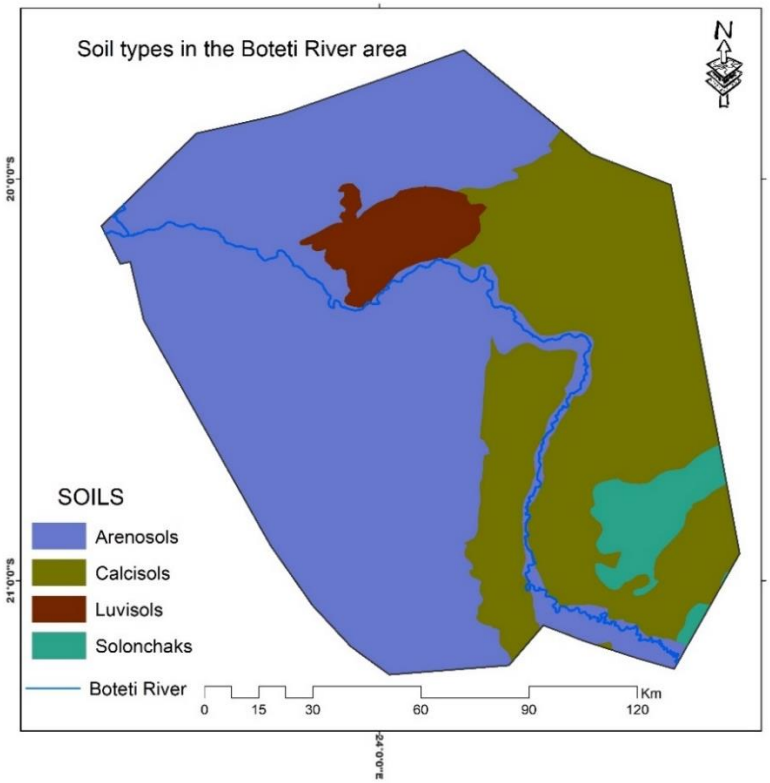

Figure 2-3 Soil types in the Boteti River area

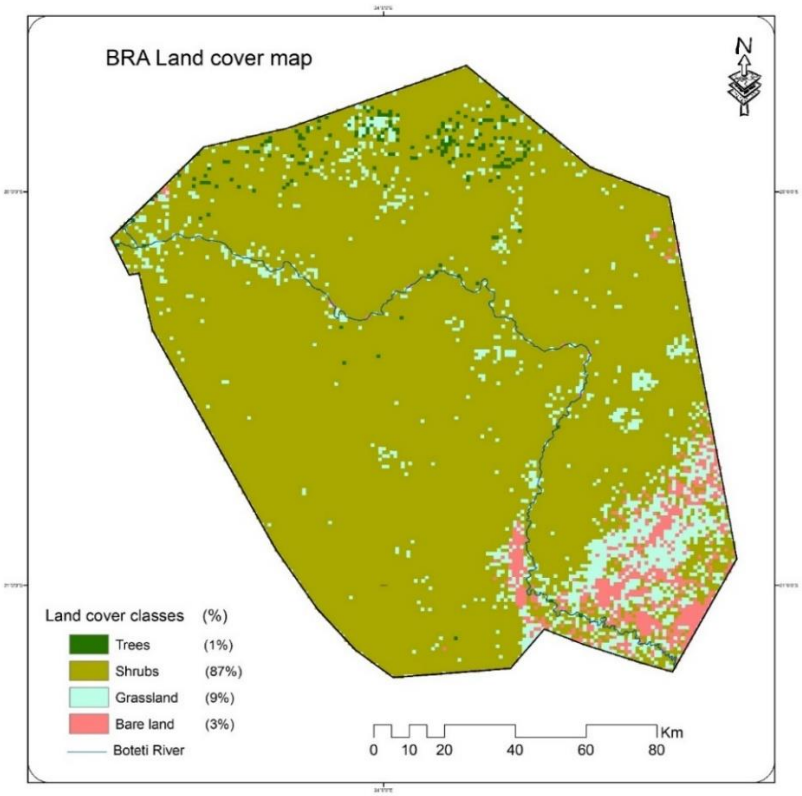

Figure 2-4 Land cover map of BRA source

2.5. BRA drainage and its paleostructure

The drainage network in the BRA is sparsely developed which is an indication of low to non-existent surface run-off related with low topographic gradient, low rainfall and high evapotranspiration rates, and soils that suppress run-off. This low gradient on the other hand, impacted the Boteti River channel meanders, changing direction at several locations through the BRA from north west to south which is an implication that the river is structurally and/or lithologicaly controlled.

The Boteti River overlaid flood plains of older alluvial deposits of the fossil Okwa and Deception river systems which were coming from the west of the BRA (McFarlane & Eckardt, 2006). The Authors reveal that the deception rivers except Okwa coming from south west and the Boteti River from north west were considered to terminate into the old lagoonal flats of the paleolake Makgadikgadi. After the water of the lake declined, the Gidikwe Ridge (see Figure 2.1) formed which was considered as a barrier and resulted in impoundment of water from the Boteti River and Okwa (currently a fossil river) on the west side of the ridge. Which is an implication for existence of thicker body of Upper Kalahari lacustrine sediments on that part compared with the eastern side. Similar Kalahari Sand thickness is schematized in this study. The ridge was eventually breached several places; then after, this impoundment drained out. There is a periodic break forming sequence of terraces adjoining the Boteti River of the body which are important to the sustenance of water in the Boteti River by conducting infiltration of rainfall, resulting in sustained seepages at the base of the river, feeding some stretches of the river. This can also add chances to groundwater recharge. In the lower reaches the Boteti River turns southwards to Lake Xau forming small deltas on the lake floor. Eventually, the river has discharged point into north east side of the lake, to Makgadikgadi Pans.

2.6. Geology

The study area is characterized by thick layer of Kalahari Sands in the lower-lying areas, Karoo groups on the elevated regions, and Sandstone and mudstones at shallower depths (Sattel & Kgotlhang, 2004). Furthermore, Kalahari Sands are grouped as upper, middle and lower formations with varying thickness. The Upper Kalahari consists of aeolian sands, pan and alluvial deposits; sequence of lacustrine clays, silts and sand define the Middle Kalahari; and the Lower Kalahari which is not present consistently, consists of sandstone and breccia-conglomerate. Figure 2.4 presents an outline of the geological features that are buried by variable thickness Kalahari group formations and consists mainly Ecca group, Ghanzi, Karoo basalts, Mamuno formation and Archean sediments.

Sinclair Group

Sinclair Group, volcanic-sediments of the Kgwebe Formation are overlain by the Kalahari Sands in an unconformable manner within the northwest part of the BRA and are in sequential to the Ghanzi Group volcanic sediments.

Ghanzi Group

The Ghanzi Group Sediments consists mainly of arkoses with some shale, mudstone, siltstone and limestone representing shallow water deltaic deposits. The Ghanzi group quartzites form the bedrock of the northwest part of the BRA overlain by a thick suit of Kalahari sand sediments and basalt

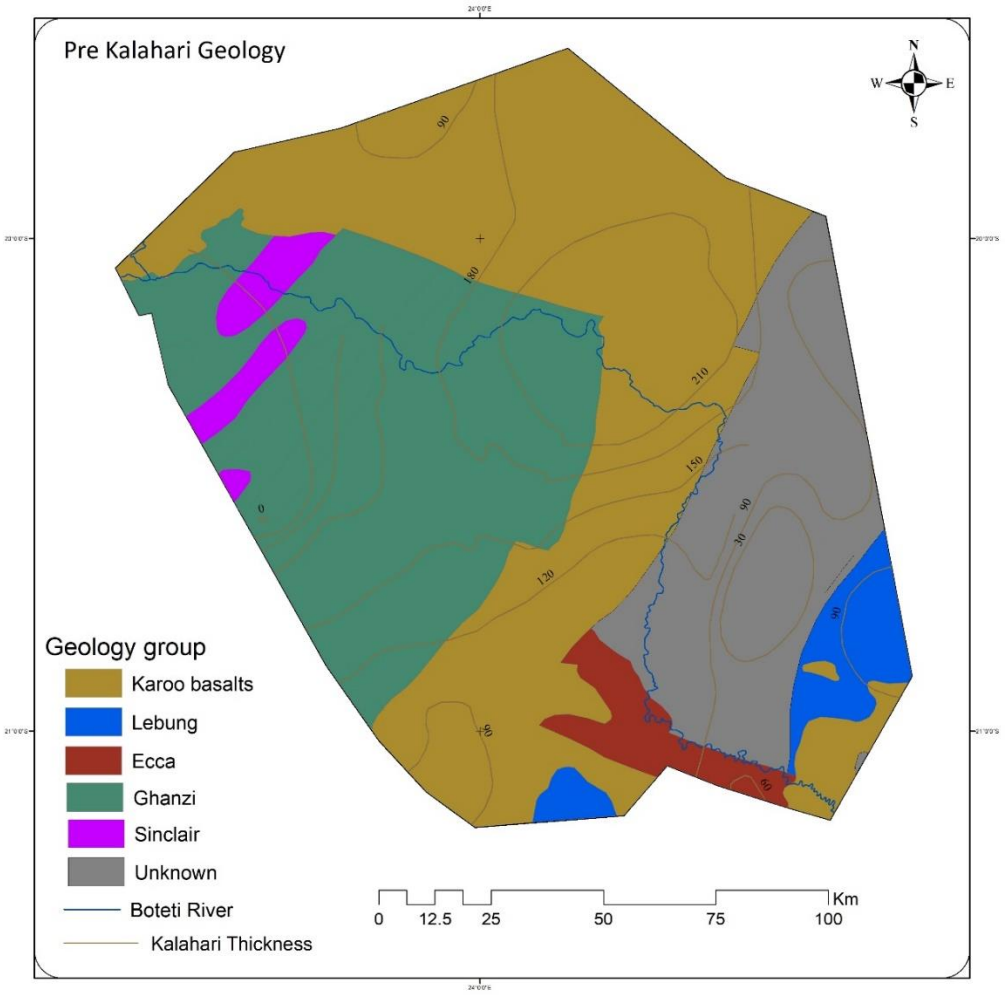

Figure 2-5 Pre Kalahari Geology map of the BRA

Ecca Group

Ecca group is formed by Tlapana and Mea Arkose formations. The Tlapana formation is characterised as a basalt carboniferous coal or shale and non-carbonaceous mudstone having upper and lower Tlapana formations. On the other hand, Mea Arkose Formations are described as white, gritty Arkose formations which develop orange, iron stained bands in weathered outcrop (Society, 2007). As national geology map of Republic of Botswana combined with the lithology of drilled boreholes within the area (MEWT, 2007) the stratigraphic sequence is presented in (Table 2.2)

Table 2-2 Stratigraphy of the BRA (adapted from MEWT DWNP, 2007)

AGE	STRATIGRAPHIC UNIT			LITHOLOGICAL DESCRIPTION
	Supergroup	Group	Formation	
Tertiary to Recent	Kalahari Beds	Kalahari	Upper	Alluvial sediments, aeolian sands, calcrete & silcrete
			Middle	Green or pink silcrete, friable sandstone, siltstone & clay
			Lower	Dark green highly calcareous quartzose siltstones & conglomerate
Late Carboniferous to Early Jurassic	Karoo	Stormberg Lava		Basalt lava sheets & intrusives (doleritic dykes and sills)
		Lebung	Ntane Sandstone	Fine red and pink sandstone, grey-green when reduced
			Mosolotsane	Sandstones, usually red (Mosu Sandstone, upper member). Siltstones & mudstones (red to black, lower member). Northern Belt of Central Karoo.
			Ngwasha and Pandamatenga	Sandstones, siltstones and mudstones, grey to green. North East Karoo.
		Ecca	Thlabala	Dark grey, brown and green (towards the top) non-carbonaceous mudstone
			Thlapana	Dark grey carbonaceous mudstones & coal
			Mea Arkose	Fluvio-deltaic white-pinkish sandstones and siltstones
		Dwyka	Dukwe	Varved siltstones & mudstones(upper member) Siltstones & tillites (lower member)
Late Proterozoic	Damara	Ghanzi	Ngwango	Purple arkosic mudstone
			D'kar	Green arkosic sandstone, siltstone & mudstone
			Mamuno	Purple red arkosic sandstone, limestone & siltstone
Early Proterozoic		Molopo Farms Complex		Basic and ultra-basic intrusives
Archaean Basement				Unexposed metamorphosed rocks of uncertain lithology.

Karoo Super group

A succession of sedimentary and volcanic rocks that are formed during Carboniferous and Jurassic times are constituents of the Karoo Supper group.

Lebung Group

The Lebung Group lies on the Ecca Group unconformably. It is composed of the Mosolotsane Formation unconformably overlain by the Ntane Sandstone formation. The Ntane Sandstone consists two members, the upper aeolian member which is characterized as pure quartz, orange to pinkish orange in colour, uniform and at the top it is weakly consolidated and very porous when covered by basalt. The lower member consists of sandstones characterized by coarse grained and gritty cross bedded. On the other hand, mixed sequences of sandstone, siltstone and mudstone all having red-brown colour are grouped under Mesolotsane Formation.

Stormberg Lava Group

Stormberg Lava Groups are tholeiitic continental flood basalts characterized by massive, grey-green, black in colour with green amygdales. The report by (MEWT DWNP, 2007) indicated that to the east of the BRA

basalt overlies Ntane sandstone. In areas where the Karoo supper group is absent, the basalt unconformably overlying Ghanzi Group sediments.

Kalahari Group

Kalahari Group sediments, from Cretaceous to recent Kalahari rests unconformably on the Karoo and pre-Karo rocks and totally obscure the underlying rocks. These formations extend throughout the study area with varying thickness.

Aeolian, alluvial and lacustrine lithological units are grouped under the Kalahari group sediments. The aeoline sediments can be easily differentiated into 'red sands' and represent the older arid period than "un-reddened' sands. The aeoline deposits comprise loose quartz sands variously consolidated with depth, interbedded calcrete, silcrete, silts and silicified sandstones. The lacustrine sediments are overlain by the Boteti deltaic and flood plain deposits which contain medium to fine grained sands and silts.

2.7. Hydrology and Hydrogeology of the BRA

The Boteti River, the only contemporary river and main surface water body, within the Boteti district is the main source of people's water supply and livelihoods. Study by (VanderPost & McFarlane, 2007) indicates the river had stopped flowing since 1991 then have been started flowing since 2010 to date. The river discharge was recorded from stations Samedupe and Rakops (see Figure 2.1).

The main groundwater resources that are exploited found in the Kalahari Group sediments including the Boteti River Alluvium and in the Karoo Sandstones. The Kalahari Group aquifers are of three classes i.e. shallow calcrete usually associated with pans, Middle Kalahari silicified sandstones, silcrete and calcrete and the lower consisted of sandstones. The Stormberg basalt, Ghanzi Formation sediments and the Archean Basement complex are not recognized as potential aquifers.

Review of the groundwater level map of the area shows that the regional groundwater flow in the BRA is from west to south east and the lateral groundwater flow gets into the interest aquifer system from the neighboring Central Kalahari Basin aquifers at the western part (Lekula, et al., 2018) and discharged a few kilometers distant from the modelled area in the Makgadikgadi Pans.

2.8. Review of Hydrology and Drainage of the Okavango Delta

The Okavango Delta, in the Kalahari Desert sands in Botswana is produced due to the interaction of local, regional and basin-wide factors which resulted for a seasonal flooding through Cubango and Cuito Rivers originating from the Angola highlands. As revealed by (Milzow, et al., 2010) the summer rain fall (January to February) from the Angola highlands first seeps the parched ground before rivers start flowing; later, the river continues flowing through a 1,500 km way in around one month resulting in flooding in the dry winter months peaking in April at the entry to the Okavango Delta. Due to quite flat topographic gradient and swamp vegetation which slows the water movement, the flood travels about three to four months (March to June) while filling dry and hot ground through crossing a 250 Km by 155 Km wide Delta from Mohembo (inlet) to Maun (outlet). As cited by (Shinn, 2018) the reports from the Okavango Research Institute (ORI) stated that the inflow into the Delta from 2008 to 2011 hydrological years increased by $5{,}700*10^6$ m^3 i.e. from $7,800*10^6$ m^3yr^{-1} to $13,500*10^6$ m^3yr^{-1} respectively; peaking in 2010; which is likely the main reason for the Boteti River started flowing in that year from no flows of about two decades. Figure 2.5 a & b below shows the long-term flood event and water level at the inlet and outlet of the Delta respectively. Figure 2.6. shows Okavango Delta annual flood charts: a) discharge at the inlet into the Delta, at Mohembo (Source: http://www.eyesonafrica.net/ and b) Water level of Thamalakane River at the outlet of the Delta, in Maun (at the inlet into Boteti River) (Keotshephile, et al., 2015).

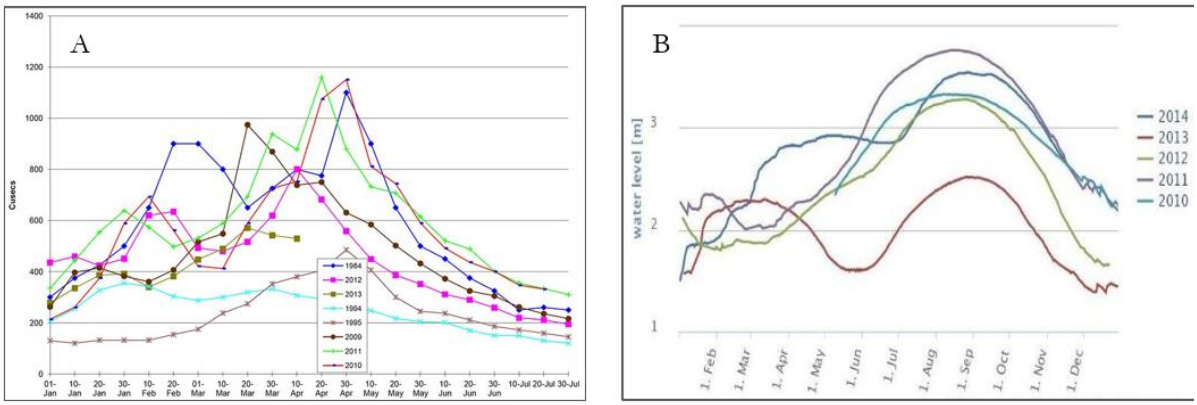

Figure 2-6 Discharge [m^3s^{-1}] presented on a hydrological yearly basis at Mohembo (A) and Thamalakane River stage [m] at Maun (B) from 2010 to 2014)

3. RESEARCH METHODOLOGY

3.1. Methodological flow chart

The steps and work flow of the study is presented on the flow chart shown in (Figure 3.1) below with brief descriptions in the subsequent sections.

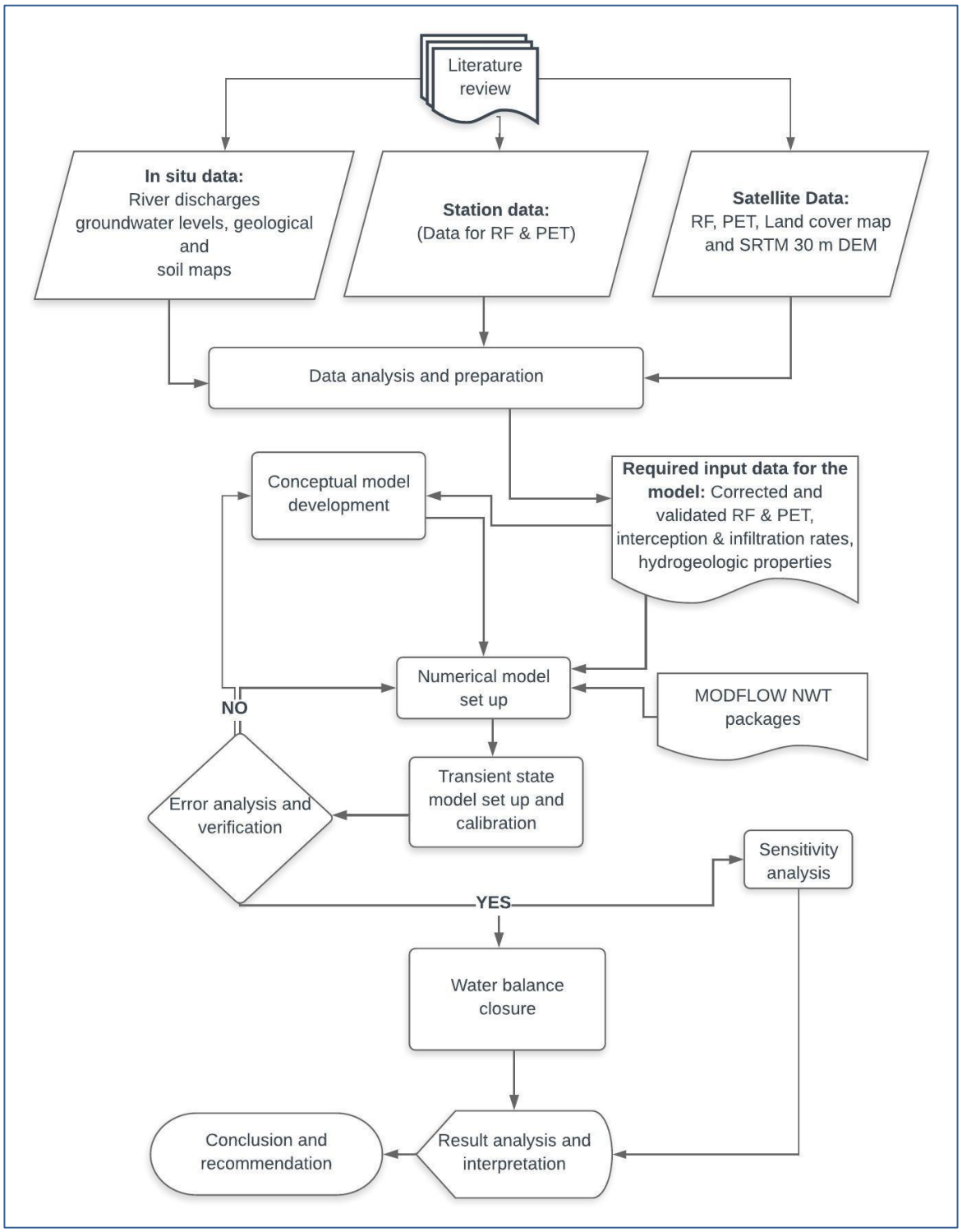

Figure 3-1 Methodology flow chart

3.2. Data processing

The necessary spatio-temporal data was processed, organized and corrected. Furthermore, the consistency and goodness of the data was checked in a form viable for the MODFLOW-NWT under ModelMuse GUI model input. The data status and source of the data is shown in (Table 2.1) above.

3.2.1. Ground-based meteorological data

Figure 3-2 Recorded length of RF for stations [mmd^{-1}]. Precipitation and potential evapotranspiration are the main driving forces for IHM. In situ weather data for seven weather station which are located inside and near by the study area was obtained from DWA of Botswana and retrieved from online source SASCAL http://www.sasscalweathernet.org/ for the period of 1st September 2014 to 31st August 2017. However, the stations encounter data gaps.

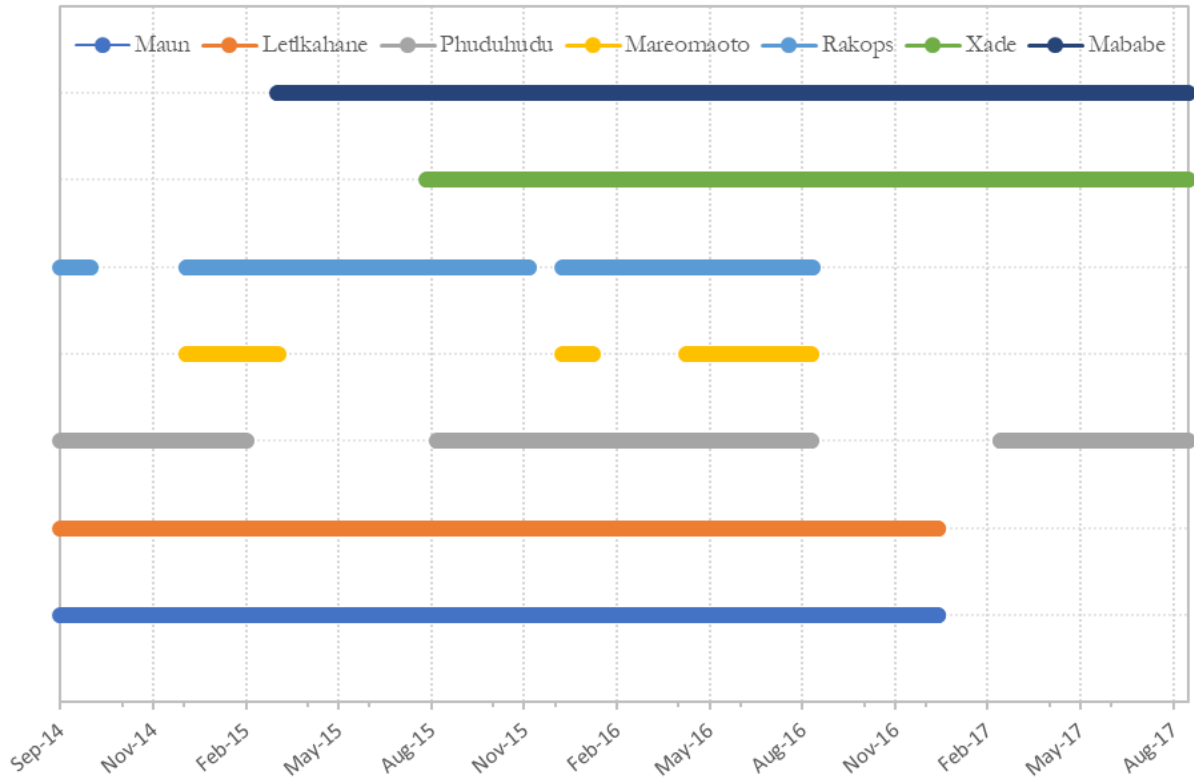

Figure 3-2 Recorded length of rainfall for available stations [mmd^{-1}]

The missing values of precipitation can be estimated using different estimation methods. Teegavarapu & Chandramouli, 2005 tested methods like kriging, stochastic interpolation techniques and inverse distance weighting method (IDWM) to estimate the missing precipitation values. The study showed that IDW method is better to estimate the missing values and was used for this study too. The missed rainfall at specified station was predicted using (Equation 1) below.

$$Px = \frac{(\sum_{i=1}^{n} Pi)*(dxi)^{-k}}{\sum_{i=1}^{n}(dxi)^{-k}} \quad (1)$$

$$where, \ [\frac{(dxi)^{-k}}{\sum_{i=1}^{n}(dxi)^{-k}}] \quad is\ the\ inverse\ distance\ weight\ at\ prediction\ location$$

P_x is prediction at the base station x, P_i is the observation at station i, d_{xi} is the distance from the location of station i to station x; n is the number of stations; and k friction distance that ranges from 1 to 6 (Teegavarapu & Chandramouli, 2005) and $(dxi)^{-k}$ is the weighting factor.

The inverse distance weights were obtained from Arc GIS software in geostatistical analyst tool, geostatistical wizard based on distance from the predicted point, latitude and longitude, and power. The

assigned power lets the user to control the influence of known values on the predicted values. The power of one smoothens the interpolated surface whereas the weights of points which are farther apart from estimation point becomes too small, nearly zero when the power increased. As recommended by (Chen & Liu, 2012) the power of 2 which increases the influence of neighbor values is used for this study.

Potential evapotranspiration (PET) can be calculated by multiplying reference crop evapotranspiration (ET_o) with crop coefficient. The crop coefficient varies with the land cover classes within the area. However, for this study, as the agricultural crops hardly exist in the BRA and the area is mainly covered with grasses, shrubs and trees which have the Kc value of about 1 (Allen et al., 1998) which has no much effect on the value of PET to be calculated. Thus, ET_o is considered as PET. ET_o was calculated from FAO Penman-Monteith equation as a function of maximum and minimum temperature, relative humidity, wind speed and sun shine hours which is also called FAO-56 the standardized reference evapotranspiration equation (McMahon, et al., 2013).

$$ETo = \frac{0.408\Delta(Rn-G)+\gamma\frac{900}{Ta+273}\,\mathrm{u2}\,(es-ea)}{\Delta+\gamma(1+0.34\mathrm{u2})} \quad (2)$$

where, ET_o is the daily reference crop evapotranspiration (mmd-1), Ta is the mean daily air temperature (◦C), u2 is the daily average wind speed (ms-1) at 2 m height, Rn is net radiation (MJm2d-1), G is soil heat flux density (MJm2d-1), es and ea are saturation and actual vapour pressure values (KPa) respectively, Δ is slope of vapour pressure curve (KPa°C-1) and γ is psychrometric constant (KPa -1).

3.2.2. Station-based Satellite Products

3.2.2.1. Precipitation

The distribution of rain gauge network specially in arid and semi-arid regions of developing countries, like the BRA, is sparse and ground-based monitoring data are scarce. Thereby the available data are insufficient for characterization and analysis of spatio-temporally variable rainfall and water resources management (Lekula, 2018). This limitation can be solved by using another option, i.e. by remote sensing methods (Satellite Products). However, remote sensing products exhibit errors, so in principle can't be used directly by hydrological models; instead they need to be validated and eventually bias-corrected using available in situ measurements where possible (Habib et al., 2014, Lekula et al., 2018).

For this study the satellite rainfall estimate (SRE) of Climate Hazards group Infrared Precipitation with Stations (CHIRPS V2.0) was used. The product was chosen due to: 1) its fine spatial (0.05°) and temporal (daily) resolution for the entire simulation period of this study. 2) The performance of the product was evaluated by Toté et al., (2015) in Mozambique and the performance of an IHM (MODFLOW NWT under ModelMuse GUI) by Kipyegon, (2018) in the Central Kalahari basin who used the product as input was found well. 3) The station that this study considered (Maun station) was not inherently used to calibrate CHIRPS which is confirmed from:
(ftp://ftp.chg.ucsb.edu/pub/org/chg/products/CHIRPS2.0/diagnostics/list_of_stations used/monthly/). Nearest stations like Mababe, Xede and others were used for validation. The data was downloaded from ILWIS software using ISOD toolbox. The product (CHIRPS version 2.0) Algorithm details and validation results are found in (Funk et al., 2015).
The precipitation gaps of four weather stations within the study area was filled considering additional three stations which are nearby to the BRA, seven stations in total. The correlation of each stations was determined by displaying coefficient of determination, R^2 value and consistency between stations was checked using double mass curve method. Both correlation and consistency found as poor (see Appendix 1) and inconsistent. This is an implication that rainfall is highly variable in time and space; as large gaps are filled and stations from farthest distance were considered. Due to the above-mentioned reasons the gap

filled data was discarded and the rainfall for one station, Maun was retrieved from online source GSOD, ISOD tool box, ILWIS for the whole simulation period and used for validating the satellite product.

Bias decomposition was performed and analyzed in terms of hit bias, missed rainfall bias and false rain bias and described in Table 3-1.

Table 3-1 Description of bias components (mmd-1)

Type	Description	Equation
Hit bias	The total bias when both satellite and gauges detect RF	$\sum(R_s - R_G) \mid (R_s > 0 \ \& \ R_G > 0)$
Missed rain bias	The bias when satellite detects nothing but recorded by gauges	$\sum(R_G \mid (R_s = 0 \ \& \ R_G > 0)$
False rain	The bias when satellite detects RF, but nothing is recorded by gauges	$\sum(R_s \mid (R_s > 0 \ \& \ R_G = 0)$

Where, R_S is RF estimated by satellite and R_G is RF recorded by the gauges.

The capability detection for SREs and the RF recorded by gauges was evaluated by applying categorical statistics on the following detection capability indicators.

Table 3-2 Categorical statistics for satellite and gauge detection capability indicators (Lekula, et al., 2018)

Detection capability indicators	Description (Equations)	Acceptable range, Best value
Probability of detection (POD)	$POD = \frac{Hits}{Hits + miss}$	0 to 1, 1
False alarm ratio (FAR)	$FAR = \frac{False\ Alarm}{Hits + False\ Alarm}$	0 to 1, 0
Critical success index (CSI)	$CSI = \frac{Hits}{Hits + False\ Alarm + miss}$	0 to 1, 1

Bias Correction

The satellite rainfall estimates (SREs) was corrected by applying a multiplicative bias correction factor on the uncorrected SREs which was obtained from ratio between SREs and gauge measurements. Bias correction factor can be formulated in different schemes as time and space variable, time and space fixed and time variable (Habib et al., 2014). As the validation of the satellite product relies on one station, a bias formulation schemes of time variable (TV) which is pixel based at daily scale was used for this study.

$$BF_{TV} = \frac{\sum_{t=d}^{t=d-l} S(i,t)}{\sum_{t=d}^{t=d-l} G(i,t)} \quad (3)$$

Where BF_{TV} is temporally variable and spatially lumped bias correction factor, S (i, t) SRE at i^{th} time and space and G (i, t) gauge estimate at i^{th} time and space, l is length of time window for bias calculation.

Evaluating the performance of the satellite rainfall estimates (SREs) with respect to gauge record helps to be certain on the corrected and validated satellite products thereby to use it as model input.

3.2.2.2. Potential Evapotranspiration

Reference evapotranspiration (ET_o) was provided from FAO-WaPOR database the US-based GMAO GOES-5 model which computes the RET through Global Data Assimilation System (GDAS) analysis fields (Tomaso et al., 2014) based on FAO-56 Penman-Monteith model from climate parameter data i.e. air temperature, atmospheric pressure, wind speed, relative humidity, and solar radiation) which were obtained from http://gmao.gfsc.nasa.gov. As stated in detail in (Section 3.2) the calculated ETo from in situ measurements was considered as PET; thus, RET from model (satellite) is also used as PET satellite in this study.

The correlation between PET from model and the calculated PET based on station data was performed via Pearson correlation coefficient.

$$CC = \frac{\sum(Gi-\overline{G}) * (Si-\overline{S})}{\sqrt{\sum(Gi-\overline{G})^2} * \sqrt{\sum(Si-\overline{S})^2}} \quad (4)$$

Where CC is the correlation coefficient, G and S are the calculated values at gauges and satellite respectively whereas $\bar{G}$ and $\bar{S}$ their average values.

3.2.3. River Discharge

As stated earlier the Boteti River sourced from Okavango Delta flows into the BRA from the northwest direction and crosses about 305 km way southwards to Lake Xau; which eventually discharged to Makgadikgadi Pans towards the eastern part of the modelled domain but currently it does not. The present study considered two gauging stations, Samedupe at the upstream and Rakops at the downstream of the Boteti River (Figure 2.1). The measured daily flow rates (discharge) for both gauging stations were obtained from DWA, Botswana. However, the flow rates encountered large data gaps. As the inflow at the upstream gauge was used as a driving force for the model (calibration control), these data gaps were filled based on the available data through nonlinear trend regression gap filling (curve fitting) method.

Based on location of discharge gauges the Boteti River was divided into five parts (stream segments) for modelling purposes. Through modelling on SFR2 package the location of gauging stations were assigned as the last stream reach (grid cell) of the stream on MODFLOW ModelMuse under MODFLOW packages and programmes, SFR package, MODFLOW Features, gauges pane.

3.2.4. Digital Elevation Model (DEM)

In addition to representing the topography of the study area (Figure 2.1), the SRTM 30 m DEM values at the specified location together with the groundwater table depth data can be used to calculate the hydraulic heads which further used for potentiometric surface development and model calibration.

DEM can be created from digitized topographic maps, field data collected from GPS receivers, and digital aerial photographs or satellite images (Elkhrachy, 2016). For this study The NASA Shuttle Radar Topographic Mission (SRTM) digital elevation model was downloaded from https://earthexplorer.usgs.gov/ through earth explorer as SRTM 1-arc second in Geo TIFF format and processed in ArcGIS. However, due to the influence of vegetation and land cover, system parameters during data acquisition, and data processing steps the SRTM DEM might not be certain. Therefore, it is crucial to validate the accuracy of DEM obtained from satellite image. As the study by Elkhrachy (2016) reveals vertical accuracy of DEM can be assessed with respect to the techniques listed above. The Author performed accuracy assessment of SRTM 30 m DEM with respect to reference data (GPS observations and Digitized topographic map); the GPS reference elevation data in the absence of trees, buildings and vegetation was found more accurate than digitized topographic map.

Reference control points with orthometric height (corrected) for the whole Botswana boundary was obtained from Botswana Survey and Map Agency. Study area polygon, SRTM 30 m DEM and reference control points were transformed to WGS 1984 UTM Zone 35S. The reference control points within the study area was clipped by study area polygon and pixel values corresponding to reference control points were extracted using extract values to point tool in ArcGIS. Following the recommendation by Elkhrachy (2016), this study considered thirty-six reference control points with orthometric height and the correlation was checked with SRTM 30 m DEM and found to be 0.9072; indicating a good agreement (see Figure 3.3). However, uncertainties or outliers were observed from the correlation graph. As confirmed by displaying the reference control points, on the study area DEM, the outliers of the SRTM DEM above the trend line are measurements at highest elevation whereas the outliers below the trend line are measurements taken at lower depressions and quite near the river course. For example, the point located at (X, Y) UTM: (214910, 7753190), enclosed by red circle is measurement taken relatively at higher elevation and the point located at (X, Y) UTM: (231074, 7742100) enclosed by green circle is measured quite near the river course.

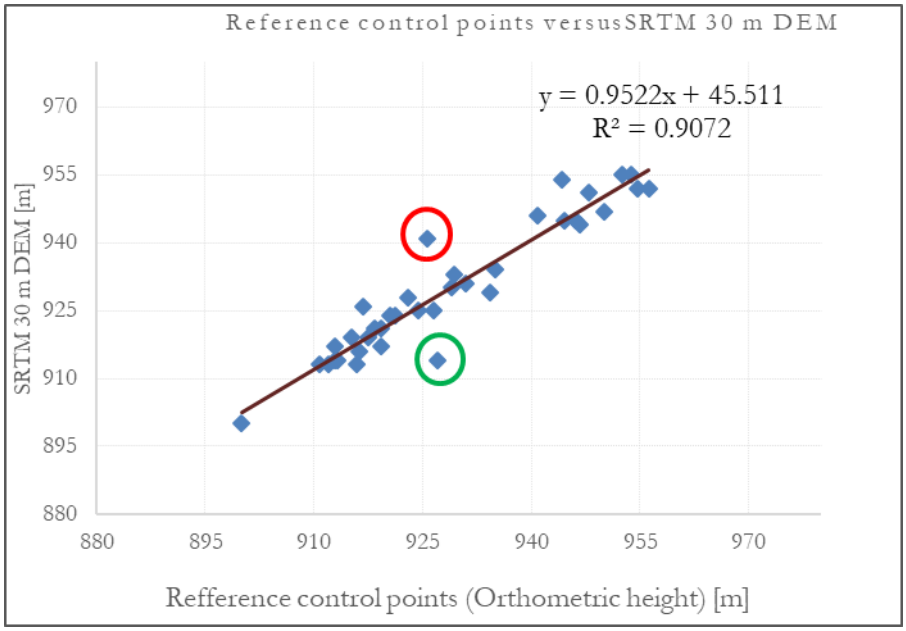

Figure 3-3 Corrected reference control points versus SRTM DEM 30 m

Eventually, the SRTM 30 m DEM values for specified location together with the groundwater table depth data was used to calculate the hydraulic heads and DEM showed the topography of the study area.

3.3. Conceptual model

A conceptual model is a qualitative representation of what is known about the system or site. A hydrologic conceptual site model entails natural and artificial processes that determine and facilitate the movement of groundwater within the system and can give information about from where the groundwater comes (sources), where it is going (sinks), through what type of porous media it is flowing (hydrogeology and stratigraphy), the behavior of the groundwater in the past and its future change based on different processes (M. Anderson & Woessner, 1992; Neven K & Alex M, 2011). Boundary conditions can be either physical such as surface topography, faults and water bodies and/or hydraulic boundaries like specified flow and specified head boundary conditions and determines the mathematical boundary conditions of the numerical model thereby strongly influence the flow pattern and direction of groundwater (Anderson & Woessner, 1992; & Lekula, et al., 2018).

3.3.1. Hydro-stratigraphic units

The BRA is located within the Kalahari Basin which is covered by varying thickness Kalahari Group sediments at the top and underlain by Archaen rocks, by Proterozoic rocks of the Damara Supper Group, Jurassic and Carboniferous sediments and by the volcanics of the Karoo Group at the bottom. The sequence of the stratigraphy within the study area is indicated in (Table 2.2). In addition, Having sparsely located available borehole logs information the thickness map for Kalahari Sand was identified through inverse distance weighting interpolation method in ArcGIS tool.

A one-layer unconfined aquifer which includes Upper, Middle and Lower Kalahari formations (Thomas & Shaw, 1990) with both saturated and unsaturated zones is the main interest for this study. The Lower Kalahari Gravels or basalt conglomerates are cemented by calcretes, silcretes or mixture of these materials and experience high yielding due to fracturing. The Middle Kalahari sediments are characterized by thick lacustrine sediments, clays, silts and sands which are commonly green in color. On the other hand, Upper Kalahari (fluvial deposits) are characterized by Pleistocene and Holocene lacustrine or pan deposits and aeolian sands including extensive spreads of deltaic sediments.

3.3.2. Model boundary conditions

Except of the Thamalakane River extending along the fault line, the other boundary conditions were conceptualized based on the potentiometric map prepared from groundwater level observations of 53 borehole logs obtained from DWA of Botswana and (MEWT DWNP, 2007) report. The boundaries along the equipotential lines represent inflows or outflows depending on the hydraulic gradient direction while boundaries perpendicular to equipotential lines represent no flow boundaries. Groundwater levels were measured in different times and laid inside and outside the modelled domain. The hydraulic heads for each borehole log were determined by subtracting the groundwater depth below ground surface from the respective cell values of SRTM 30 m DEM (see section 3.2.4) for details. Contour lines and contour map of the modelled domain with a 6 m vertical interval were produced by applying kriging interpolation method in ArcGIS tool. Borehole observations considered outside the study area helps to extend contour lines and able to distinguish the direction of groundwater inflow and/or out flow boundaries.

3.3.3. River-groundwater interactions

Deriving a consistent conceptual model for a river-groundwater interaction is difficult and needs extensive study of river and groundwater dynamics. Such interactions can be discussed through a series of alternative model representations that represent the range of observed behaviors (Newman et al., 2006). As modelled by (Newman et al., 2006), the following four models represent the river-groundwater interactions in arid and semi-arid regions. Model A represents flow of river but there is no water in aquifer rather it can recharge a deep aquifer system. Which is also called losing river. Such a situation most probably happens when there is low recharge and high groundwater abstraction rates. Model B represents case of no river flow but saturated zone with specified water level below the riverbed. In this case there is no river-groundwater interactions indicating lower aquifer storage and sort of dry river. In case of model C there is river flow plus groundwater in the aquifer. The flow is from river to the aquifer eventually the level of groundwater increases and will result in exfiltration (outcrop of groundwater to the surface). Model D represents a type of gaining stream/river where the water flows from the aquifer to the river. This situation likely happens in semi-arid regions with higher elevation and high annual precipitation at the end of wetter season.

The Boteti River, originated from the Okavango Delta is the only contemporary surface water body in the BRA and flows through the semi-arid regions of Botswana Kalahari, the area with erratic and variable rainfall and high evaporation rate. The river-aquifer interactions likely resemble to model C stated in (Figure 3.4) above; kind of losing river which in turn results for positive change in storage.

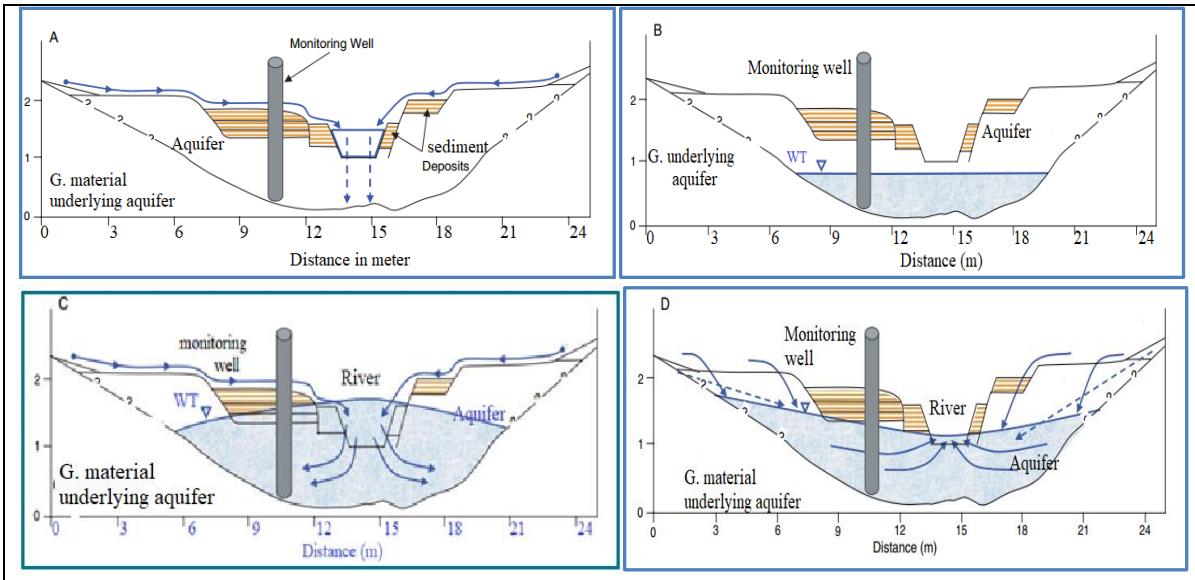

Figure 3-4 River-aquifer interactions conceptual models (Modified from (Newman et al., 2006)

3.3.4. Sources and Sinks

The Boteti River sourced from the Okavango Delta and rainfall during summer seasons (November to March) are the main source of water for surface and subsurface systems. The main external sources of water for the subsurface zone (recharge conditions of flow system) are: 1) gross recharge from rainfall infiltration; 2) seepage from the river; 3) lateral groundwater inflow through specified flow boundary from the western side of the modelled domain (lateral groundwater outflow boundary of Lekula, et al., (2018)); 4) lateral groundwater inflow from the southern part and 5) lateral channel seepage along Thamalakane River (sourced from Okavango Delta) through northern and north-western boundaries.

The main sinks from the saturated zone system (discharge conditions) were 1) groundwater evapotranspiration; 2) surface leakage (exfiltration); 3) discharge into river and 4) lateral groundwater outflow through the GHB and drain (DRN) boundaries from southern and southwestern parts.

All the components of sources and sinks were quantified through modelling and represented as:

$$\text{Inflow} - \text{Outflow} = \pm\frac{\Delta \mathbf{S}}{\Delta \mathbf{t}} \qquad (5)$$

Where, ΔS is change in storage and Δt is change in time.

3.4. Numerical model setup

Numerical model is the third step in modelling protocol following establishment of the modelling purpose and development of a conceptual model as first and second steps respectively (Anderson & Woessner, 1992) . It is a mathematical representation of the groundwater flow system and flow follows Darcy's law. Numerical modelling includes grid design, aquifer parameterization and model selection to mention some.

3.4.1. Model selection and description

MODFLOW NWT (Niswonger et al., 2011) with packages such as unsaturated zone flow (UZF1) and stream flow roughing (SFR2) was used for simulating river-groundwater interactions of the BRA. MODFLOW-NWT is the formulation of MODFLOW 2005 (Harbaugh, 2005). The model is selected because: 1) It can solve especially problems representing surface-groundwater interaction in unconfined aquifers i.e. problems related with drying and rewetting non linearities (Niswonger et al., 2011). 2) The software is open source, public domain and operates under ModelMuse GUI which allows the user to see the front, side and top views of the model which supports editing and 3-D view for displaying properties of

the model. 3) Calibration was done through trial and error method which enables the user to understand the relationship among parameters and about the whole model functionality compared with automatically calibrating models.

3.4.2. Model setup, aquifer geometry and grid design

The study area is about 19, 550 km2 and is discretized into 1 km2 square model grids in 174 rows and 168 columns which are consistent with EPSG 32735 Botswana Coordinate system. Convertible-type, a single layer unconfined aquifer, Kalahari Aquifer with both saturated and unsaturated zones is the main interest of this study. As there is no enough borehole log data about the detail stratigraphy of the geologic formations within the BRA but having spatially non-uniform Kalahari Sand thickness of larger than 100 m as a reference, the model aquifer was set to 70 m b.g.s fixed thickness and the model aquifer top was considered as surface elevation. Similar schematization was made by Baroncini-Turricchia et al., (2014) to model a single layer unconfined aquifer at Carrizal Catchment, Spain but they considered the shallowest inversion depth.

3.4.3. Driving forces

Precipitation, potential evapotranspiration and well abstraction rates are the main driving forces for integrated hydrological models. For the present study including the river inflow from Okavango Delta precipitation and potential evapotranspiration were the main driving forces of the MODFLOW NWT unsaturated zone flow model (UZF1) in a daily basis for a period of three years, beginning of September 2014 to end of August 2017. However, due to lack of data well abstraction rates are considered as negligible.

3.4.3.1. Precipitation and Potential Evapotranspiration

The difference between the bias-corrected CHIRPS and spatially variable interception rate map, which is referred as effective rainfall or applied infiltration rate (El-Zehairy et al., 2018) was prepared and used as an input for the UZF1 package in MODFLOW NWT under ModelMuse GUI to calculate groundwater recharge and evapotranspiration (Niswonger, et al., 2006). The map calculation can be made either in ILWIS and/or ArcGIS environments or in MODFLOW ModelMuse using user defined formula. All the maps were resampled to 1 km2 spatial resolution using nearest neighbor resampling technique to meet the model grid cell size and converted to ASCII raster format which is viable for MODFLOW NWT under ModelMuse GUI.

Spatio-temporally variable reference evapotranspiration rate supplied from US-based GMAO GOES-5 model at 20 km spatial resolution was used as PET (see section 3.2.2.2). Later the map was resampled and converted to the same cell size and format as infiltration rate map and finally used as model input.

3.4.3.2. Inflow from Okavango Delta

The present study considered two gauging stations, Samedupe at the upstream and Rakops at the downstream of Boteti River in the BRA (see Figure 2.1). As stated earlier the gap filled inflow rate (discharge) at the upstream lateral boundary was used as input to the MODFLOW ModelMuse model under MODFLOW packages and programmes, SFR package, MODFLOW Features, Flow (flow into the upstream end pane). However, the inflow rate was measured inside the modelled domain few kilometres in from the lateral boundary, at the Samedupe gauging station. Therefore, that amount was multiplied by user defined constant (factor), 1.04 to account the losses and undefined water use between the lateral boundary and the gauging station where the discharge is measured.

3.4.4. Model External boundaries

As stated above in section 3.3.2, external model boundary conditions (lateral boundaries) that are used in the numerical model are specified head boundary to the north west of the modelled area, no flow boundary

to north, GHB to the south, drain boundary to south east, and specified flux boundary to the west. The position of external model boundaries is presented in (Figure 3.5) below.

3.4.4.1. Time-Variant Specified-Head (CHD)

Time-Variant Specified-Head Package (CHD) allows constant head cells to take on different values for each time step. Sometimes it is also called constant head boundary; abbreviated as CHD. Large water bodies i.e. major rivers, lakes, reservoirs and oceans that are not affected by stresses in the system is better represented by specified head boundaries (M. Anderson & Woessner, 1992). For this study the constant head boundary is assigned as a poly line object at the north western boundary (line AB in Figure 3.5) where the Boteti River flows into the interest area and the modelled domain is also bounded by Thamalakane River at that side.

3.4.4.2. Flow-Head Boundary (FHB)

FHB was developed for the U.S Geological Survey 3D finite-difference modular groundwater flow model, MODFLOW and allows the user to specify flow or head boundary conditions that vary at times other than starting or ending times of stress periods and associated time steps (Leake, et al., 1997). The values of the flow and/or head at each time step (not corresponding model time steps) are calculated by linear interpolation of user specified values.

The specified flow can be also applied using recharge (RCH) or well (WEL) packages. However, in RCH package the user should specify the options how stress period and time step dependent flux [LT-1] is applied; like on the Top layer, a Specified layer or Top active cell as well as should be decided either to ignore previously applied recharge rate (if any) or take it as total sum for the given grid cells. On the other hand, specified volumetric flow [LT-3] on stress period intervals can be applied using well (WEL) package.

For the present study the FHB boundary was assigned as polyline object at the western lateral boundary of the modelled domain (line EA in Figure 3.5) where the hydraulic contour lines are parallel with the model boundary polygon (perpendicular to groundwater flow direction) at that side. On top of that, the stated boundary is groundwater outflow boundary of Lekula, et al., (2018) IHM of Central Kalahari Basin. Finally, time step independent specified flux [LT-1] was determined based on aquifer cross section and parameters across that boundary per grid cell through Darcy's law and applied to the model.

3.4.4.3. General Head Boundary (GHB)

Head dependent flux boundaries can be simulated by using GHB package. The flux into (or out of) the saturated zone system at the boundary and head in the cell has a linear relationship. For GHB a reference head and conductance are specified by the user. For the present study the GHB was defined by a polyline object (line DE in Figure 3.5) to account for the pronounced inflow and/or outflow groundwater across that boundary.

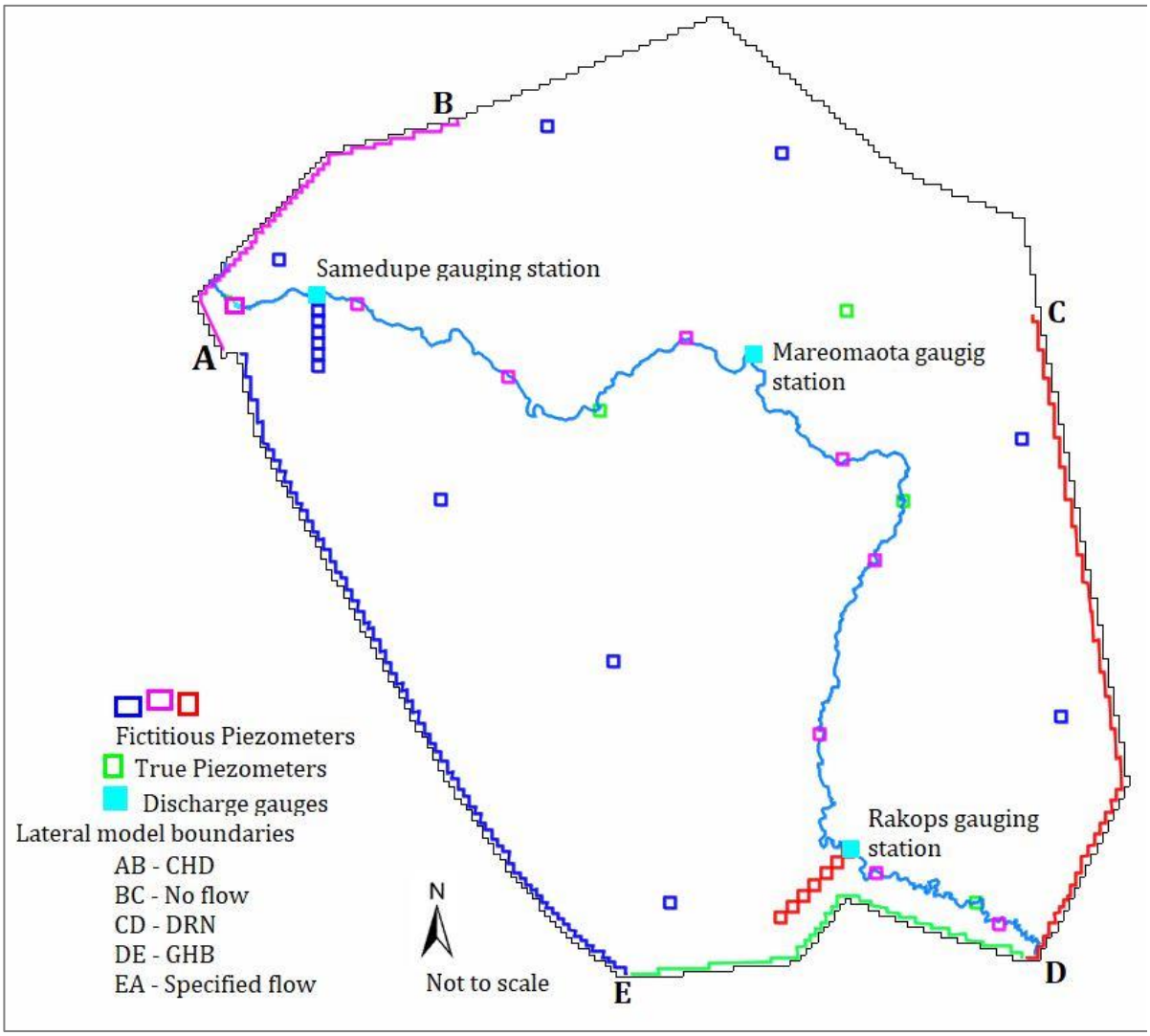

Figure 3-5 Location for sets of fictitious piezometers and lateral model boundaries

3.4.4.4. Drain (DRN) Boundary

The drain only removes water from the modelled domain groundwater system so that the drain is active only when the head in the aquifer is higher than drain elevation.

The present study model aquifer (Kalahari Aquifer) DRN boundary (line CD in Figure 3.5) was used to account for the out flow of water from the saturated zone system through the south-easterly direction which is discharged into the Makgadikgadi Pans.

3.4.5. Internal model boundaries

Unsaturated Flow Package (UZF1)

The UZF1 package, which is the substitution for the Recharge and Evapotranspiration packages of MODFLOW-2005 simulates percolation through an unsaturated zone between land surface and water table (Niswonger et al., 2006). The main input parameters of the model, infiltration rate and evapotranspiration demand were simulated and partitioned internally into unsaturated zone evaporation, gross recharge, groundwater evapotranspiration and groundwater exfiltration by UZF1 package. The package uses infiltration rate, evapotranspiration demand, initial unsaturated water content, saturated water content, Brooks-Corey exponent, vertical hydraulic conductivity of unsaturated zone, evapotranspiration extinction

depth and evapotranspiration extinction water content as input to proceed the underlined process (Niswonger et al., 2006). The flow is assumed to occur in the vertical downward direction in an isotropic and homogeneous zone. The package simulates one dimensional, vertical unsaturated flow via kinematic wave approximation to Richard's equation using (Equation 7). Vertical unsaturated flow is assumed to gravity driven only and neglects negative potential gradients (Niswonger et al., 2006).

$$\frac{\partial \theta}{\partial t} + \frac{\partial K(\theta)}{\partial z} + i = 0 \qquad (6)$$

where θ is the volumetric water content, volume of water per volume of rock (L3L-3), q is water flux, volume of water per time per unit area (LT-1), z is elevation in the vertical direction (L), K (θ) is the unsaturated hydraulic conductivity as a function of water content (LT-1).

The Brooks-Corey function (Equation 8) relates unsaturated zone hydraulic conductivity and water content.

$$\mathrm{K}(\theta) = Ks[\frac{\theta - \theta r}{\theta s - \theta r}]^{\epsilon} \qquad (7)$$

Where, Ks is the saturated hydraulic conductivity, θr is residual water content, θs is saturated water content and ε is the Brooks-Corey exponent.

Streamflow-Routing (SFR2) Package

SFR2 package, a modification to SFR1 is used to simulate stream-groundwater exchange and unsaturated zone flow beneath streams (Niswonger & Prudic, 2010). Whenever the water table (head in MODFLOW) is below the elevation of stream or river bed, SFR2 package simulates unsaturated flow independently of the saturated flow within each model cell based on a kinematic wave approximation to Richard's equation by method of characteristics (Smith, 1983). Method of characteristics is used to reduce one dimensional partial differential equation to an ordinary differential equation that is solved by analytical integration. As the flow is assumed vertical in the saturated region below streams, SFR2 fills the pore space in the unsaturated zone from top to down and the saturated region below the stream will be relatively narrow which contrasts with saturating vadose zone from bottom to up where portion of groundwater flow will be horizontal and much more pore space will be needed to be filled in order to saturate the unsaturated zone beneath streams. Therefore, streams that are hydraulically disconnected from the aquifer will be much more likely to reconnect to the aquifer through SFR2 and can reduce the vertical hydraulic gradient and decrease the amount of seepage loss from the stream (Niswonger & Prudic, 2010).

Streambed thickness and width, streambed hydraulic conductivity, stream flow network, stream slope, streambed top, channel roughness, flow into upstream end and unsaturated zone parameters such as saturated and initial water content, maximum unsaturated zone vertical hydraulic conductivity, Brooks Corey exponent are all in put parameters for SFR2 package in MODFLOW-NWT.

The volume of water that seeps from the stream is calculated by multiplying the infiltration rate by the wetted area of the stream and is similar to the method used in River Package (Niswonger & Prudic, 2010). By considering the gap (distance) between unsaturated zone and aquifer, infiltration rate (flux out of the stream) to aquifer is calculated using (Equation 8).

$$Q = \frac{KwL}{m}(\mathrm{hs} - \mathrm{ha}) = C(\mathrm{hs} - \mathrm{ha}) \qquad (8)$$

Where Q is volumetric flow between a given section of stream and volume of aquifer (L^3T^{-1}), K is the saturated hydraulic conductivity of stream bed sediment (LT^{-1}), w is with of the stream (L), L is length of the stream corresponding to a volume of aquifer (L), m is thickness of the stream bed deposit extending from top to bottom as specified by the user (L), h_s is the heads in the stream determined by adding the

stream depth to the elevation of the streambed (L) and h_a is the head in the aquifer beneath the streambed (L), and C is streambed conductance (L^2T^{-1}).

3.4.6. Model Parametrization

Newton Solver (NWT)

Basic options for NWT, Head tolerance (HEADTOL) [L], Flux tolerance (FLUXTOL) [L3T-1], Maximum number of outer iterations (MAXITEROUT) and Portion of cell thickness used for coefficient adjustment (THICKFACT) were set to default values i.e. 0.0001, 100, 100 and 0.00001 respectively. Matrix solver is set as Chi MD (2) and Print solver convergence information (IPRNWT) was selected. Model complexity (OPTIONS) was set as complex following (Hassan et al., 2014, Niswonger et al., 2011 and Teketel, 2017)

3.4.6.1. UZF1 Parametrization

Satellite products of precipitation and evapotranspiration demand were processed, and maps prepared as outlined in (section 3.2.2). Interception rate and extinction depth values were sourced from literature (as discussed below) and maps were produced with respect to the land cover map of the interest area. Later, all maps were resampled to 1 km2 grid cell size and converted to file format viable for MODFLOW ModelMuse, i.e. ASCII raster and imported to the model. Daily infiltration rate was calculated by subtracting interception map from daily precipitation maps. Daily rates for each time step were used for transient state model simulation. Extinction water content [L3L-3], saturated water content [L3L-3], Brook's Corey exponent and vertical hydraulic conductivity of the unsaturated zone [LT-1] was allocated as 0.12, 0.3, 3.5, 1.25 respectively.

Furthermore, recharge and discharge location option (NUZTOP) as "Top layer (1)", vertical hydraulic conductivity source (IUZFOPT) as "specify vertical hydraulic conductivity (1)", number of trailing waves (NTRAIL2) as "15", number of wave sets (NSETS2) as "20" was assigned. And "route discharge to streams, lakes, or SWR reaches (IRUNFLG)", "simulate evapotranspiration (IETFLG)", "print summary of UZF budget terms (IFTUNIT)", and "calculate surface leakage (inverse of NOSURFLEAK)" were selected.

Interception and infiltration rates

Interception loss is the amount of rainfall captured by the canopy of the plant like leaves and stem, and successively absorbed and evaporated from it. It depends on the land cover and climate type of the area. Canopy size, amount of rainfall and evapotranspiration rates are major factors for variation of interception rate within the interest area. For this study spatially variable interception rate values were considered based on a 20 m resolution land cover map of the BRA (Figure 2.3) which is mainly covered by shrubs, grassland, trees and bare land. The amount of precipitation intercepted per grid cell was calculated using (Equation 10) below. The findings by (Le Maitre, et al., 1999 and Miralles et al., 2010) reveal that the interception rates of trees, shrubs cover areas, grass land and bare land are summarized as 0.12, 0.04, 0.02 and 0 respectively.

$$I = P * (It * At + Is * As + Ig * Ag + Ib * Ab) \quad (9)$$

Where, I is interception per grid cell [md-1], P is precipitation per grid cell [md-1], It, and Is, Ig, Ib are interception rates by trees, shrubs, grasslands and bare land [%], and At, As, Ag, Ab are area ratio coverage per grid for trees, shrubs, grasslands and bare land respectively.

Extinction depth and Extinction water content

Extinction depth is the depth in subsurface where evapotranspiration terminates and is one of input for unsaturated zone flow (UZF1) package. It depends on the maximum rooting depth of the land cover classes and spatially variable rooting depth map was produced based on 20 m resolution land cover map. Canadell et al., (1996) and Obakeng, et al., (2007), suggested the maximum rooting depth as 25 m, 4 m and 2 m for

trees, shrubs and grassland respectively. Extinction depth of the dominant soil in the BRA, sandy soil (J. H. Kgaswanyane, 1996), was adapted from (Shah, et al., 2007), and found to be 0.1. The rooting depth values were assigned to land cover map and resampled to 1 km2 spatial resolution to fit model grid size later used as input for the model under UZF package. Equation (11) below was used to determine extinction depth per grid cell.

$$Extd = Rdt * At + Rdsh * Ash + Rdg * Ag + Rd + Rdb * Ab \quad (10)$$

Where Extd is Extinction depth per grid cell [m], Rdt, Rdsh, Rdg and Rdb are rooting depths of trees, shrubs, grassland and bare soil respectively per grid cell [m].

The amount of water removed from a cell as evapotranspiration is limited by the volume of water stored in the unsaturated zone above the extinction depth. If the saturated zone extends up to the vicinity of evapotranspiration extinction depth, the rate of ET removed decreases linearly from maximum at land surface and zero at the ET extinction depth (Niswonger et al., 2006). The method is the same as used in the Evapotranspiration package (McDonald, 1988).

Extinction water content (EXTWC) is the water below which evapotranspiration cannot be removed from the unsaturated zone. Extinction water content has a value between saturated water content minus specific yield and saturated water content (Niswonger et al., 2006). For the present study spatially uniform EXTWC value of residual water content plus 0.01 was applied.

3.4.6.2. Streamflow-Routing (SFR)

The river was simulated as separate stream segments based on gauging locations (Figure 2.1) and segment number and reach for streams was assigned from upstream to downstream chronologically thereby simulated through SFR2 package. Streambed properties (ISFROPT) as "specify some streambed properties by reach (can't inactivate streams)" and Unsaturated flow (ISFROPT) was selected. Tolerance [L3T-1] (DKEAK), Number of trailing wave increaments (NSTRAIL), Maximum number of trailing waves (NSFRSETS), Maximum number of cells to define unsaturated zone (ISUZN), Number of divisions per time step for kinematic waves (NUMTIM), Time weighing factor for the kinematic wave solution (WEIGHT) and closure criterion for the kinematic wave solution (FLWTOL) were set as 0.0001, 10, 30, 10, 1, 1 and 0.0001 respectively. Streambed top (STRTOP) as "Model Top" for all streams and Reach length (RCHLEN) as "Object intersect length" was assigned. Stream slope (SLOPE) as 0.02 to 0.05, Streambed thickness (STRTHICK) as 0.8 to 2 m, streambed Kv (STRHC1) as 0.005 to 0.9 m/day and for unsaturated zone below streams similar value as UZF1 package i.e. for saturated volumetric water content (THTS), Brooks corey exponent (EPS), and Maximum unsaturated vertical hydraulic conductivity (UHC) were assigned. Stream width as 1 to 4m, Mannings Channel roughness as 0.035, Stream horizontal hydraulic conductivity as the horizontal hydraulic conductivity (Kx) of the respective zone were assigned for all streams and all adjusted during calibration. In addition, the measured dailly stream flows at the upstream lateral boundary, inlet of the Boteti River into the modelled domain was assigned as model input under SFR2 package, flows (flow into upstream end) pane.

SFR2 package allows the user to add or subtract water from streams due to runoff, precipitation, and evapotranspiration (Prudic et al., 2004); and allow the simulation between stream connections by assigning number for stream segments in a sequential order from upstream to the downstream.

3.4.6.3. GHB and CHD

For a GHB condition defined by a poly line object, head at the boundary was assigned based on the values of initial heads across the GHB boundary as "Model To-15" and adjusted through calibration. GHB Conductance was assigned based on the horizontal hydraulic conductivity of the respective zone as 12.5 md^{-1} and both adjusted during model calibration. GHB conductance multiplier was assigned as 1.

CHD boundary condition is specified as a polyline object and, starting and ending heads were assigned as equivalent fresh water level of mean sea level along the CHD boundary.
The summarized model parametrization (model inputs) are found in (Table 3.3) below.

Table 3-3 Model parametrization (Summarized model inputs) for IHM of the BRA

MOD Packages (Option) used	Parameter (model input)	Min. value	Max. value	Unit	Reference	Variability	Remark
UZF1	Infiltration rate	0.0011	0.0017	md^{-1}	Corrected and validated CHIRPS after subtracting interception rate	Spatially and temporally variable	Fixed
	PET	0.0060	0.0062	md^{-1}	Validated satellite PET of 20 km resolution		Fixed
UZF1	THTS	0.1	0.4	m^3m^{-3}	Soil moisture studies by Obakeng et al., (2007)	Spatially uniform	-
	THTI	0.1	0.1	m^3m^{-3}	Following Niswonger & Prudic, (2010) Set as equal to THTS minus Sy		-
	EXTDP	0.1	25	m	Canadell et al., (1996)	Spatially variable	Fixed
	EXTWC	0.1	0.16	m^3m^{-3}	Calculated and assigned value of between WCr and THTS and adjusted	Spatially uniform	Calibrated
	Kv	0.019	3.1	md^{-1}	Assigned as 1/10 of Kh and adjusted	-	Calibrated
SFR2	WIDTH1	1	3	m	-	-	Calibrated
	STRHC1	0.05	0.8	m	-	Spatially variable	Calibrated
	STRTOP	0.8	2.5	m	-	-	Calibrated
	STRTHICH	0.8	1.5	m	-	-	Calibrated
	SLOPE	0.01	0.01	[-]	-	-	Fixed
	n	0.035	0.035	[-]	-	-	
DRN	COND	0.05	300	m^2d^{-1}	Assigned through calibration	Spatially variable	Calibrated
GHB		0.05	50				Calibrated
UPW	Kh	0.025	31	md^{-1}	From studies by (de Vries et al., 2000)		Calibrated
	Sy	0.27	0.33	[-]	Assigned during calibration following Lekula et al., (2018)	Assigned throughout the model domain	-
FHB	Specified flux	0.3	0.3	md^{-1}	Calculated	-	-

Where:
PET – Potential evapotranspiration, THTS – Saturated volumetric water content, THTI – Initial volumetric water content, EXTDP – evapotranspiration extinction depth, EXTWC – Evapotranspiration extinction water content, WCr – residual water content, Kv – Maximum unsaturated zone vertical hydraulic conductivity, Kh – Horizontal hydraulic conductivity, WIDTH1 – stream width, STRHC1 – Streambed hydraulic conductivity, STRTOP – Streambed Top, STRTHICH – Streambed thickness, SLOPE – Stream slope, COND – DRN and GHB Conductance, n – Manning's roughness coefficient and Sy – Specific yield.

3.4.7. State variables

State variables are spatially as well as temporally variable ground measured values which have relevant information about the system and used as a reference during model calibration. The simulated values from the model are compared with ground measured values (true conditions) to attain the best model fit and to fix the calibration parameters. Due to lack of transient piezometric data, river flows are the only state variables with temporally varying data. However, five piezometers with one-time measured values (September 2018) were used for calibration in line with flows considering: 1) As Obakeng et al., (2007) fluctuation of groundwater level with in the Botswana Kalahari is not much varying. They found the annual average groundwater level fluctuation within that region is 0.2 m to 0.6 m; but can be about 3 m and above in some regions; 2) regarding calibrating heads, the present study mainly focused to control groundwater level below surface elevation through calibrating river flows and closing the water balance of the system. 3) the groundwater abstraction rates which might have substantial influence on the fluctuation of the groundwater level are considered as negligible.
The Boteti River is diverted from the outlet of Okavango Delta, Thamalakane river (see Section 2.8). As stated in (section 3.2.3) based on location of discharge gauges within the river, Boteti River was divided into five parts (stream segments) for modelling purposes. Boteti River at each discharge gauge stations were calibrated through SFR2 package based on the respective stream cross sections and SFR parametrization stated in (section 3.4.6.2). As stated by (Niswonger & Prudic, 2010) the flow, if SFR2 are routed through a network of channels, flow is always in the same direction along channels.

3.4.8. Initial conditions

The initial heads were assigned for all active model cells to define the groundwater condition at the start of model run. The interpolated heads from available borehole data was used to warm up the model and later kept as it is for transient state modelling.
The initial soil moisture content was assigned following (Niswonger & Prudic, (2010)) as saturated soil moisture content minus specific yield; based on the saturated soil moisture content from soil moisture studies of (Obakeng, et al., 2007). The initial hydraulic conductivity and specific yield values were assigned following (Lekula et al., 2018) of the surficial unconfined Kalahari Sand unit layer and both were adjusted during calibration. The GHB and DRN conductance values was initially assigned based on the hydraulic conductivity values of the zones across the GHB and DRN boundaries.

3.5. Model calibration

This study focused on transient state model set up and calibration by aiming to match the simulated heads and flows with the measured values and closing with reasonable water balance for the simulation period from beginning of September 2014 to end of August 2017. The first one-year data was used as spinoff (initialization) period to get the model response for daily variation of state variables under applied driving forces. Later, without discarding the spinoff data in similar manner as (Teketel, 2017 & Kinoti, 2018) but contrary to (El-Zehairy et al., 2018, Hassan et al., 2014 & Baroncini-Turricchia et al., 2014) transient state model calibration for 1096 daily stress periods and time steps was carried out. The modelling units were set on the model, MODFLOW options pane as days for time and meter for length.

A forward calibration procedure, manual trial and error method was carried out to achieve the desired objectives. The calibration continues until the final calibrated model has: i) an acceptable agreement between simulated and measured stream discharges; ii) simulated piezometric heads that match single measurements of heads and do not exceed the ground surface; iii) a realistic water balance with a discrepancy value of < 1% (Anderson & Woessner, 1992). Percent discrepancy is defined as difference between inflow and outflow less change in storage divided by the average of inflow and outflow multiplied by 100.

Horizontal hydraulic conductivity, maximum unsaturated vertical hydraulic conductivity, conductance of the GHB, conductance of the drain and streambed hydraulic conductivity were main adjusted parameters during model calibration. Specific yield (Sy) also called drainable porosity which is volume of water released from storage by gravity from unconfined aquifer per unit surface area of aquifer per unit decline of the water table also was used as a calibration parameter. MODFLOW calculates the amount of storage in the unconfined aquifer and therefore, maintain the continuity between the unsaturated zone and aquifer (Niswonger & Prudic, 2010).

3.6. Model performance evaluation

Model performance was carried out for both hydraulic heads and stream flows based on error assessment which was ascertained from observed and simulated values through statistical analysis and water balance closure in terms of discrepancy between total inflows and outflows. In addition, the performance of the model was checked based on visual inspection of plots i.e. by checking the observed and simulated scatter plots of hydraulic heads and/or hydrographs of flows.

For hydraulic heads, statistical analysis that includes; ME (mean of errors), MAE (mean absolute error) and RMSE (root mean square error) as presented in equations (11) to (13) was used to evaluate the model performance.

$$\text{ME} = \frac{1}{n}\sum(\text{Hm} - \text{Hs}) \quad (11)$$

$$\text{MAE} = \frac{1}{n}\sum(abs(\text{Hm} - \text{Hs})) \quad (12)$$

$$\text{RMSE} = \sqrt{\frac{1}{n}(\sum(\text{Hm} - \text{Hs})\text{^}2)} \quad (13)$$

Where, n – is number of observations, Hm and Hs are measured and simulated heads respectively.

As (M. Anderson & Woessner, 1992), a small value of ME indicates the unbiased overall model fit i.e. the simulated values are on average with respect to the measured or true values. However, as the negative and posive residuals are included in the average value, the errors may be cancelled eachother and is not sufficient indicator of model fit. MAE and RMSE are used to measure the average magnitude of errors. The possible value range for MAE is from 0 to ∞ and for RMSE is from -∞ to ∞. In both cases value close to zero is prefferable.

Simulated versus observed hydrographs of river flows were compared through objective functions which measure the closeness of the simulated value from the model with respect to the observed (field measured) values. As recommended by (Rientjes, 2015; Seibert & Vis, 2012 & Nash & Sutcliffe, 1970) most commonly used objective functions are relative volumetric error (RVE), Nash-Sutcliffe (NS) and over all model performance (Y). Detail description of objective functions is shown in (Table 3-4).

Table 3-4 Description of objective functions (Rientjes, 2015)

Objective functions	Description	Equations	Acceptable range, Best value
Relative volumetric error	Q_{sim} versus Q_{obs} volumetric balance	$RVE = \frac{\sum Q_{sim} - \sum Q_{obs}}{\sum Q_{obs}} \; x \; 100$	Best value 0, ±5% to ±10% acceptable
Overall model performance	An indicator of Overall model performance	$Y = \frac{NS}{1 + \lvert RVE \rvert}$	0 to 1, best value 1, acceptable >0.6
Nash-Sutcliffe	Indicates shape fitness between the observed and simulated discharge	$NS = 1 - \frac{\sum(Q_{obs} - Q_{sim})^2}{\sum(Q_{obs} - \overline{Q_{obs}})\text{^}2}$	-∞ to 1, acceptable >0.6

Where, Qsim, Qobs and $\overline{Q_{obs}}$ are simulated discharge, observed discharge and mean of observed discharges, respectively.

3.7. Model sensitivity analysis

The main objective of sensitivity analysis is to identify the parameters which have the most influence on model results thereby to identify the sources of model uncertainty (M. Anderson & Woessner, 1992). The Sensitivity analysis was performed based on optimized parameters as a reference and changing one parameter sequentially by increasing or decreasing through user specified percent factor, for example as -30% to +30% case of this study. Sensitivity analysis of saturated and unsaturated zone fluxes i.e. unsaturated zone evapotranspiration, groundwater evapotranspiration, groundwater exfiltration, gross recharge and net recharge to changes in saturated water content, maximum unsaturated vertical hydraulic conductivity, extinction depth and specific yield was assessed.

3.8. Spatial and temporal effect of the river on groundwater level

To characterize the spatio-temporal impact of Boteti River on groundwater levels, sequence of fictitious piezometers were allocated near the two discharge gauges (Figure 3.5) as blue piezometers from Samedupe gauge, upstream of the river and red piezometers from Rakops gauge, downstream of the river with varying distance increments from the gauges; starting 1 km for the nearest piezometer then increased sequentially by 2 km for each piezometer. (El-Zehairy et al., 2018) postulated the same method to characterize variation of groundwater levels with respect to lake stage. The initial water level of the fictitious piezometers was assigned as surface elevation and their spatial and temporal variation was assessed. It has to be noted that during calibration process, the water level of the piezometers was kept below the respective surface elevation to be certain that the water table is below surface level.

3.9. Water balance

As stated earlier, an integrated 3D transient state hydrological model, MODFLOW NWT under ModelMuse GUI coupled with UZF1 & SFR2 packages that integrates surface, unsaturated and saturated zones of the system, and simulate surface, unsaturated and saturated zone water fluxes (Lekula et al., 2018; El-Zehairy et al., 2018; Hassan et al., 2014 & Niswonger et al., 2011) was used for this study.

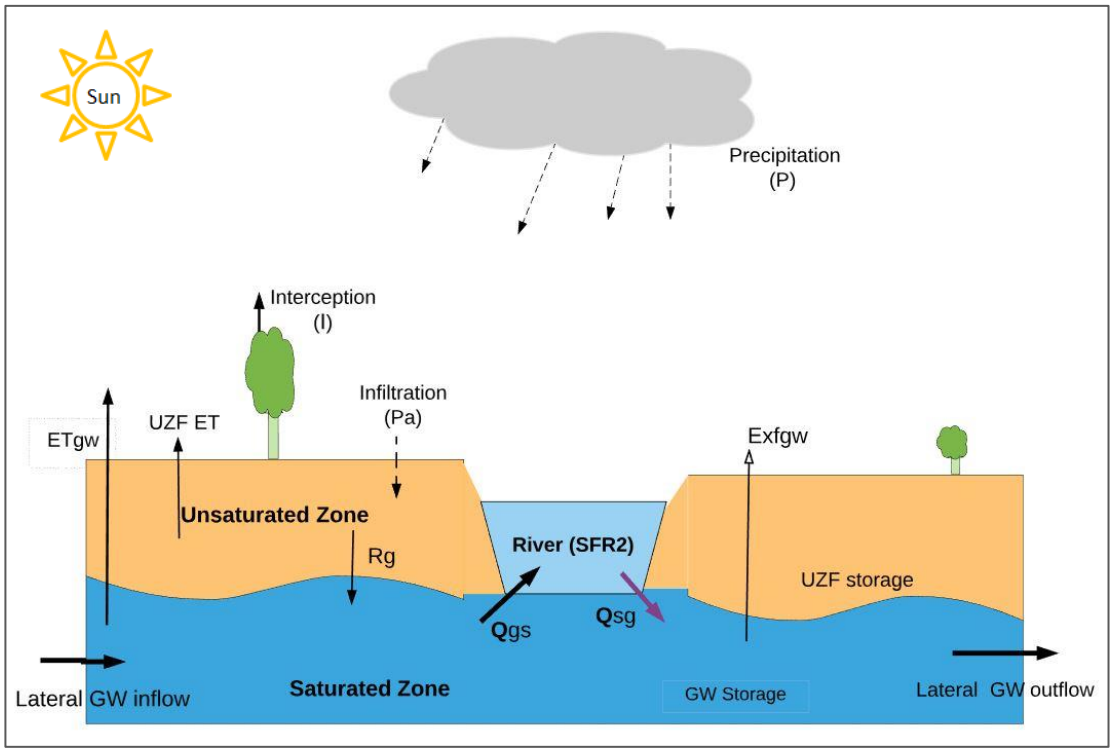

Figure 3-6 Schematic diagram of model setup and water balance components of the BRA; Qgs and Qsg accounts leakage from groundwater to river and river to groundwater respectively.

The diagram on (Figure 3-6) represents the water balance components of the BRA. The following water balance equations (Equation 15 to 22) for each section of the model are essential to assess and understand the dynamics of river-groundwater interactions of the BRA.
The water balance of the whole model domain can be expressed as follows:

$$P + \mathrm{Q_{in}} + Q_{CHD} + \mathrm{Q_{FHB}} + Q_{GHBin} = ET + Q_{out} + \mathrm{Q_{DRN}} + Q_{GHBout} + \Delta S \qquad (14)$$

Where, P is precipitation rate, Qin is river inflow at the inlet of the modelled area, QCHD is lateral groundwater inflow into the modelled domain across constant head boundary, QFHB is lateral groundwater inflow through specified flow boundary, QGHBin is lateral groundwater inflow through GHB, ET is total evapotranspiration rate, Qout is river outflow from the modelled area, QDRN is lateral groundwater outflow from the modelled area across the drain boundary; QGHBout is lateral groundwater outflow across GHB and ΔS is total change in storage.

Total evapotranspiration and total change in storage can be expressed as follows:

$$ET = ET_{uz} + ETgw + I \qquad (15)$$

$$\Delta S = \Delta S_{uz} + \Delta Sgw \qquad (16)$$

Where, ETuz and ETgw are unsaturated and saturated zone Evapotranspiration rates respectively; I is amount of precipitation intewrcepted; and Suz and Sgw are unsaturated and saturated zone storage changes respectively.

River flow at the outlet of the modelled area can be expressed as:

$$Q_{out} = Q_D + Q_H + Q_B \qquad 17$$

Where QB is base flow calculated as difference between leakage from river to groundwater and leakage from groundwater to river, QH and QD are of infiltration excess runoff (Huttonian) and saturation excess runoff

(Dunnian) respectively. On the other hand, land surface and unsaturated zone water balance are expressed as (Equation 18 & 19 respectively).

$$P_e + Exfgw = P_a + Q_D + Q_H \quad (18)$$

$$P_a = Rg + ET_{uz} \pm \Delta S_{uz} \quad (19)$$

where, Pe is effective rainfall (P - I), Exfgw is groundwater exfiltration, Pa is actual infiltration rate through the unsaturated zone (El-Zehairy et al., 2018) , Rg is gross recharge.

Finally, water balance of the saturated zone can be expressed as:

$$Rg + Q_{CHD} + Q_{FHB} + Q_{GHBin} + Q_{sg} = ETgw + Q_{DRN} + Q_{GHBout} + Exfgw + Q_{gs} + \Delta Sgw \quad (20)$$

Net recharge is the amount of water that reaches the saturated zone. Thus, it plays indispensable role to estimate groundwater storage and constitutes part of the groundwater flow to the discharge areas (Hassan et al., 2014). It can be expressed as equation (21) below.

$$Rn = Rg - (Exfgw + ETgw) \quad (21)$$

4. RESULTS AND DISCUSSION

4.1. Data processing results

4.1.1. Precipitation

Figure 4-1 show correlation of CHIRPS against Maun station gauge rainfall (2014-2017). An R^2 of 0.7 shows an acceptable and good agreement between the satellite estimate and ground measured values. The values on the ordinate (Y-axis), satellite estimates > 0 and gauge records 0 as well as the values on the abscissa (X-axis), gauge records > 0 and satellite estimates 0 are errors (bias) and removed while checking the correlation.

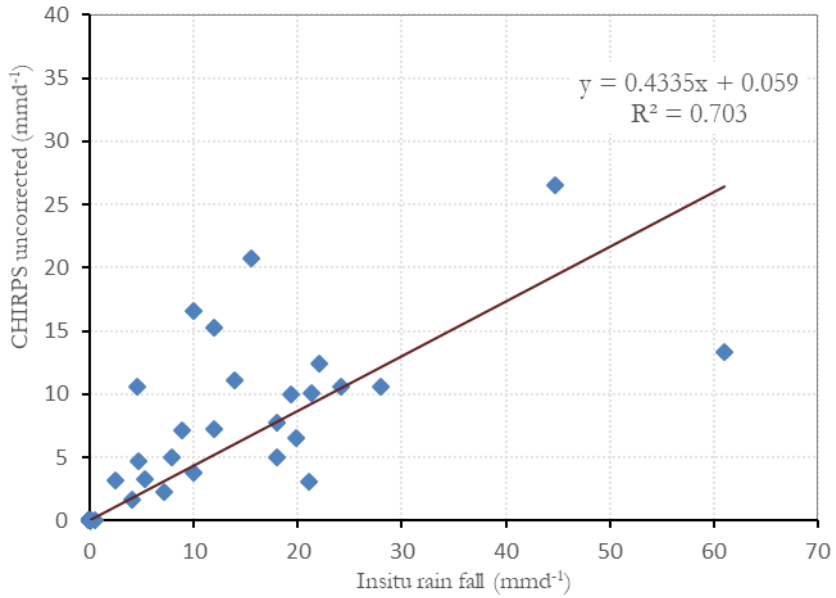

Figure 4-1 Scatter plot of daily station rainfall against uncorrected CHIRPS at Maun station

Performance evaluation of Satellite rainfall estimates can be determined by applying categorical statistics (Lekula et al., 2018). In the present study the performance of CHIRPS was determined by applying categorical statistics in terms of Probability of Detection (POD), False Alarm Ratio (FAR) and Critical Success Index (CSI). As the results reveal, frequency of detection in terms of POD was found quite good. The detection capability in terms of FAR and CSI was fair. The results as indicated in (Table 4.1) and (Figure 4.2) are in line with Toté et al., (2015) who Found POD and FAR statistics results of CHIRPS as 0.89 and 0.29 for Mozambique.

Table 4-1 CHIRPS Frequency of detection with respect to in situ rainfall at Maun station

Indicator	Value	Range, best value
POD	0.83	0 to 1, 1
FAR	0.39	0 to 1, 0
CSI	0.54	0 to 1, 1

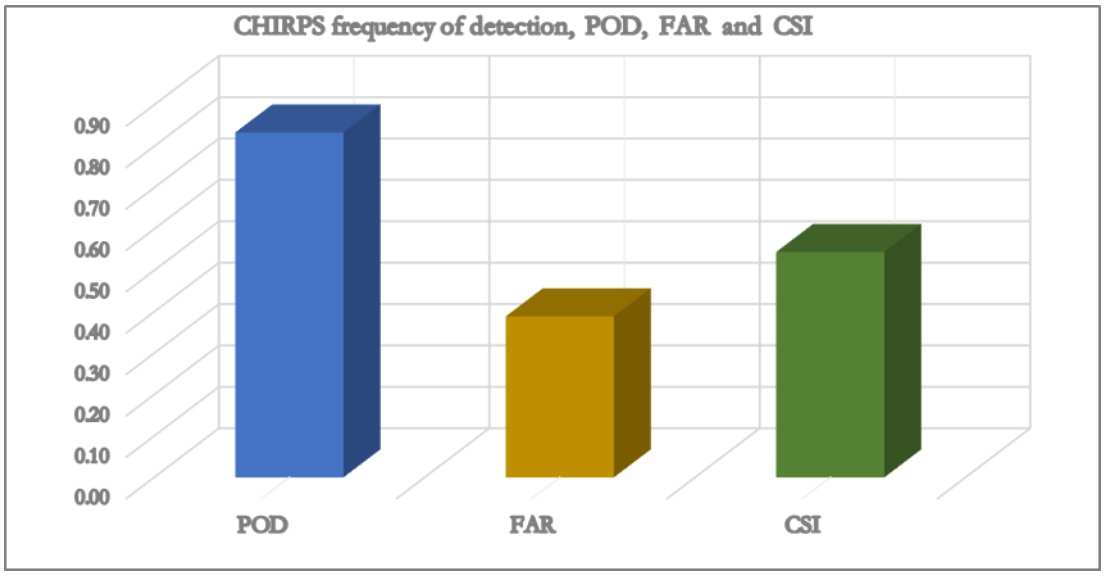

Figure 4-2 Capability of detection indicators for CHIRPS and gauge records at Maun station

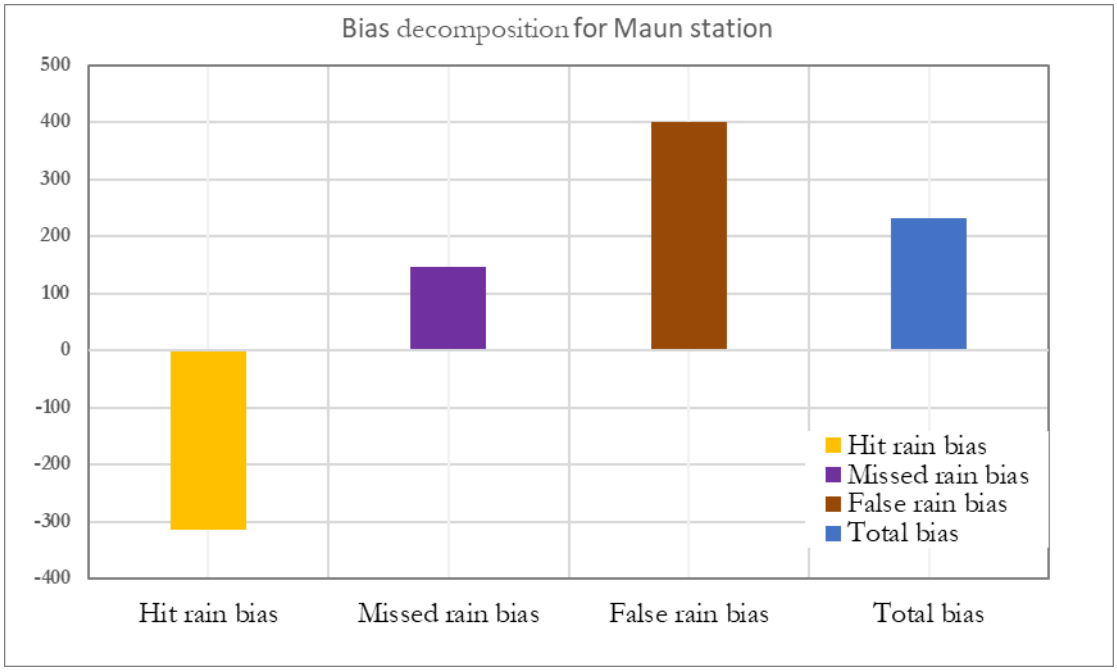

Figure 4-3 Bias decomposition

Figure 4-3 shows the total bias in terms of hits, missed rain and false rain bias. The negative value of hit bias indicates that the underestimation of CHIRPS and also the under estimation of CHIRPS is clearly seen from (Figure 4-1). However, this under estimation reflects when both satellite and gauge record rain fall i.e. only the hit component. Similar results were revealed by Kipyegon, (2018) for the Central Kalahari basin and Toté et al., (2015) in Mozambique.

As shown Figure 4-4 on the cumulative graph due to overall over estimation of CHIRPS there is high bias from 2014 to 2015. However, bias hardly exists from end of 2015 to 2016. This indicates that more rain fall is recorded by gauges than satellite estimates during this period and the bias canceled out. Later, accumulation of error resulted in an increase in bias. The overall over estimation of CHIRPS was found to

be 70.5 mm throughout the whole simulation period. After bias correction the over estimation was reduced to 29.83 which is about 42.3% of the total overestimated amount.

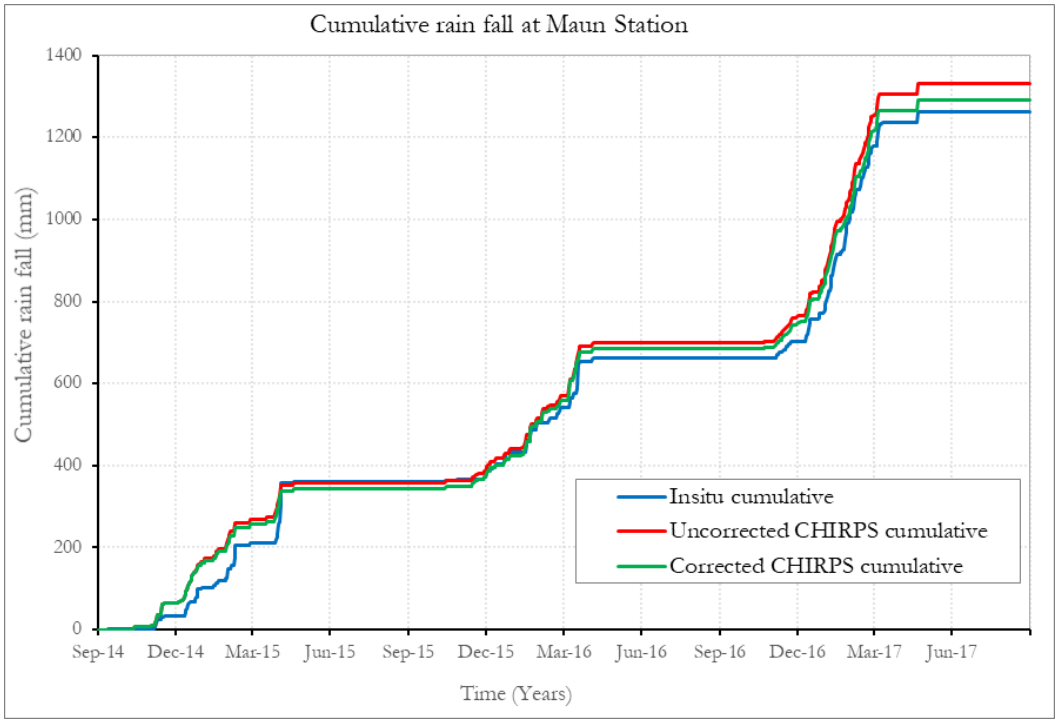

Figure 4-4 Cumulative rainfall at Maun Station (01 September 2014 to 31 August 2017)

In addition, spatial averaging, a 3x3 low pass filter was applied to reduce the overall over estimation. The method distributes (smoothen) the high pixel values to the neighboring pixels and reduces the bias. As shown on (Table 4.3) below, hit and missed rain bias reduced by 4.5% and 4.9% respectively. However, false rain bias shows an increment; this increment is due to the pixels which have no values previously might assigned by new value after applying the method. Frequency of detection after averaging showed an increase in POD and FAR but slight decrease in CSI. This decrease in CSI is due to an increase FAR.

Table 4-2 Frequency of detection indicators before and after averaging

Bias	Bias before averaging	Bias after averaging
Hit rain bias	-314.44	-287.48
Missed rain rias	145.8	132.08
False rain bias	399.61	551.84
Total	230.97	396.45

Table 4-3 Bias decomposition before and after averaging

Indicator	Value before averaging	Range, best value	Value after averaging
POD	0.83	0 to 1, 1	0.88
FAR	0.39	0 to 1, 0	0.45
CSI	0.54	0 to 1, 1	0.51

Although spatial averaging was applied to reduce the bias, it gives large total bias and reduce the value of CSI. Therefore, uncorrected CHIRPS prior to averaging was consider for bias factor estimation.

As multiplicative factor was determined based on one station data (Maun) through (Equation 3), the same correction factor was applied to other stations too. After correction, the correlation between Maun and other stations was checked. Good agreement between stations was found (see Figure 4.5). However, the correlation decreases as the distance between the stations increase. 5 km² resolution CHIRPS was resampled to 1 Km² (grid cell size) and converted to ASCII raster format to meet the model requirement. Finally, spatially uniform temporally variable correction factor was applied to each grid cell (pixel) of precipitation maps and input into the model.

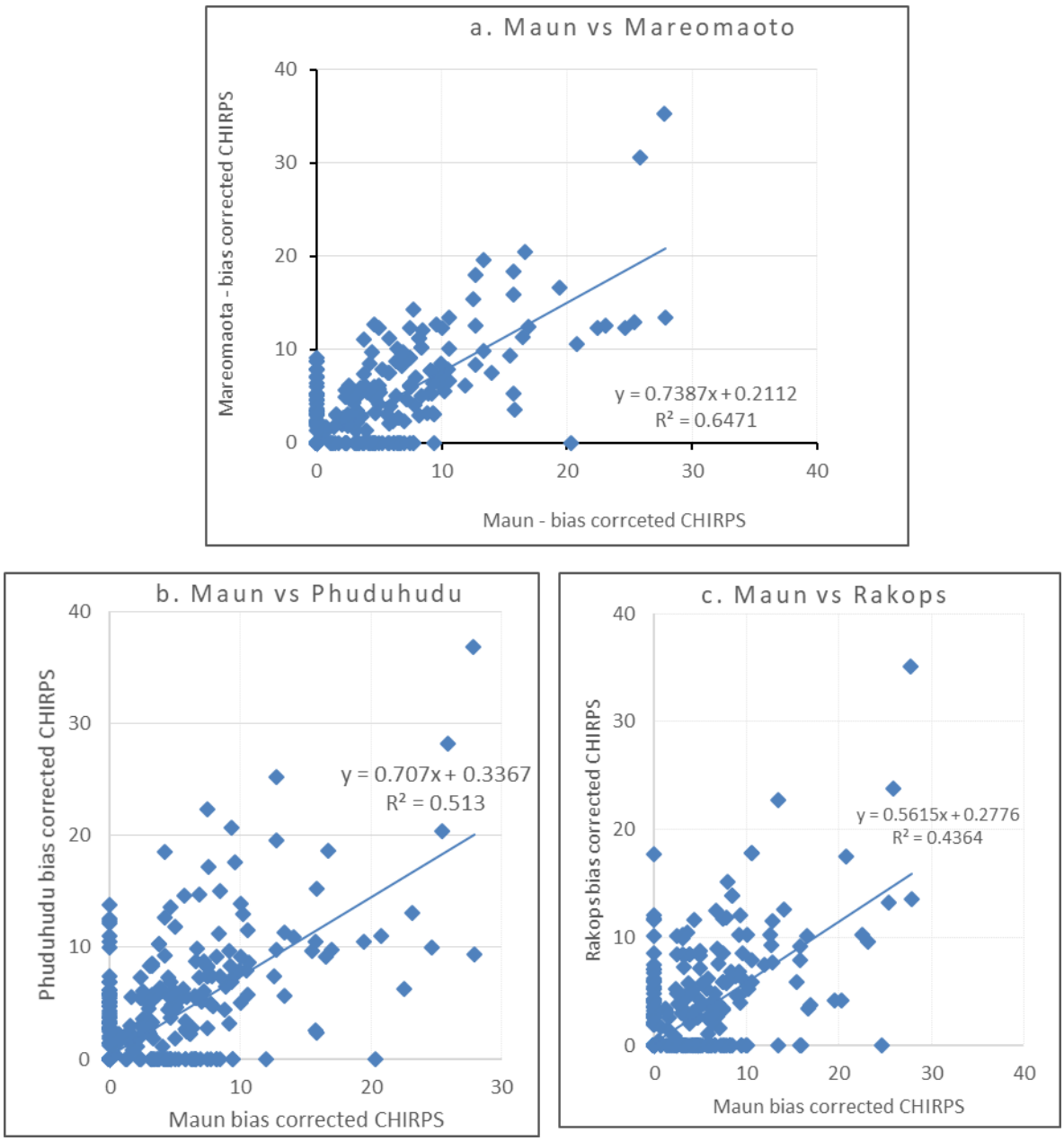

Figure 4-5 Correlation of bias corrected CHIRPS between Maun and nearby stations (A to C); the stations are presented in Figure 2-1.

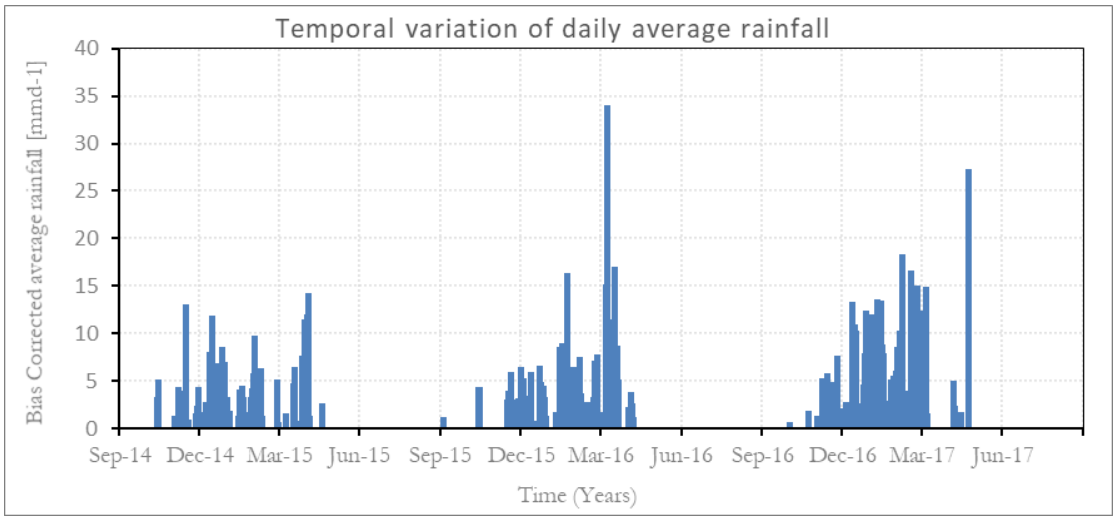

Figure 4-6 Temporal variation of bias corrected daily average rainfall for the whole BRA

As shown in (Figure 4-6) temporal variation of rainfall within BRA from Sep 2014 to August 2017, follows an experienced weather episode of the region and can be seen as three rainy seasons and four dry seasons including the first incomplete dry season. The variation follows the long-term rainfall pattern shown in (Figure 2-2). The spatial distribution of rainfall in BRA is shown in (Figure 4.7) above. As the topography of the area is quite flat (Figure 2.1) and experiences a convective type rainfall (Lekula, et al., 2018), with small daily average rainfall variations, the rainfall distribution seems following the land cover; high in tree cover areas at the northern and North west boundaries and lower on the bare areas of southern and south eastern parts.

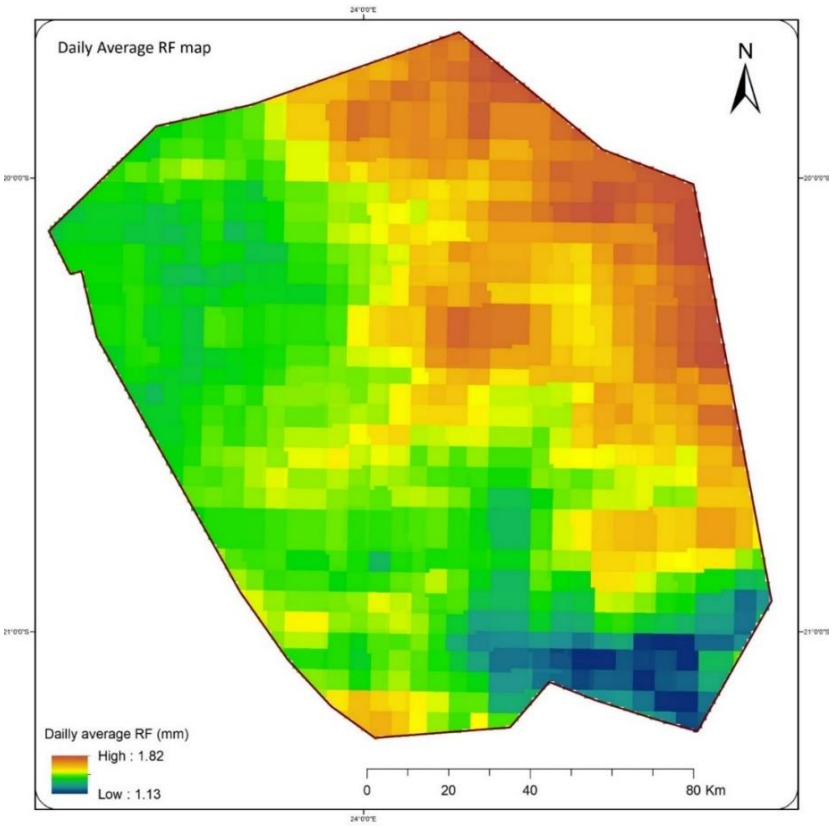

Figure 4-7 Spatial variability of daily average rainfall in BRA from September 2014 to August 2017

However, most of the area is covered by shrubs. On top of that, the distribution is still low at low land areas of the southern depressions.

4.1.2. Interception and Infiltration rates

Spatially variable interception rate map was produced based on the land cover map of the BRA. The interception rate was high for tree cover areas in the northern side and low for bare land in the lowlands of the southern part. About 87% of the area is covered by shrubs which accounts an interception loss of about 4% of the total rainfall.

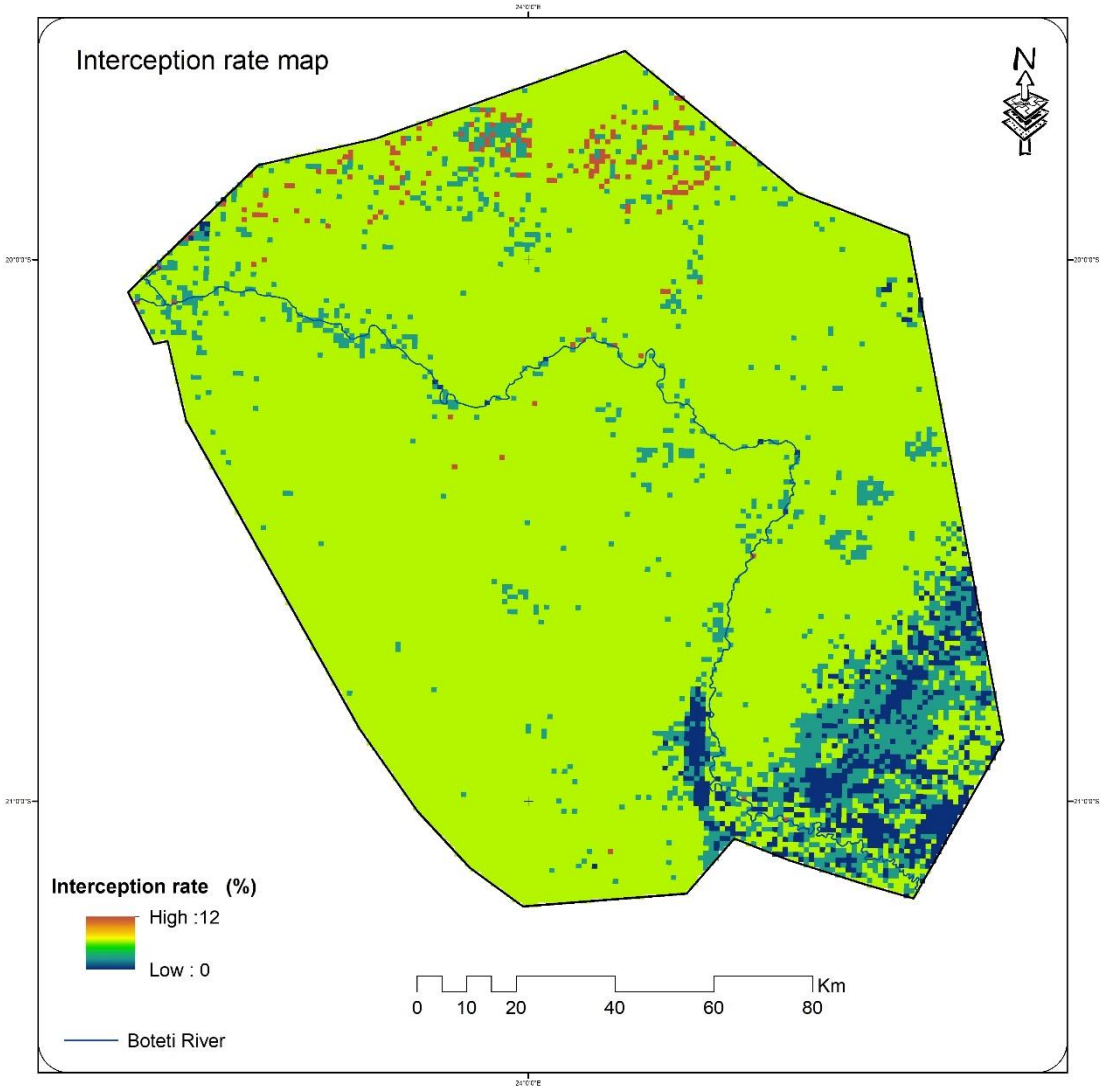

Figure 4-8 Interception rate map of the BRA (0 for Bare land to 12% for Trees); the land cover classes are present in Figure 2-3.

The infiltration rates for the model was calculated by subtracting the amount of interception loss from the total amount of rainfall in a daily basis for each grid cell. Detail description about interception and infiltration rates is found in (section 3.4.6.1).

4.1.3. Potential Evapotranspiration

As stated in section 3.2 above PET was calculated using the FAO Penman Monteith method and its correlation with PET retrieved from US-based GMAO GOES-5 model at 20 km resolution was checked

using statistical and graphical methods. A good agreement (match) was seen and the correlation coefficient was found to be 0.68.

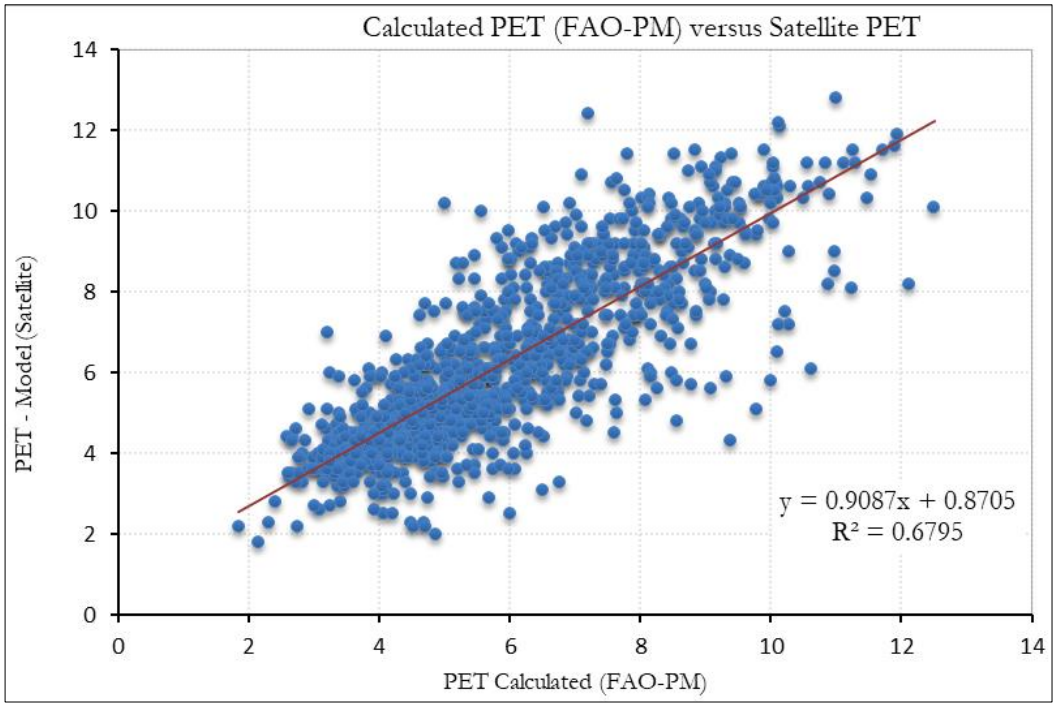

Figure 4-9 Scatter plot for calculated PET (FAO-PM) versus PET from satellite [mmd-1] for Maun station

Temporal variation of PET

The temporal variability and fluctuation of PET (Figure 4.10) above follows the seasonal variations that has been experienced with in the study area; hot-humid seasons (October to March), and dry-cold season (April to September). Air temperature, relative humidity and net radiation which affects PET, are high in hot-humid seasons and resulted in high PET estimation. As indicated by the overall pattern of PET throughout the simulation period, there is uncertainty on some days from November 2014 to January 2015 and December 2016 to March 2017 between PET estimated by the satellite and the calculated PET. As the season is humid and rainy, these uncertainties are attributed to noise (attenuation) due to clouds that might hinder the satellites during estimating the climatic variables. Similar results were revealed by Kipyegon, (2018). However, he studied for FEWSNET PET of 1° spatial resolution at the Central Kalahari basin. The small variations that have been seen from PET satellite estimate and PET calculated was assumed as insignificant.

Spatial variation of PET

Figure 4-11 shows the spatial variation of daily average potential evapotranspiration within BRA. It can be seen that the spatial variation of PET is low. In contrast to spatial the temporal variability of PET is distinct both daily and seasonally (Figure 4-10). PET retrieved from satellite at 20 km was resampled to 1 km² cell size via nearest neighbor method and converted to ASCII raster format which finally used as model input.

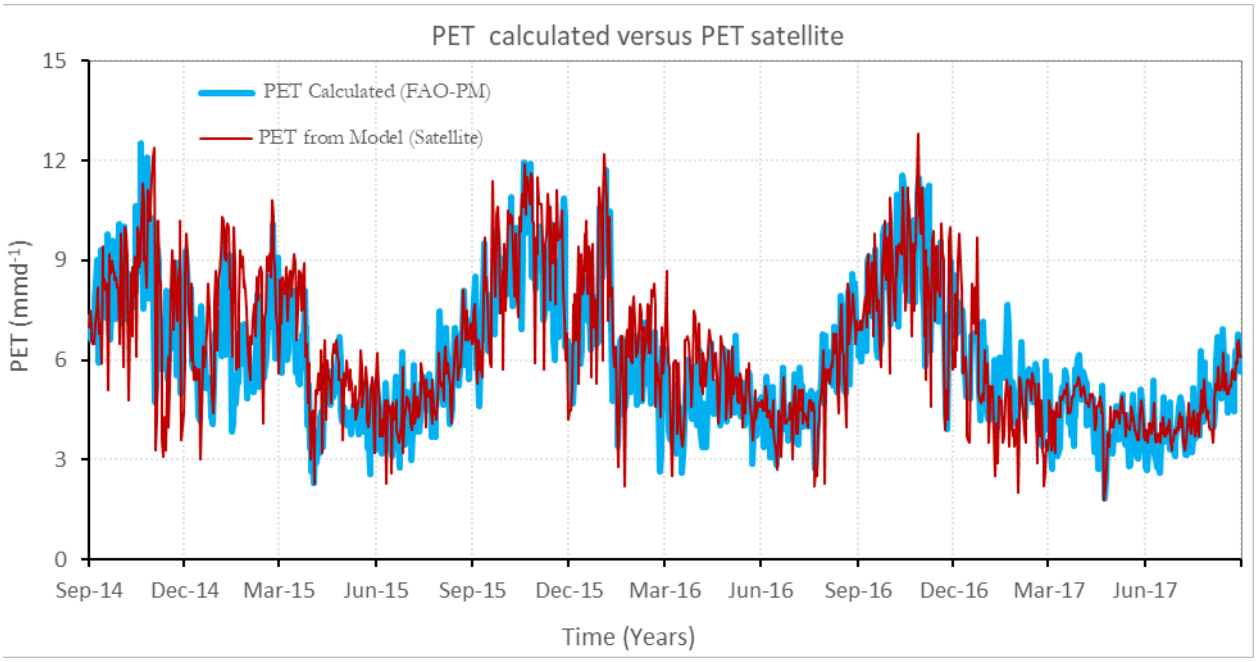

Figure 4-10 Temporal variation of PET calculated (FAO-PM) and PET (Satellite) in BRA

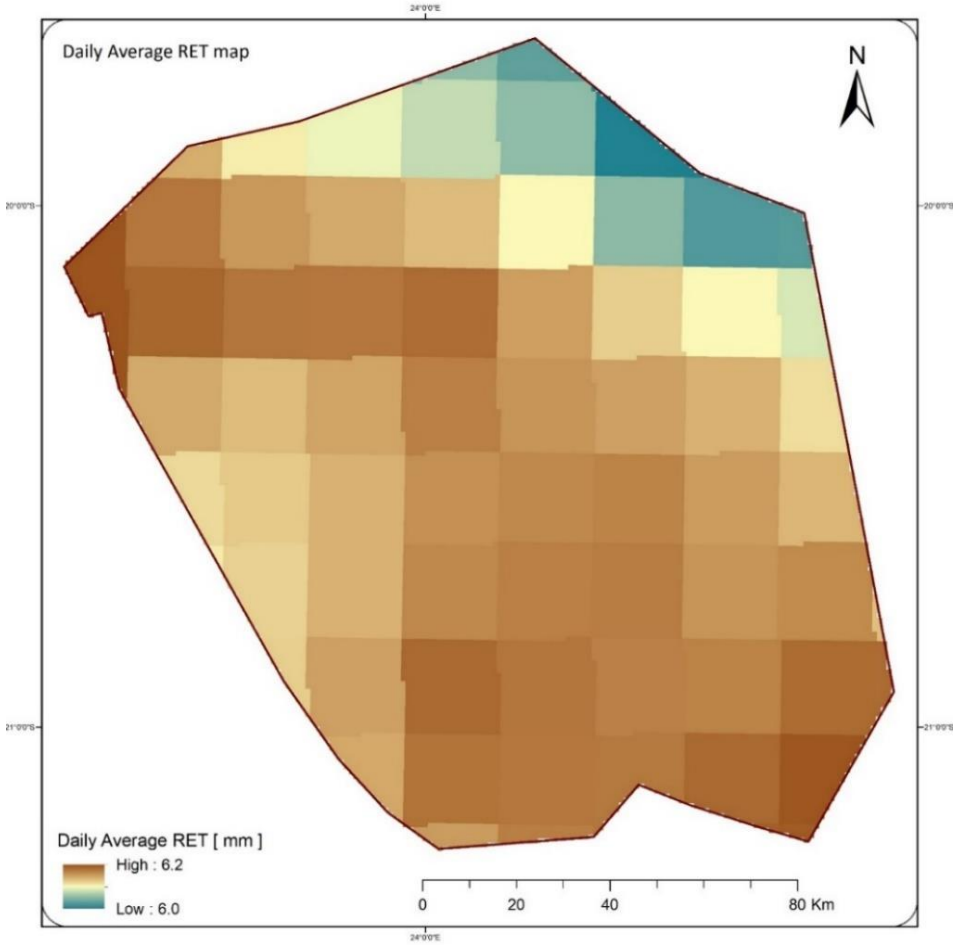

Figure 4-11 Spatial variation of daily average PET in BRA (01 September 2014 to 31 August 2017)

4.1.4. Evapotranspiration Extinction depth

Based on the land cover classes of the BRA, ET extinction depth was briefly described in (section 3.4.6.1). As shown in (Figure 4.12) the spatial variation of ET extinction depth varies from 0.1 to 25 m below the surface for sandy soil and Kalahari trees respectively. However, most of the area is covered by shrubs which have a rooting depth of 4 m which means, in most of the grid cells evapotranspiration occurs up to a depth of 4 m below ground surface.

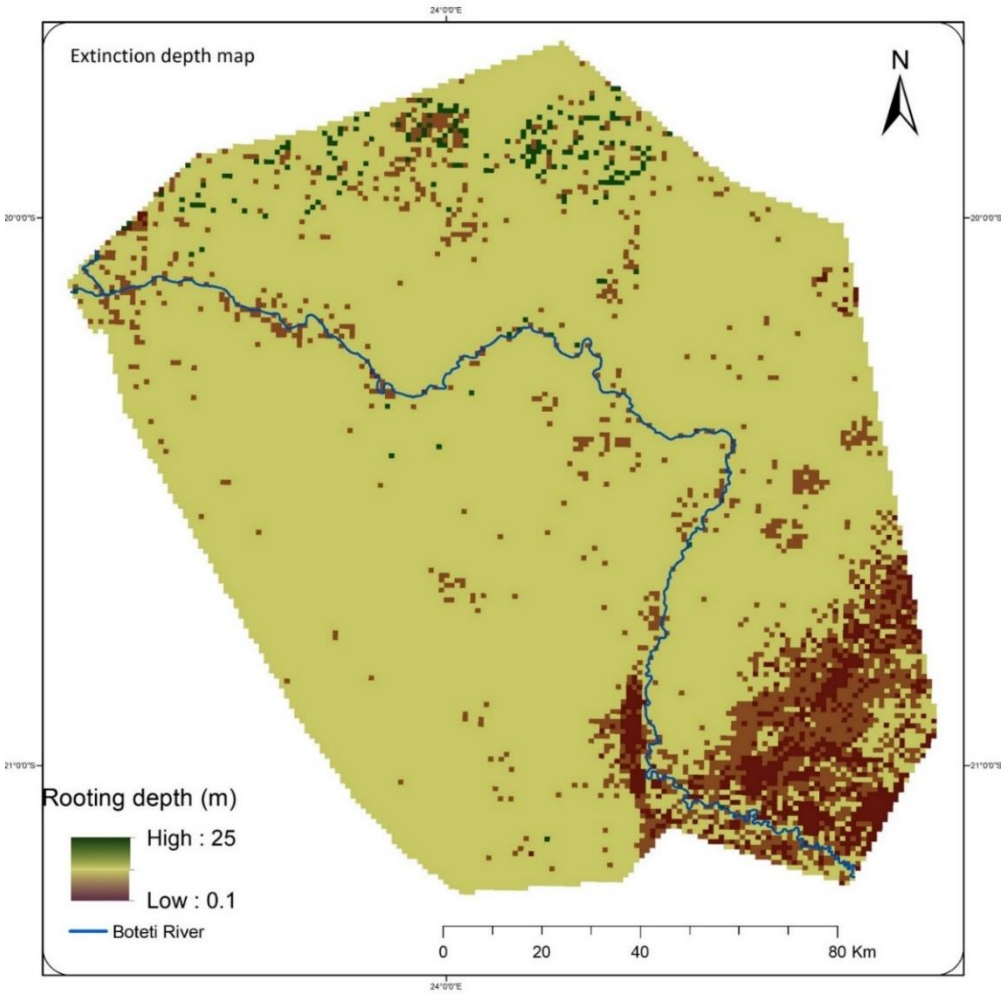

Figure 4-12 Extinction depth map of the BRA

4.1.5. River discharge – Rainfall relationship in BRA.

Figure 4.13 shows the transient variation of river flows at Samedupe and Rakops river gauge stations against the transient daily average rainfall in BRA. Oval shaped objects on the graph shows that the river flows are not much influenced by rainfall variation within the area. This is because the main source of water for the flows of Boteti River is from Okavango Delta through Thamalakane River (Milzow, et al., 2010; CN, BP, & JC, 2018; Shinn, 2018). The seasonal variability of the Boteti River flow is in line with the water levels at the outlet of Okavango Delta, Thamalakane River in Maun (see section 2.8 and Figure 2.5 b).

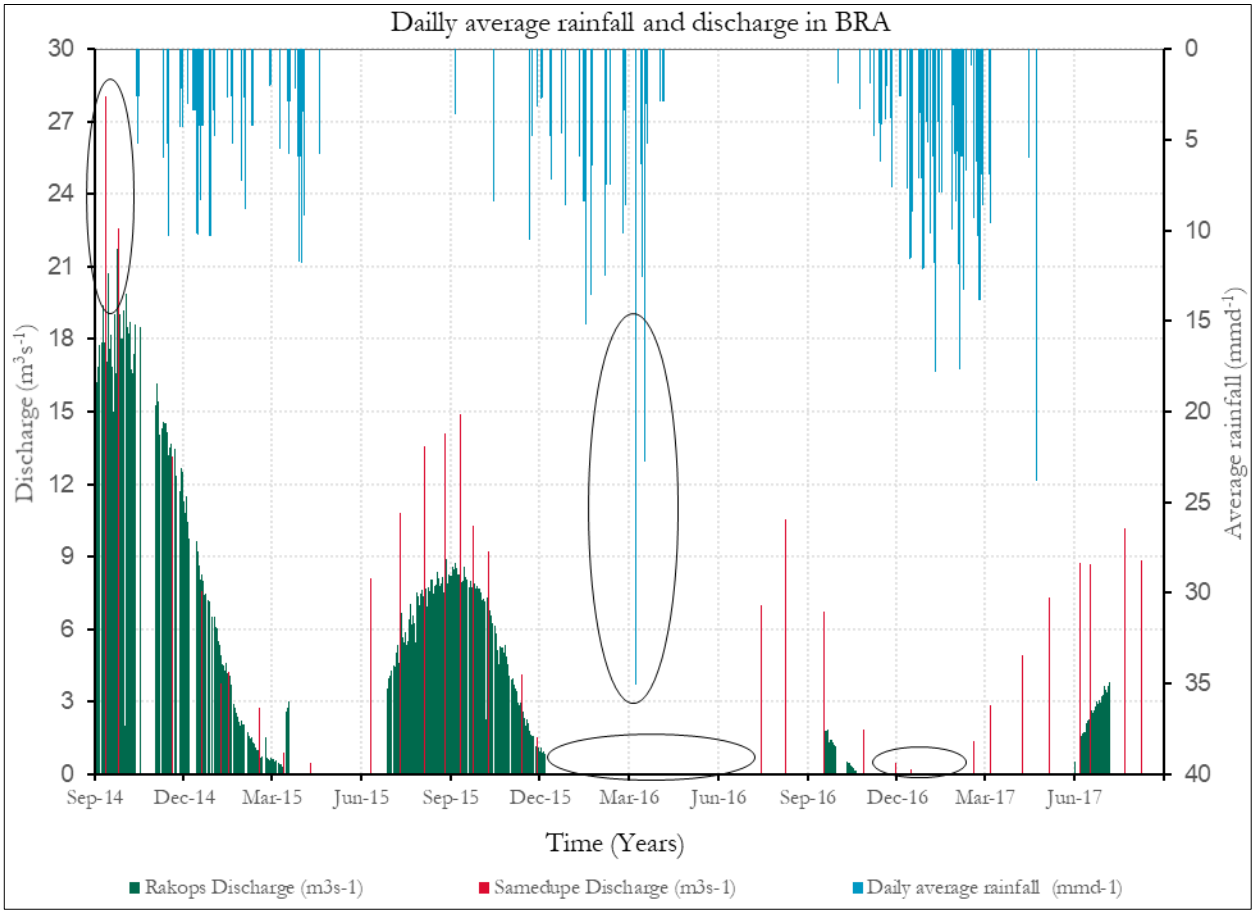

Figure 4-13 Daily average rainfall versus river flows in BRA

4.1.6. Kalahari Sand thickness

The (Figure 4.14) shows variation of the Kalahari Group sediments thickness which has continuous coverage throughout the modelled domain. The thickness varies from 3 m upper Kalahari Sand Formations in the east to more than 100 m for lower Kalahari Formations in the west. The study focused on a one-layer unconfined aquifer with both saturated and unsaturated parts. Similar layer thickness schematization was stated by (McFarlane & Eckardt, 2006) (see section 2.5).

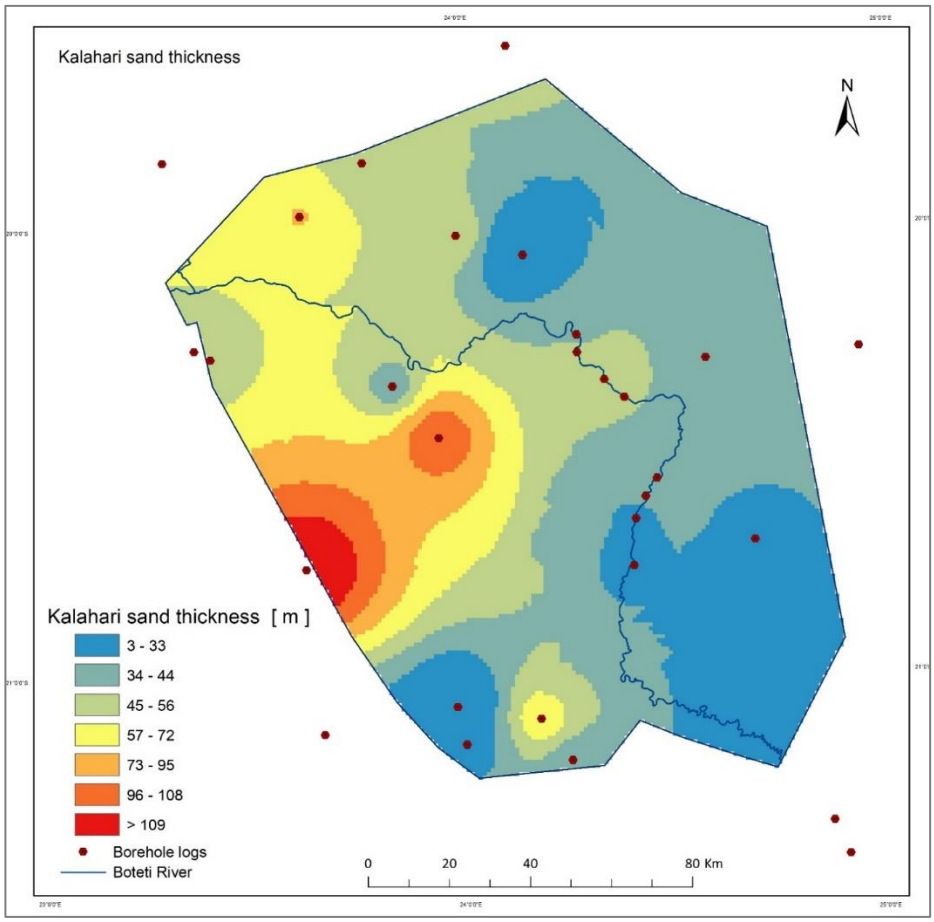

Figure 4-14 Kalahari Sand thickness map

4.1.7. Numerical model boundaries

The potentiometric surface derived from the available regional borehole data shows that the direction of groundwater flow into the model domain is from west and south west directions which is also the outflow boundary of (Lekula, et al., 2018) and converges to the south easterly direction few kilometers far from the modelled area, in the Makgadikgadi Pans. In addition, the flow follows the topography (Figure 2.1), which is directed from higher elevated regions of west and north west of the region to lower depressions in the south eastern part.

The boundaries of the system were assigned as indicated by colour boundary lines shown in (Figure 4.15); Constant head boundary to the north-west direction as purple polyline object where the Boteti River gets into the area and the modelled domain is also bounded by Thamalakane River at that side; no flow boundary in the north as black polyline object; head dependent boundary (GHB) to the south as blue dashed lines where in and out flow of groundwater flow is pronounced; drain boundary in the south east as red dashed lines where the lateral groundwater flow gets out of the modelled domains; specified flow boundary to the west as blue polyline where the lateral groundwater flows is into the model domain and stream-flow routing (SFR) for the river. The lateral inflow and out flow of groundwater from the system was indicated by headed arrow lines. Parametric values for all boundaries were assigned accordingly with brief description as stated in (Section 3.4.6).

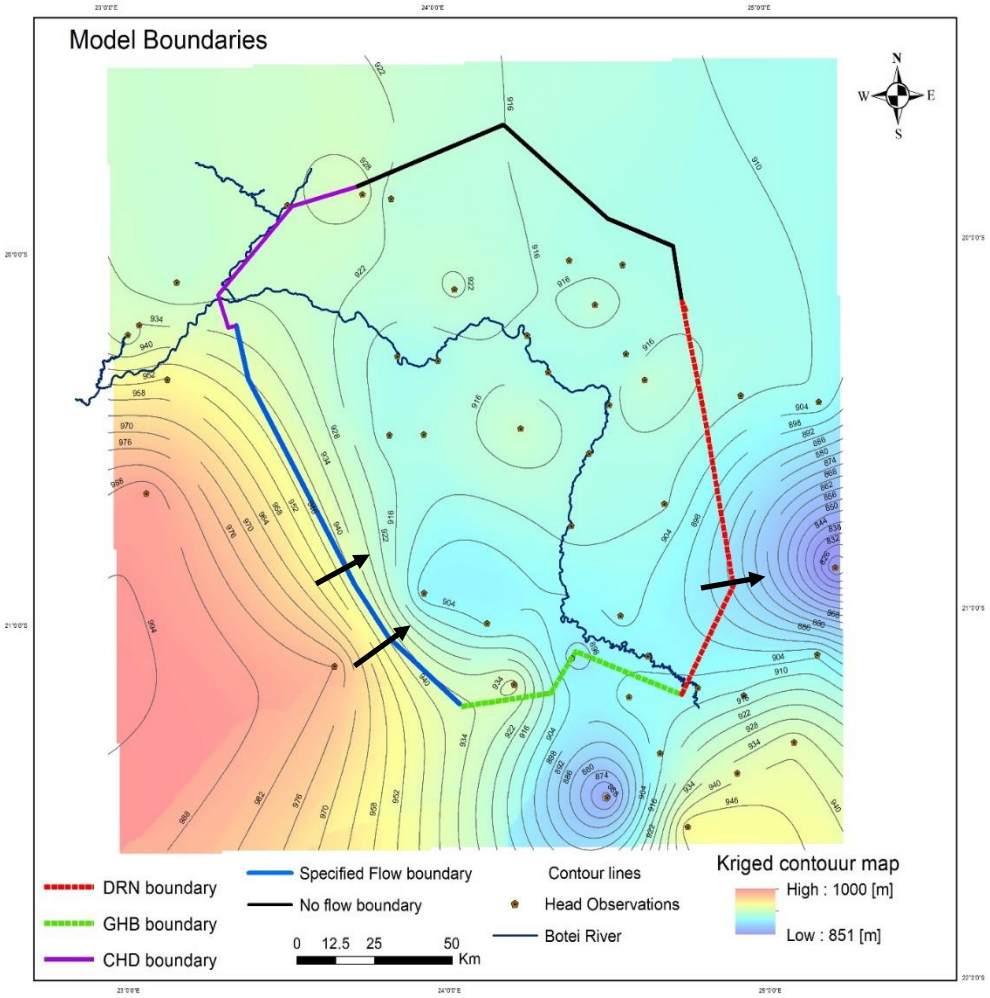

Figure 4-15 Numerical model boundaries with potentiometric surface map

Determination of specified flow

The specified flow into the model domain was determined from Darcy's law (Equation 22/23).

$$Q = KA\frac{\Delta h}{L} \qquad (22)$$

where, Q is total flow into the model domain [L^3T^{-1}], K is hydraulic conductivity of the aquifer material [LT^{-1}], $\frac{\Delta h}{L}$ is hydraulic gradient, change in hydraulic head per length [LL^{-1}], A is cross sectional area [L^2] and L is the length between two piezometers of h1 and h2 [L].

Flow for a single cell can also be determined by considering a single grid cell area as width of grid multiplied by thickness of the aquifer as follows:

$$Qi = K * (wi * \frac{(h2 + h1)}{2} * \frac{\Delta h}{L} \qquad (23)$$

where, Q_i is flow through a single grid cell which has width w_i equal to cell size width and $\frac{(h2+h1)}{2}$ is saturated thickness of the aquifer. The total inflow is flow through a single cell multiplied by the number of cells that the specified flow is assigned.

The gradient was determined from potentiometric surface considering two piezometers of 10 km apart with water levels of 970 m and 946 m a.s.l and found to be $2.4x10^{-3}$. Hydraulic conductivity of the geologic material along the FHB boundary was specified as 12.5 md^{-1}. As stated above in (Section 4.1.6) the non-uniform Kalahari Sand thickness was found larger than 100 m. However, the thickness of a single layer unconfined aquifer was set to 70 m fixed thickness b.g.s. Based on available data an average water level depth of 16 m b.g.s was assumed. So that the saturated thickness of the aquifer is found to be 54 m. The flow per single model cell per area was calculated using (Equation 23) as follows:

$$Qi = (12.5\frac{\mathrm{m}}{\mathrm{d}} * 1000\ m * 54\ m * 0.0024)$$

$$qi = \frac{Qi}{Ai} \quad = \quad 0.0016\ \mathrm{md}^{-1}\ per\ cell.$$

where, q_i is flux across a single grid cell and A_i is area of single grid cell.

A specified flow (FHB) boundary was specified on a total of 181 cells and allowed total flux of 0.3 md^{-1} which finally was used as input for the model through flow and head boundary (FHB) package.

4.2. Transient state model

4.2.1. Transient state model calibration

Transient state model calibration was carried out through manual trial and error method aiming at reducing the differences between the simulated and observed stream flows and hydraulic heads. However, the simulation didn't consider transient vatriation of hydraulic heads; instead, as stated in (section 3.4.7). The simulated time series of hydraulic heads were tuned to match one time measured hydraulic heads and also were controlled not to rise above the surface.

Calibration was challenging: 1) due to the limitted amount of data the groundwater level (heads) were calibrated considering the latest data; and large data gaps of stream flows were created problems on the output i.e. unmatch between the calibtrated and true hydrographs. Thus, if future studies in the Boteti River area consider on time measured daily variation of hydraulic heads, stream flows and abstraction rates data, this study results should be used with caution; 2) as the dialy and spatially variable model setup with many different varuables and diverse boundary conditions, the calibration was very complex and time consuming taking about one hour for each complete model run.

As the MODFLOW ModelMuse UZF package used the dailly input variables, the simulation period of 01 September 2014 to 31 August 2017 was discretized into 1096 stress periods and a time step.

4.2.2. Calibrated Parameters

The integrated hydrological model of river-groundwater interactions of the BRA with one-layer, convertible type unconfined aquifer was calibrated considering UZF and SFR2 package parameters in transient state conditions. The values of all calibrated parameters are outlined in (Table 3.3).

The spatially variable horizontal hydraulic conductivity of the aquifer was assigned in zones ranging in value from 0.09 to 37 md-1. The final hydraulic conductivity distribution of the modelled aquifer is presented in (Figure 4.16). The highest hydraulic conductivity zones as high as 37 md-1 were found in Boteti alluvial sediments pretty near the river course and to the south eastern side of the modelled domain where thinner lacustrine sediments are found compared with the western side (McFarlane & Eckardt, 2006 & see Figure 4.14). Tthe lower hydraulic conductivity zones were observed in the western side of the modelled area. Spatially uniform calibrated specific yield of the modelled aquifer was found to be 0.24.

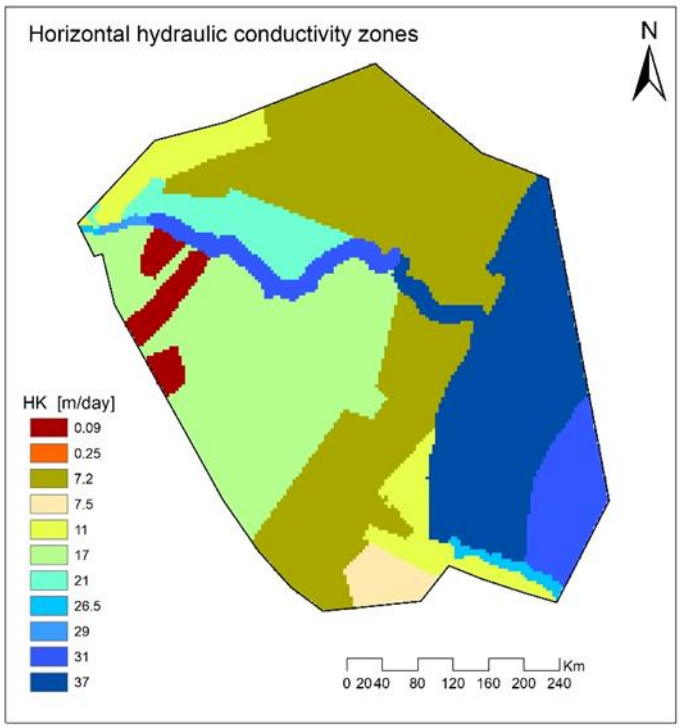

Figure 4-16 Horizontal hydraulic conductivity distribution within the BRA.

4.2.3. Head calibration results

As stated earlier, the study didn't consider the daily variations of groundwater levels; the simulation was carried out with respect to heads measured in September 2018. The coordinates, observed heads, simulated heads and error assessment for the observation points is presented in (Table 4.4). The error assessment was based on ME, MAE and RMSE calculated from the equations (12), (13), and (14) respectively. The assessment results were 0.29, 1.31, and 1.56 for ME, MAE and RMSE respectively. However, BH8117 showed clear overestimation on the respective observed heads; which might be resulted from the rise of water table due to continues channel seepage via CHD boundary at that side and couldn't be reduced using the realistic parametric values. For example, increasing the hydraulic conductivity around that zone resulted in overestimation of inflow through CHD boundary.

All the simulated heads presented in Figure 4.17 showed response to rainfall; especially an abrupt rise in groundwater level is pronounced at boreholes BH9849 and Phuduhudu BH in 2017 due to high cumulative rainfall from November to March and additional unusual high rainfall intensity in May during that year which in turn resulted in high recharge rate. As postulated by Hu et al., (2016) such event can be better represented by grid refinement (densifying model grids). However, the response of heads for rainfall is delayed which is likely due the thick unsaturated zone of the Kalahari Sand Unit layer of the Botswana Kalahari (Lekula, et al., 2018).

In general, the uncertainties between the observed and simulated heads arose likely due to: 1) the error in setting conceptualization and parametrization of the model; 2) the difference in the simulation period and measured time of observed heads; 3) due to geologic heterogeneity (not represented in the present study) and sub-grid scale altitude variability i.e. mismatch between observed and simulated heads at the observation point during start of simulation (Hassan et al., 2014); which is seen from the three of the boreholes in figure 4.17. 4) unaccounted groundwater abstraction rates. 5) uncertainties and errors in driving forces.

Through the calibration process the water table depth was compared to the surface elevation, SRTM 30 m DEM of the modelled domain to control the water table to be below the surface elevation. As a result, all

true and fictitious piezometers (presented in Figure 2.1 and Figure 3.5) water levels were found below surface elevation.

Table 4-4 Frequency of detection indicators before and after averaging

Table 5 Location of observed heads, and error assessment.

Borehole name	Easting	Northing	H_{obs}	H_{sim}	H_{obs}-H_{sim}	ABS(H_{obs}-H_{sim})	(Hobs-Hsim)^2
BH8117	120022.016	7770705.1	926.77	929.32	-2.55	2.55	6.50
Phuduhudu BH	230837.342	7768887.1	926.86	926.00	0.86	0.86	0.74
BH9849	186478.98	7768887.1	925.74	924.72	1.02	1.02	1.04
BH8837	241043.3	7734909.7	919.20	919.05	0.15	0.15	0.02
BH9544	254058.18	7662781.2	910.08	908.11	1.97	1.97	3.88
Sum					1.45	6.55	12.18
STD					1.72	0.95	2.70
Min					-2.55	0.15	0.02
Max					1.97	2.55	6.5
Mean					0.29	1.31	2.44
					ME	MAE	RMSE
					0.29	1.31	1.56

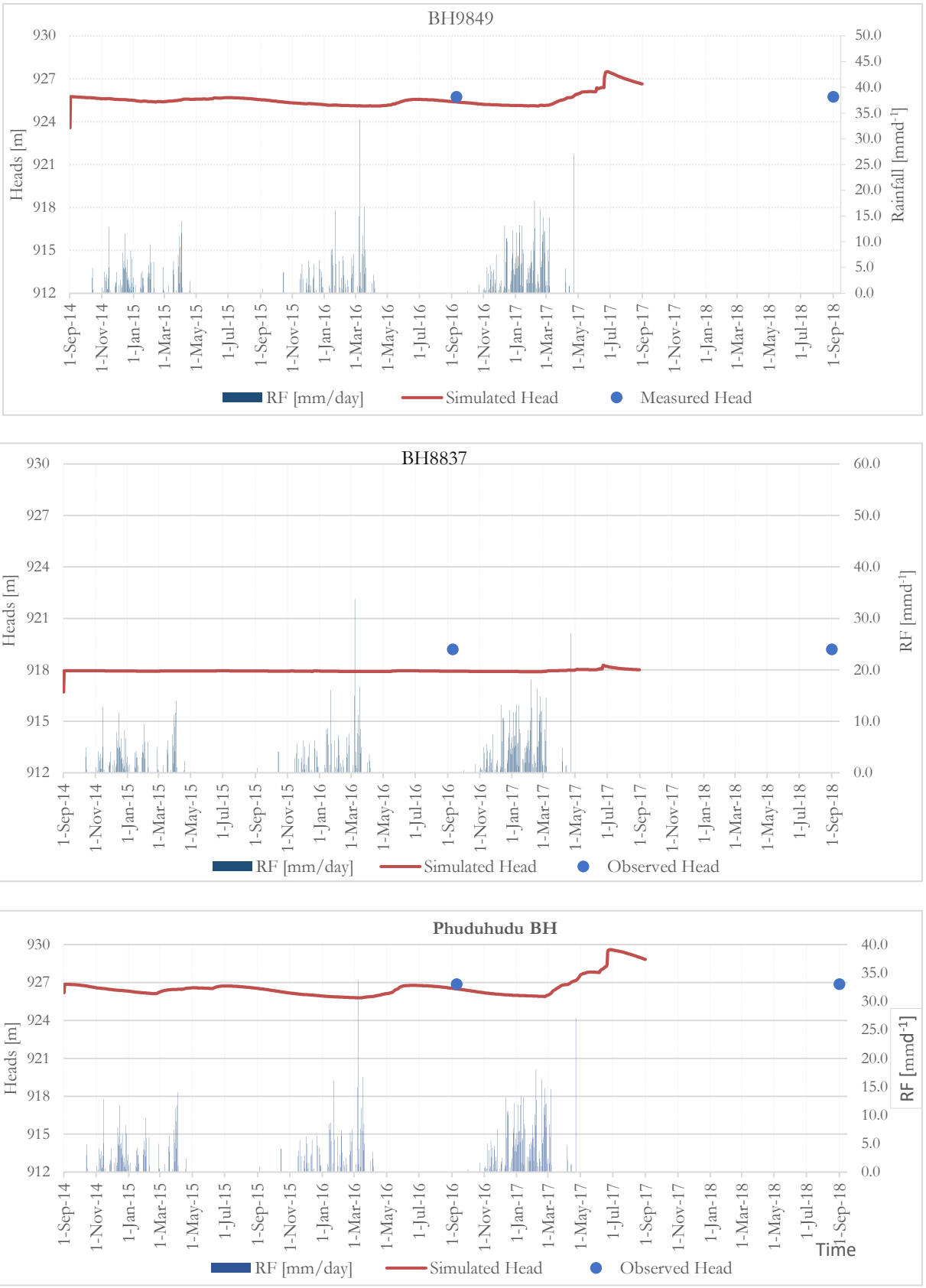

Figure 4-17 Simulated heads for Boreholes BH9849, BH8837 and Phuduhudu BH; heads measured in September 2018.

4.2.4. Calibrated river flows

The calibration was performed targeting to match the hydrographs of the simulated stream discharges with the respective observed stream discharge hydrographs. Due to lack of data for other gauging stations river flows at the two discharge gauging stations, Samedupe and Rakops were calibrated.

The locations and error assessment for both gauging stations is shown in Table 4-5 below. The values of NS and RVE were found to be 0.76 and -30.87 respectively. The model performs reasonably well in terms of NS. The shape of the simulated discharge hydrographs follows the trends of the discharge measured. However, the performance in terms of volumetric error was poor and the simulated hydrograph show mismatch particularly at the beginning of the model simulation. It is remarkable that match between simulated and measured discharges was far better at the end of the simulation period than at the beginning which is an indication that the mismatch between the two hydrographs at the beginning of the simulation period was likely due to the warming up time needed by the model to get on track. Due to time constraints the results are taken as they are. For further studies, more warming up time with sufficient input data should be considered and the parameters should be optimized for better representation of simulated hydrographs with respect to the true (measured) hydrographs.

For Rakops gauging station the values of NS and RVE were found to be 0.52 and -6.78 respectively. The volumetric error, -6.78 which is between ±5% and ±10% is an indicator for reasonable performance of the model. However, the model didn't perform well in terms of NS and hydrograph fit. The hydrograph of this gauging station is presented in Appendix 4.

Table 6 locations and error assessment for Samedupe and Rakops gauging stations; the error assessment is based on the available data and its corresponding simulated values.

Station Name	Latitude (degrees)	Longitude (degrees)	NS	RVE
Samedupe	-20.100	23.517	0.76	-30.87
Rakops	-21.033	24.400	0.52	-6.78

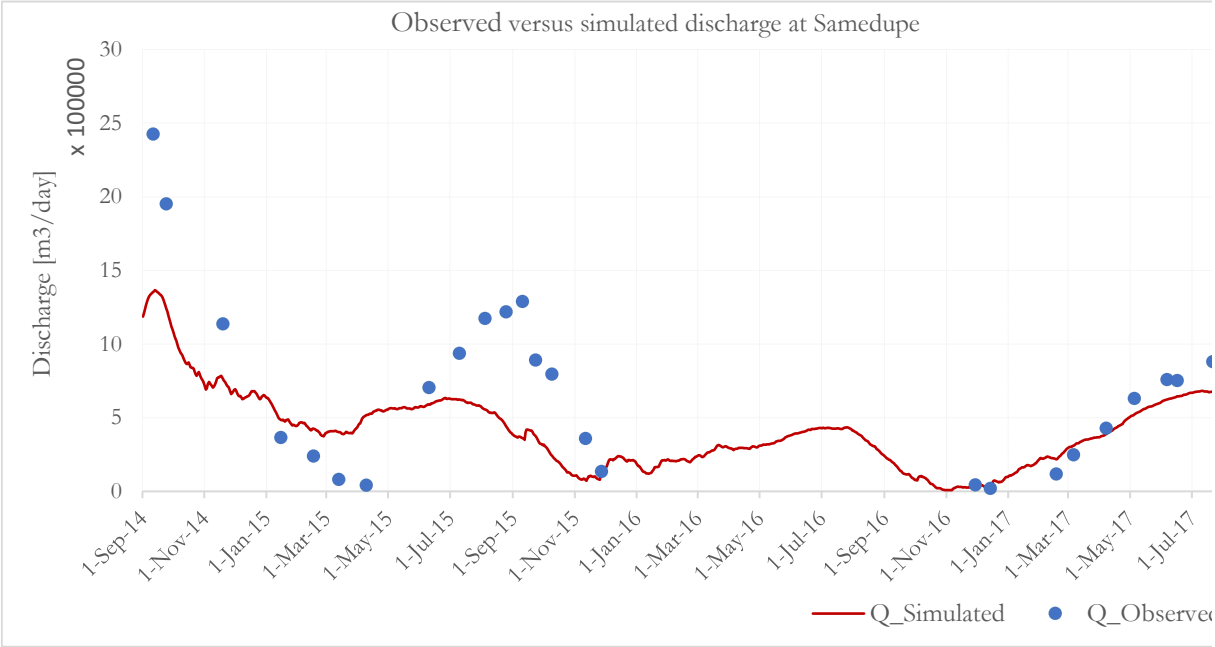

Figure 4-18 Observed versus simulated flows for Samedupe gauging station

4.2.5. Water balance

The annual water balance of three years transient state simulation for river-groundwater interactions is presented in Table 4.5. However, due to the model calibration warm-up time uncertainty, the water balance of the first year was disregarded as unreliable; so the statistics of the water balance was based on considering the last two hydrological years. The water balance of the BRA for (2016-dry and 2017-moderately wet) hydrologic year was discussed in three sections based on equations (14) to (21).

The total yearly inflow at the upstream of the Boteti River, Samedupe gauging station accounts $8.98*10^8$, $9.0*10^8$ and $8.98*10^8$ m^3yr^{-1} for the 1st, 2nd and 3rd hydrological year respectively. The water balance of the whole model domain as equation (14) includes input components: P (81.73% of IN), Q_{in} (16.30% of IN), CHD_{in} 2.88% of IN), FHB (0.1% IN), the inflow through GHB boundary was negligible. On the other hand, the outflow of the whole model domain accounts ET (91.60% of OUT) followed by Q_{out} (3.24% of OUT), Q_{DRN} (1.93% of OUT), and GHB_{out} (0.42% of OUT). Within the e groundwater storage showed radical change, decreased from 108 $mmyr^{-1}$ in the second simulation year (September 2014 to August 2015) to -121 $mmyr^{-1}$ in the third simulation period (September 2016 to August 2017). This is likely due to an increase in ETuz and exfiltration despite an increase in R_g and R_n in that year.

The water balance of the land surface and unsaturated zone as equations (18) and (19) includes input components: effective precipitation (Pe = P – I), which is applied to the land surface of the area; later infiltrates to the soil zone and partitioned into different components by UZF package acounts (96.23% of P), Exfgw (0.62% of P) and output components: R_g (66.32% of P) followed by ET_{uz} (33.79% of P) and (Q_H + Q_D)s (40% of P).

The inflow of water into the saturated zone was dominated by gross recharge which accounts 85% of total groundwater inflow (GWin) followed by leakage from river (Q_{sg}) (10.12% of GW_{in}), the channel seepage across Thamalakane River through CHD boundary (4.78% of GWin), FHB (0.15% of GW_{in})and GHB_{in}

(0.01% of GW_{in}); and five outflow fluxes of the saturated zone system, outflow dominated by ET_{gw} (81.07% of the total GW outflow (GW_{out})), followed by groundwater leakage to streams (14.82% of GW_{out}), DRN (2.68% of GW_{out}), Exf_{gw} 0.85% of GW_{out}) and GHB_{out} (0.58% of GW_{out}).

In a nutshell, gross, leakage from river to groundwater and the lateral seepage across the Thamalakane River through the CHD boundary are the main inputs of the saturated zone system. The main groundwater outputs are groundwater evapotranspiration and aquifer leakage to the river. Overall, the river is gaining water from the aquifer. which is likely attributed to the substantial diffuse recharge from rainfall (Rg) through permeable Kalahari Sands maintaining groundwater levels generally above the river stages. The lateral boundary inflows also contribute to that.

The total yearly inflow at the upstream of the Boteti River, Samedupe gauging station accounts $8.98*10^8$, $9.0*10^8$ and $8.98*10^8$ m^3yr^{-1} for the 1st, 2nd and 3rd hydrological years respectively.

Table 7 Summary of annual water balance [mmyr-1] of the entire transient state model of the BRA (from the beginning of September 2014 to end of August 2017)

Hydrological year	Driving forces (Model inputs)				UZF					Gw in					ΔSg_{in}	GW out					ΔSg_{out}
	P	PET	I	Pe	Pa	Q_H+Q_D	ET_{uz}	Rg	ΔS_{uz}	$CHDi_n$	$GHBi_n$	FHB	Qsg	Rn		Q_{DRN}	GHB_{out}	Qgs	ETg	Exfg	
	[mmyr^{-1}]				[mmyr^{-1}]					[mmyr^{-1}]						[mmyr^{-1}]					
01-Sep 2014 to 31-Aug 2015	305.26	2377.60	11.54	293.72	288.16	8.27	72.32	322.40	-92.62	16.08	0.00	0.53	33.06	-95.89	168.42	10.10	2.15	53.00	415.58	2.70	57.16
01-Sep 2015 to 31-Aug 2016	321.23	2416.20	12.14	309.09	290.65	20.98	84.30	204.26	-178.5	16.26	0.00	0.53	34.17	-99.31	146.77	9.09	1.92	48.72	301.04	2.54	38.84
01-Sep 2016 to 31-Aug 2017	570.43	2139.99	21.56	548.87	216.19	335.65	216.99	360.38	-2.62	15.49	0.001	0.53	33.10	129.96	67.12	8.40	1.78	47.94	227.45	2.97	187.81
Average	398.98	2311.26	15.08	383.89	265.00	121.63	124.54	295.68	-91.24	15.95	0.00	0.53	33.44	-21.75	127.43	9.20	1.95	49.89	314.69	2.74	94.60
Averages of 2nd and 3rd years	445.8	2278.1	16.9	429	253.4	178.32	150.65	282.3	-90.6	15.88	0.0005	0.5	33.64	15.33	106.95	8.75	1.9	48.3	264.25	2.76	113.33
Standard deviation	148.70	149.58	5.62	143.08	42.29	185.46	80.29	81.41	87.94	0.40	0.00	0.00	0.63	131.39	53.34	0.85	0.18	2.73	94.80	0.22	81.24
Maximum	570.43	2416.20	21.56	548.87	290.65	335.65	216.99	360.38	-2.62	16.26	0.00	0.53	34.17	129.96	168.42	10.10	2.15	53.00	415.58	2.97	187.81
Minimum	305.26	2139.99	11.54	293.72	216.19	8.27	72.32	204.26	-178.5	15.49	0.00	0.53	33.06	-99.31	67.12	8.40	1.78	47.94	227.45	2.54	38.84

The water balance components of the transient solution: precipitation (P), potential evapotranspiration (PET), Interception (I), effective rainfall (Pe), actual infiltration rate through the unsaturated zone (Pa), runoff which is an output from model as UZF water balance components and accounts both Huttonian and Dunnian runoff, unsaturated zone evapotranspiration (ETuz), gross recharge (Rg), unsaturated zone storage change (ΔSuz), inflow through specified head boundary (CHD_{in}), inflow through the specified flow boundary (FHB), inflow and out flow through general head boundary (GHB_{in} & GHB_{out}), inflow into and from the river (Qgs & Qsg), change in groundwater storage (ΔS_{in}) and out (ΔS_{out}), which resulted for total change in storage as (ΔS_{in} - ΔS_{ou}), groundwater evapotranspiration (ETgw) and groundwater exfiltration (Exfgw). All based on equations (14) to (21).

4.2.6. Temporal variability of recharge and groundwater evapotranspiration

Figure 4.18 shows the temporal variability of the simulated gross recharge and groundwater evapotranspiration by the UZF package and net recharge calculated (following Equation 21). As shown below gross recharge, groundwater evapotranspiration and net recharge all follow the dry (May to September) and wet (October to March) seasons experienced in the Boteti River area. The trend shows an increase in gross recharge and groundwater evapotranspiration in most of wet seasons. However, the net recharge pattern depends on the state of the two fluxes, gross recharge and groundwater evapotranspiration. An increase in gross recharge is resulted from high infiltration rated due to rainfall increment. In addition, room for availability of water from rainfall and the applied daily average high PET (see Figure 4.11) triggers groundwater evapotranspiration to increase. As a result, a decrease in net recharge is observed. During time of high groundwater evapotranspiration, as high as 2.28 mmd^{-1} in October 2014, the net recharge follows the pattern of groundwater evapotranspiration. while during low groundwater evapotranspiration seasons as low as 0.2 mmd^{-1} and high gross recharge as high as 2.28mmd^{-1} for example, in June 2017, the net recharge showed an increase in value as high as 1.66 $mmd^{-1}$and proportionally follows the pattern of gross recharge. Similar fluxes variations were observed by (Kipyegon, 2018) in the Central Kalahari Basin. The two years average net recharge is found to be positive despite negative groundwater change in storage for that years (see section 4.2.5)

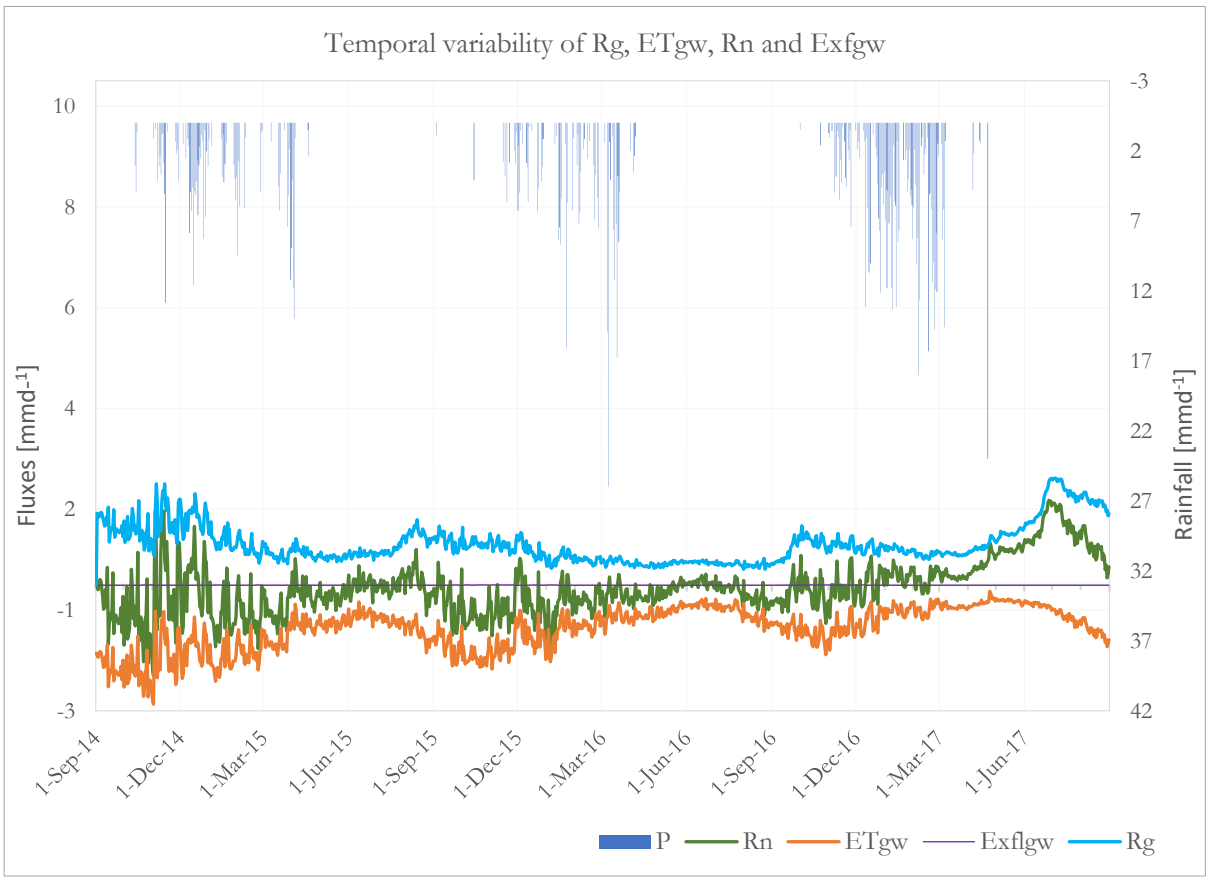

Figure 4-19 Temporal variability of simulated groundwater fluxes of the transient state model

4.2.7. Spatial and temporal effect of the river on groundwater level

To test the spatio-temporal impact of the Boteti River on the groundwater levels fictitious piezometers were set at the upstream and downstream of the Boteti River, in perpendicular direction from Samedupe and Rakops gauging stations (Figure 4-18 A&B). At both locations there is an interaction between the river and groundwater and in both cases hydraulic gradient is oriented towards the river channel indicating prevailing groundwater flow from the aquifer to the river. A noticeable difference is seen in groundwater fluctuation at the upstream and downstream gauging stations. For instance, the fluctuation of the groundwater level from the upstream gauging station (Samedupe) is highly pronounced near the river course during river flow seasons (July to September) but gradually decline in the fluctuation away from the river course and in seasons of low flows (December to May).

The groundwater level at the downstream section (Rakops gauging station) is not much varying compared with the upstream section. This is likely due to 1) the groundwater coming from western and north western lateral boundaries which might add more groundwater to that area discharged to the Makgadikgadi Pans through this point; 2) the groundwater level at this location is shallower than at the upstream section which might be resulted by more ground leakage to the river than gaining. Similar groundwater level fluctuation at areas with shallow water table was examined by (El-Zehairy et al., 2018) from their study of lake-groundwater interactions. . The seasonal river flow variability is presented in Figure 4.13.

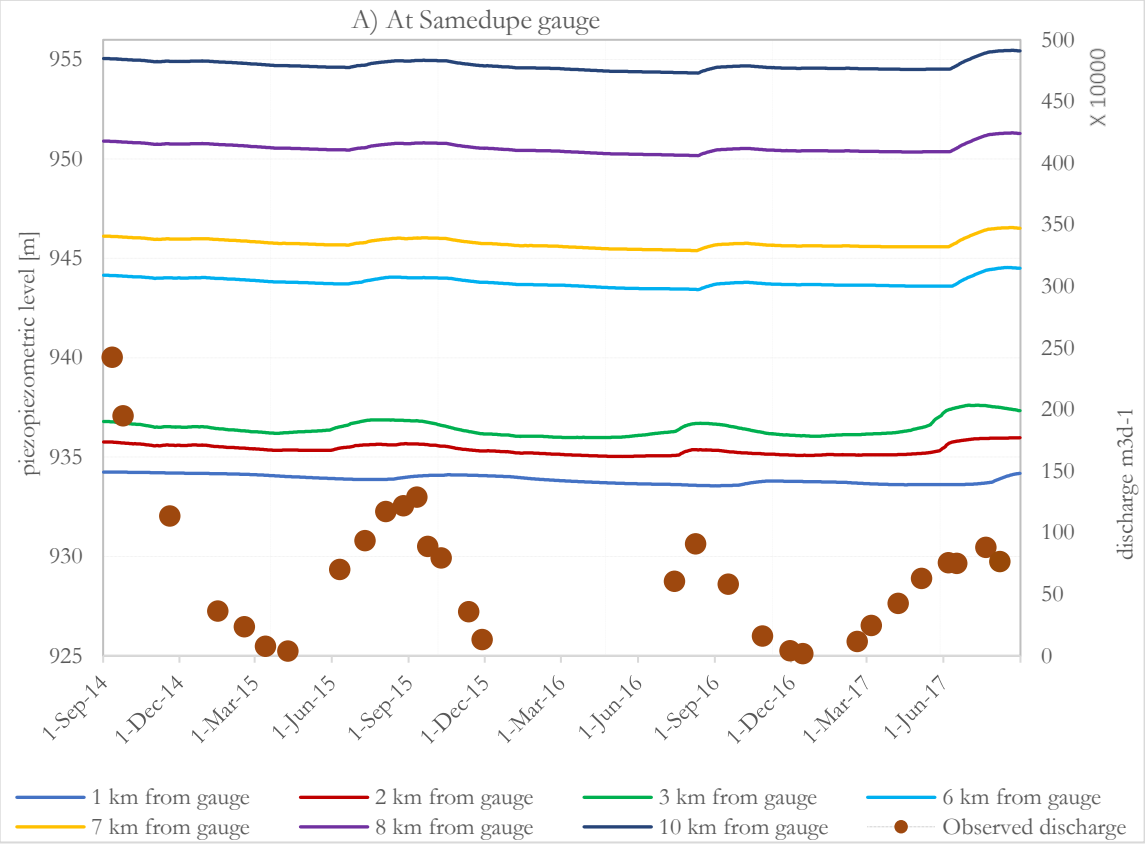

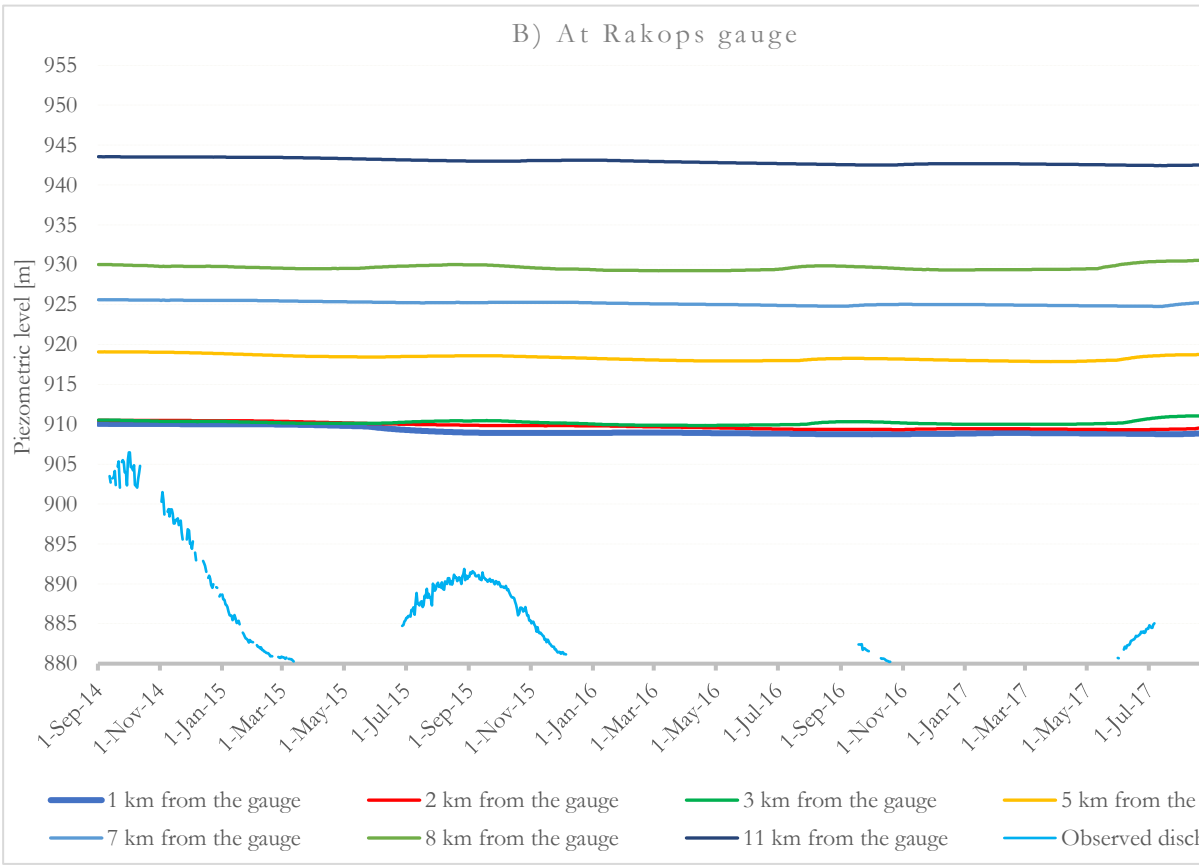

Figure 4-20 Spatial and temporal impact of the river on the groundwater level from A) Samedupe and B) Rakops gauging stations; (the location of the gauging stations is presented on Figure 3-5).

4.2.8. River-aquifer interaction

River-groundwater interactions were analysed based on model results of water leakage into and out of the groundwater system. There was an interaction (exchange of water) between the two systems throughout the simulation period. The total loss of water from the Boteti River to Kalahari Aquifer system throughout the two hydrological years 2016 and 2017 was 67 mm and the direct or indirect groundwater discharge to Boteti River was 99 mm. As a result, the river was gaining water from the aquifer throughout the simulation period with net water gain of 32 mm. Similar river-aquifer interaction was examined by (Li et al., 2016). However, that interaction between river and aquifer of that study was changed to losing river after increment in the groundwater pumpage.

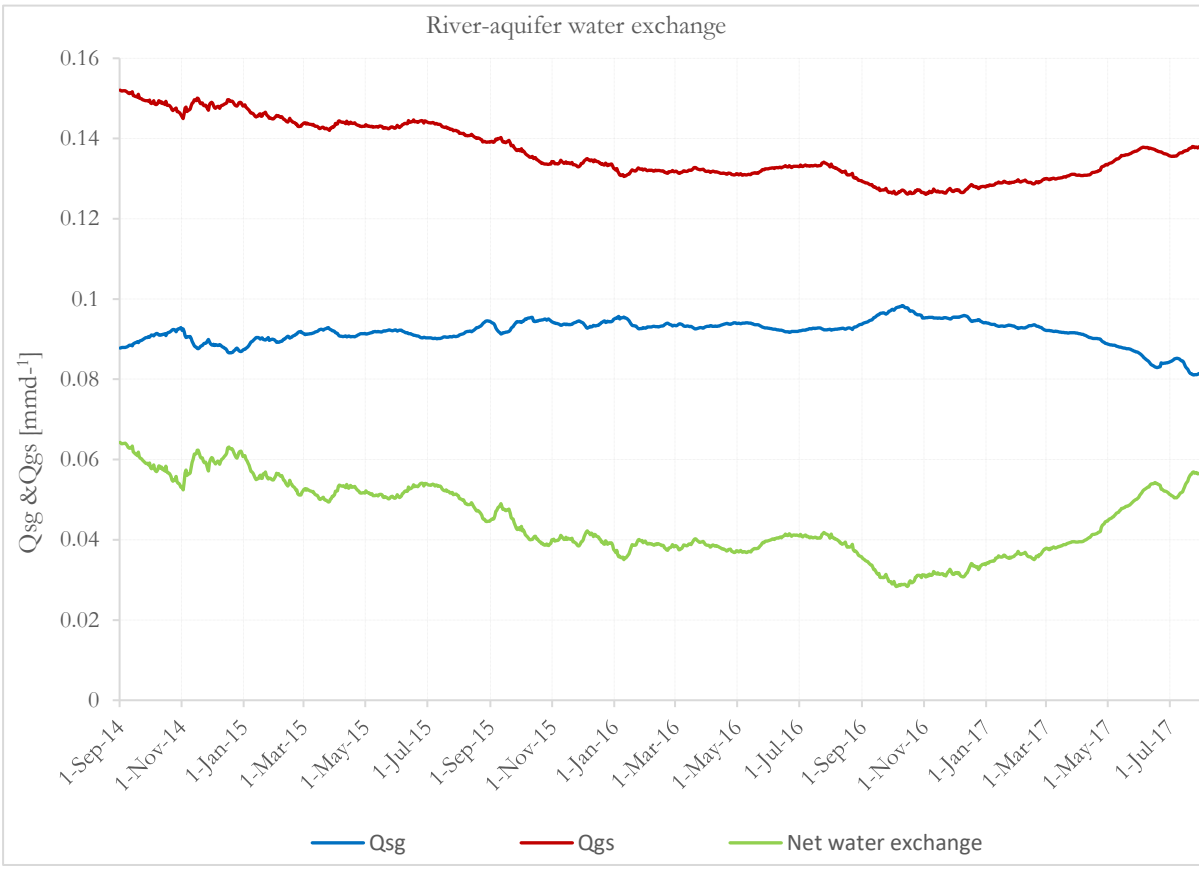

Figure 4-21 Exchange of water between river and modelled aquifer system with in the BRA

5. CONCLUSION AND RECOMMENDATIONS

5.1. Conclusion

The study was aimed to assess the dynamics of river-groundwater interactions in the BRA. The interaction of the Boteti River with Kalahari Aquifer was modelled in transient state by MODFLOW-NWT with active UZF1, SFR2 Packages under ModelMuse GUI from the beginning of September 2014 to the end of August 2017 through manual trial and error calibration. One layer, unconfined aquifer assigned as convertible (i.e. variably-saturated) was discretized into 1 km by 1 km square grids and time into 1096 stress periods, each representing one time step.

The model calibration was done on a yearly basis during the 3-year period. The simulated heads matched pretty well the available single head measurements (time series of head measurements was not available). However, even such singular matching was considered acceptable because the Kalahari heads are known to be pretty stable. In contrast, the river flow calibration was difficult. The calibration of the upstream gauge, Samedupe showed that the calibration accuracy increased with time but the calibration of the Rakops gauge indicated large discrepancy, clearly pointing at needs for streamflow calibration improvement (which unfortunately could not be completed due to time limitations) and eventually also at the need for longer time series of data. Due to the model calibration warm-up time uncertainty, the water balance of the first year was disregarded as unreliable; so the statistics of the water balance was based on the last two hydrological years.

The gross recharge contributed 85.55% of the total groundwater input while groundwater evapotranspiration 83.15% of the total output. In the 2016 (rainfall 321 mm), the Rn was negative, -100 mm while in 2017 (rainfall 570 mm) the Rn was positive, +130. Such difference was determined by the difference between gross recharge and groundwater evapotranspiration, while the groundwater exfiltration had negligible impact on Rn.

Variability of groundwater fluxes, Rg and ETg followed the seasonal variation experienced within the BRA and was highest in wet seasons

The variation of the Boteti River sages with peak levels in July-September period had an impact on the groundwater levels also affecting the amount of leakage transfer between river and groundwater.
The total loss of water from the Boteti River to Kalahari Aquifer system was approximately 67 mm and the groundwater discharge to Boteti River was 99 mm for the two hydrological years i.e. 2016 and 2017. as a result, throughout the simulation period the aquifer generally loses groundwater towards the river channel with net water gain of 32 mm which is about 16 mmyr-1.

5.2. Recommendations

Hydrological (streamflow) network within the study area was not well distributed. The available data from the existing station was encountered large data gaps and the measured values of stream flows were uncertain as they are produced from insufficient data. Thus, development of well distributed hydrological stations with better discharge estimation methods play great role to acquire and utilize reliable data in order to represent clear information about what is known in the area.

The distribution of climatic (weather stations) with in the study area was poor and the available data of rainfall and climatic variables had large data gaps. Development of additional weather stations and rain gauges within the area have their own impact on the research output and in seeking researchers for better understanding of the past, present and future state/condition of the area.

Additional groundwater monitoring network installation and timely measured water levels and abstraction rates data acquisition can maximize the reliability of the data and for better representation of the information.

The calibrated hydraulic heads showed abrupt changes in water level in response to rain fall and river seepage. Such seasonal event can be better represented by refining model grids (finer than the present study, as 1 km^2 grid is course) especially the regions around river course. However, the computational power of personal computers that might restrict such model refinement should be taken in to account.

The river-groundwater interactions in the Boteti River area is mainly dependent on inflows from the Okavango Delta. As a result, hydrology and drainage of the Okavango Delta is as equally important as the hydrology and drainage of the BRA and needs attention while studying surface-groundwater interactions of the BRA.

6. REFERENCES

Allen, R. G., Pereira, L. S., Raes, D., & Smith, M. (1998). FAO Irrigation and Drainage Paper. *Fao*, *300*(56), 326. https://doi.org/10.1016/j.eja.2010.12.001

Anderson, M. P., Woessner, W. W., & Hunt, R. (2010). APPLIED GROUNDWATER MODELING Simulation of Flow and Advective Transport. *Okt 2005 Abrufbar Uber Httpwww Tldp OrgLDPabsabsguide Pdf Zugriff 1112 2005*, *2274*(November 2008), 2267–2274. https://doi.org/10.1002/hyp

Anderson, M., & Woessner, W. (1992). Applied Groundwater modeling.pdf.

Baroncini-Turricchia, G., Francés, A. P., Lubczynski, M. W., Martínez-Fernández, J., & Roy, J. (2014). Integrating MRS data with hydrologic model - Carrizal Catchment (Spain). *Near Surface Geophysics*, *12*(2), 255–269. https://doi.org/10.3997/1873-0604.2014003

Brunner, P., & Simmons, C. T. (2012). HydroGeoSphere: A Fully Integrated, Physically Based Hydrological Model. *Groundwater*. https://doi.org/10.1111/j.1745-6584.2011.00882.x

Chen, F. W., & Liu, C. W. (2012). Estimation of the spatial rainfall distribution using inverse distance weighting (IDW) in the middle of Taiwan. *Paddy and Water Environment*, *10*(3), 209–222. https://doi.org/10.1007/s10333-012-0319-1

CN, K., BP, P., & JC, B. (2018). Revisiting Hydrology of Lake Ngami in Botswana. *Hydrology: Current Research*, *09*(02). https://doi.org/10.4172/2157-7587.1000301

de Vries, J. J., Selaolo, E. T., & Beekman, H. E. (2000). Groundwater recharge in the Kalahari. *Journal of Hydrology*, *238*, 110–123. https://doi.org/10.1016/S0022-1694(00)00325-5

El-Zehairy, A. A., Lubczynski, M. W., & Gurwin, J. (2018). Interactions of artificial lakes with groundwater applying an integrated MODFLOW solution. *Hydrogeology Journal*, *26*(1), 109–132. https://doi.org/10.1007/s10040-017-1641-x

Elkhrachy, I. (2016). Vertical accuracy assessment for SRTM and ASTER Digital Elevation Models: A case study of Najran city, Saudi Arabia. *Ain Shams Engineering Journal*, *2*, 1–11. https://doi.org/10.1016/j.asej.2017.01.007

Funk, C., Peterson, P., Landsfeld, M., Pedreros, D., Verdin, J., Shukla, S., … Michaelsen, J. (2015). The climate hazards infrared precipitation with stations - A new environmental record for monitoring extremes. *Scientific Data*, *2*, 1–21. https://doi.org/10.1038/sdata.2015.66

Gokmen, M., Vekerdy, Z., Lubczynski, M. W., Timmermans, J., Batelaan, O., & Verhoef, W. (2013). Assessing Groundwater Storage Changes Using Remote Sensing–Based Evapotranspiration and Precipitation at a Large Semiarid Basin Scale. *Journal of Hydrometeorology*, *14*(6), 1733–1753. https://doi.org/10.1175/JHM-D-12-0156.1

Habib, E., Haile, A. T., Sazib, N., Zhang, Y., & Rientjes, T. (2014). Effect of bias correction of satellite-rainfall estimates on runoff simulations at the source of the Upper Blue Nile. *Remote Sensing*, *6*(7), 6688–6708. https://doi.org/10.3390/rs6076688

Harbaugh, A. W. (2006). MODFLOW-2005, The U, 1–253. https://doi.org/https://doi.org/10.3133/tm6A16

Hassan, S. M. T., Lubczynski, M. W., Niswonger, R. G., & Su, Z. (2014). Surface-groundwater interactions in hard rocks in Sardon Catchment of western Spain: An integrated modeling approach. *Journal of Hydrology*, *517*, 390–410. https://doi.org/10.1016/j.jhydrol.2014.05.026

Hu, L., Xu, Z., & Huang, W. (2016). Development of a river-groundwater interaction model and its application to a catchment in Northwestern China. *Journal of Hydrology*, *543*, 483–500. https://doi.org/10.1016/j.jhydrol.2016.10.028

J. Canadell, R.B. Jackson, J.R. Ehleringer, H.A. Mooney, O.E. Sala, & E.-D. Schulze. (1996). Maximum rooting depth of vegetation types at the global scale. *Oecologia*, *108*, 583–595. Retrieved from http://download.springer.com/static/pdf/11/art%253A10.1007%252FBF00329030.pdf?originUrl=http%3A%2F%2Flink.springer.com%2Farticle%2F10.1007%2FBF00329030&token2=exp=1484578751~acl=%2Fstatic%2Fpdf%2F11%2Fart%25253A10.1007%25252FBF00329030.pdf%3ForiginUrl%3Dh

J.H. Kgaswanyane, M. V. (1996). Agricultural Land Use Plan Letlhakane Agricultural District, (December).

Jutebring Sterte, E., Johansson, E., Sjöberg, Y., Huseby Karlsen, R., & Laudon, H. (2018). Groundwater-surface water interactions across scales in a boreal landscape investigated using a numerical modelling approach. *Journal of Hydrology*, *560*, 184–201. https://doi.org/10.1016/j.jhydrol.2018.03.011

Keotshephile, K., Oarabile, M., Thebeetsile, M., & Mike, M. H. (2015). Evaluation of maize yield in flood recession farming in the Okavango Delta, Botswana. *African Journal of Agricultural Research*, *10*(16),

1874–1879. https://doi.org/10.5897/AJAR2014.9353
Kinoti, I. K. (2018). Integrated hydrological modeling of surface and groundwater interactions in Heuningnes catchment (South Africa). Retrieved from https://webapps.itc.utwente.nl/librarywww/papers_2018/msc/wrem/kinoti.pdf
Kipyegon, S., Lubczynski Ir Gabriel Parodi ADVISOR, M., & Lekula, M. (2018). Modelling Groundwater Resources of Transboundary Okwa Basin. Retrieved from https://webapps.itc.utwente.nl/librarywww/papers_2018/msc/wrem/cheruiyot.pdf
Kumar, U. S., Suma, S., & Navada, S. V. (2008). Recent studies on surface water–groundwater relationships at hydro-projects in India using environmental isotopes. *International Food Research Journal*. https://doi.org/10.1002/hyp
LARGE AREA HYDROLOGIC MODELING AND ASSESSMENT PART I: MODEL DEVELOPMENT'. (1998). *Nutrition*, 7. https://doi.org/10.1016/S0899-9007(00)00483-4
Le Maitre, D. C., Scott, D. F., & Colvin, C. (1999). A review of information on interactions between vegetation and groundwater. *Water SA*, *25*(2), 137–152. https://doi.org/http://www.wrc.org.za
Leake, S. A., Lilly, M. R., & Johns, S. T. (1997). Documentation of a Computer Program (FHB1) for Assignment of Transient Specified-Flow and Specified-Head Boundaries in Applications of the Modular Finite-Difference Ground-Water Flow Model (MODFLOW) Open-File Report 97 571 Prepared in cooperation with the. Retrieved from http://h2o.usgs.gov/software/
Lekula, M. (2018). *Multiple data sources and integrated hydrological modelling for groundwater assessment in the Central Kalahari Basin*. https://doi.org/10.3990/1.9789036546393
Lekula, M., Lubczynski, M. W., & Shemang, E. M. (2018). Hydrogeological conceptual model of large and complex sedimentary aquifer systems – Central Kalahari Basin. *Physics and Chemistry of the Earth*. https://doi.org/10.1016/j.pce.2018.05.006
Lekula, M., Lubczynski, M. W., Shemang, E. M., & Verhoef, W. (2018). Validation of satellite-based rainfall in Kalahari. *Physics and Chemistry of the Earth*, *105*(February), 84–97. https://doi.org/10.1016/j.pce.2018.02.010
Li, Y., Yuan, D., Lin, B., & Teo, F. Y. (2016). A fully coupled depth-integrated model for surface water and groundwater flows. *Journal of Hydrology*, *542*, 172–184. https://doi.org/10.1016/j.jhydrol.2016.08.060
Markstrom, S. L., Niswonger, R. G., Regan, R. S., Prudic, D. E., & Barlow, P. M. (2008). GSFLOW—Coupled Ground-Water and Surface-Water Flow Model Based on the Integration of the Precipitation-Runoff Modeling System (PRMS) and the Modular Ground-Water Flow Model (MODFLOW-2005). *Usgs*. Retrieved from http://pubs.usgs.gov/tm/tm6d1/pdf/tm6d1.pdf
McDonald, H. and G. (1986). A modular three-dimensional finite-difference ground-water flow model. *Journal of Hydrology*, *88*(3–4), 387–389. https://doi.org/10.1016/0022-1694(86)90106-X
McFarlane, M. J., & Eckardt, F. D. (2006). Lake Deception: a new Makgadikgadi palaeolake. *Botswana Notes and Records*, *38*(2006), 195–201. https://doi.org/10.1063/1.2359574
McMahon, T. A., Peel, M. C., Lowe, L., Srikanthan, R., & McVicar, T. R. (2013). Estimating actual, potential, reference crop and pan evaporation using standard meteorological data: A pragmatic synthesis. *Hydrology and Earth System Sciences*, *17*(4), 1331–1363. https://doi.org/10.5194/hess-17-1331-2013
Milzow, C., Kgtlhang, L., Meier, P., & Kinzelbach, W. (2010). *Regional review: the hydrology of the Okavango Delta, Botswana—processes, data and modelling*. *Iranian Journal of Pharmacology and Therapeutics* (Vol. 9). https://doi.org/10.1007/s10040-009-0436-0
Miralles, D. G., Gash, J. H., Holmes, T. R. H., De Jeu, R. A. M., & Dolman, A. J. (2010). Global canopy interception from satellite observations. *Journal of Geophysical Research Atmospheres*, *115*(16). https://doi.org/10.1029/2009JD013530
Nash, E., & Sutcliffe, V. (1970). River flow forecasting through conceptual models Part I - A discussion of principles. *Journal of Hydrology*, *10*, 282–290. https://doi.org/10.1016/0022-1694(70)90255-6
Newman, B. D., Vivoni, E. R., & Groffman, A. R. (2006). Surface water–groundwater interactions in semiarid drainages of the American southwest. *Okt 2005 Abrufbar Uber Httpwww Tldp OrgLDPabsabsguide Pdf Zugriff 1112 2005*. https://doi.org/10.1002/hyp
Niswonger, R. G., Panday, S., & Motomu, I. (2011). MODFLOW-NWT , A Newton Formulation for MODFLOW-2005. *USGS Reports*, 44. https://doi.org/10.3133/tm6A37
Niswonger, R. G., & Prudic, D. E. (2010). Documentation of the Streamflow-Routing (SFR2) Package to Include Unsaturated Flow Beneath Streams—A Modification to SFR1: U.S. Geological Survey Techniques and Methods 6-A13. *US Geological Survey Techniques and Methods 6*, (April 2010), 59. https://doi.org/Techniques and Methods 6-A13 version 1.10

Niswonger, R. G., Prudic, D. E., & Regan, S. R. (2006). Documentation of the Unsaturated-Zone Flow (UZF1) Package for Modeling Unsaturated Flow Between the Land Surface and the Water Table with MODFLOW-2005. *U.S. Geological Survey Techniques and Methods*, 71.

Obakeng, O. T., de Vries, J. J. promoto., & Lubczynski, M. W. promoto. (2007). *Soil moisture dynamics and evapotranspiration at the fringe of the Botswana Kalahari, with emphasis on deep rooting vegetation*. *ITC Dissertation;141*. Retrieved from http://www.itc.nl/library/papers_2007/phd/obakeng.pdf

Panday, S., & Huyakorn, P. S. (2004). A fully coupled physically-based spatially-distributed model for evaluating surface/subsurface flow. *Advances in Water Resources*, *27*(4), 361–382. https://doi.org/10.1016/j.advwatres.2004.02.016

Rahm, D., Swatuk, L., & Matheny, E. (2006). Water resource management in botswana: Balancing sustainability and economic development. *Environment, Development and Sustainability*, *8*(1), 157–183. https://doi.org/10.1007/s10668-005-2491-6

REPUBLIC OF BOTSWANA Ministry of Minerals , Energy & Water Resources Department of Water Affairs GROUNDWATER RESOURCES INVESTIGATION IN THE BOTETI AREA Main Integrated Volume 1. (2006), *1*(July).

Rientjes, T. (2015). Hydrologic modelling for Intergated Water Resource. *Lecture Notes for Module 9-10 Surface Water Stream*, (March).

Roussouw, N., Bird, M. S., Perissinotto, R., & Gordon, N. (2018). Microalgal biomass and composition of surface waterbodies in a semi-arid region earmarked for shale gas exploration (Eastern Cape Karoo, South Africa). *Limnologica*, (January 2017), 1–13. https://doi.org/https://doi.org/10.1016/j.limno.2018.03.003

Sattel, D., & Kgotlhang, L. (2004). Groundwater exploration with AEM in the Boteti area, Botswana. *Exploration Geophysics*, *35*(2), 147–156. https://doi.org/10.1071/EG04147

Seibert, J., & Vis, M. J. P. (2012). Teaching hydrological modeling with a user-friendly catchment-runoff-model software package. *Hydrology and Earth System Sciences*, *16*(9), 3315–3325. https://doi.org/10.5194/hess-16-3315-2012

Shah, N., Nachabe, M., & Ross, M. (2007). Extinction depth and evapotranspiration from ground water under selected land covers. *Ground Water*, *45*(3), 329–338. https://doi.org/10.1111/j.1745-6584.2007.00302.x

Shinn, J. E. (2018). Toward anticipatory adaptation: Transforming social-ecological vulnerabilities in the Okavango Delta, Botswana. *Geographical Journal*, *184*(2), 179–191. https://doi.org/10.1111/geoj.12244

Society, K. C. (2007). on behalf of Ministry of Environment , Wildlife and Tourism Department of Wildlife and National Parks Artificial Watering Point Study Makgadikgadi Pans National Park, (December).

Sophocleous, M. (2002). Interactions between groundwater and surface water: The state of the science. *Hydrogeology Journal*, *10*(1), 52–67. https://doi.org/10.1007/s10040-001-0170-8

Survey, U. S. G. (2004). To Simulate Stream-Aquifer Interaction With Modflow-2000 Streamflow-Routing. *Prudic*, (August).

Swatuk, L. A., Motsholapheko, M. R., & Mazvimavi, D. (2011). A political ecology of development in the boteti river region of botswana: Locating a place for sport. *Third World Quarterly*, *32*(3), 453–475. https://doi.org/10.1080/01436597.2011.573941

Teegavarapu, R. S. V., & Chandramouli, V. (2005). Improved weighting methods, deterministic and stochastic data-driven models for estimation of missing precipitation records. *Journal of Hydrology*, *312*(1–4), 191–206. https://doi.org/10.1016/j.jhydrol.2005.02.015

Teketel, A. T., Lubczynski, M. W., & Vekerdy, Z. (2017). INTEGRATED HYDROLOGICAL MODELING OF SURFACE-GROUNDWATER INTERACTIONS The case of Denpasar-Tabanan Basin in the Southern Bali Island. Retrieved from https://webapps.itc.utwente.nl/librarywww/papers_2017/msc/wrem/teketel.pdf

Thomas, D. S. G., & Shaw, P. A. (1990). The deposition and development of the Kalahari Group sediments, Central Southern Africa. *Journal of African Earth Sciences*, *10*(1–2), 187–197. https://doi.org/10.1016/0899-5362(90)90054-I

Tian, Y., Zheng, Y., Wu, B., Wu, X., Liu, J., & Zheng, C. (2015). Modeling surface water-groundwater interaction in arid and semi-arid regions with intensive agriculture. *Environmental Modelling and Software*, *63*, 170–184. https://doi.org/10.1016/j.envsoft.2014.10.011

Tomaso Ceccarelli, Hendrik Boogaard, Ben Maathuis, T. J. (2014). a Vailability of Weather Data for Crop Modelling an Assessment of Weather Data Available Through the Geonetcast and Isod Toolboxes for a Cgms " Semi -. Retrieved from http://chg.geog.ucsb.edu/data/chirps/index.html.

Toté, C., Patricio, D., Boogaard, H., van der Wijngaart, R., Tarnavsky, E., & Funk, C. (2015). Evaluation of satellite rainfall estimates for drought and flood monitoring in Mozambique. *Remote Sensing*, *7*(2), 1758–1776. https://doi.org/10.3390/rs70201758

VanderPost, C., & McFarlane, M. (2007). Groundwater investigation in semi-arid developing countries, using simple GIS tools to facilitate interdisciplinary decision making under poorly mapped conditions: The Boteti area of the Kalahari region in Botswana. *International Journal of Applied Earth Observation and Geoinformation*, *9*(4), 343–359. https://doi.org/10.1016/j.jag.2006.11.002

Winston, R. B. (2009). ModelMuse: A Graphical User Interface for MODFLOW-2005 and PHAST. *U.S. Geological Survey Techniques and Methods 6-A29*, 52 p. Retrieved from http://pubs.usgs.gov/tm/tm6A29/tm6A29.pdf

7. APPENDICES

Appendix 1: Correlation of rainfall stations in terms of available rainfall data (from September 2014 to August 2017).

Stations	Maun	Letlkahane	Phuduhudu	Mareomaoto	Rakops	Xade	Mababe
Maun	1.00	0.57	0.21	0.26	0.20	0.29	0.34
Letlkahane	0.53	1.00	0.26	0.27	0.29	0.40	0.30
Phuduhudu	-0.01	0.62	1.00	0.62	0.58	0.51	0.44
Mareomaoto	0.05	0.27	0.62	1.00	0.33	0.39	0.62
Rakops	0.20	0.29	0.58	0.33	1.00	0.43	0.29
Xade	0.03	0.40	0.51	0.39	0.62	1.00	0.48
Mababe	0.13	0.30	0.44	0.62	0.29	0.43	1.00

Appendix 2. Cumulative in situ PET at Maun and Rakops stations

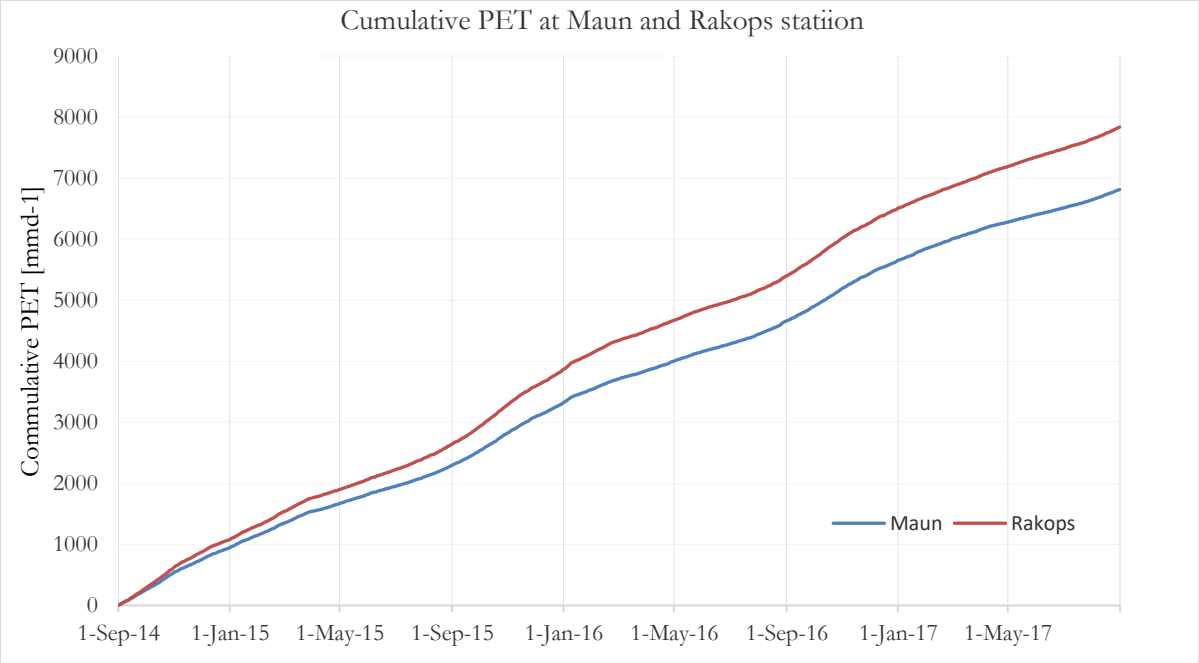

Appendix 4: Observed versus simulated discharge at Rakops gauging station

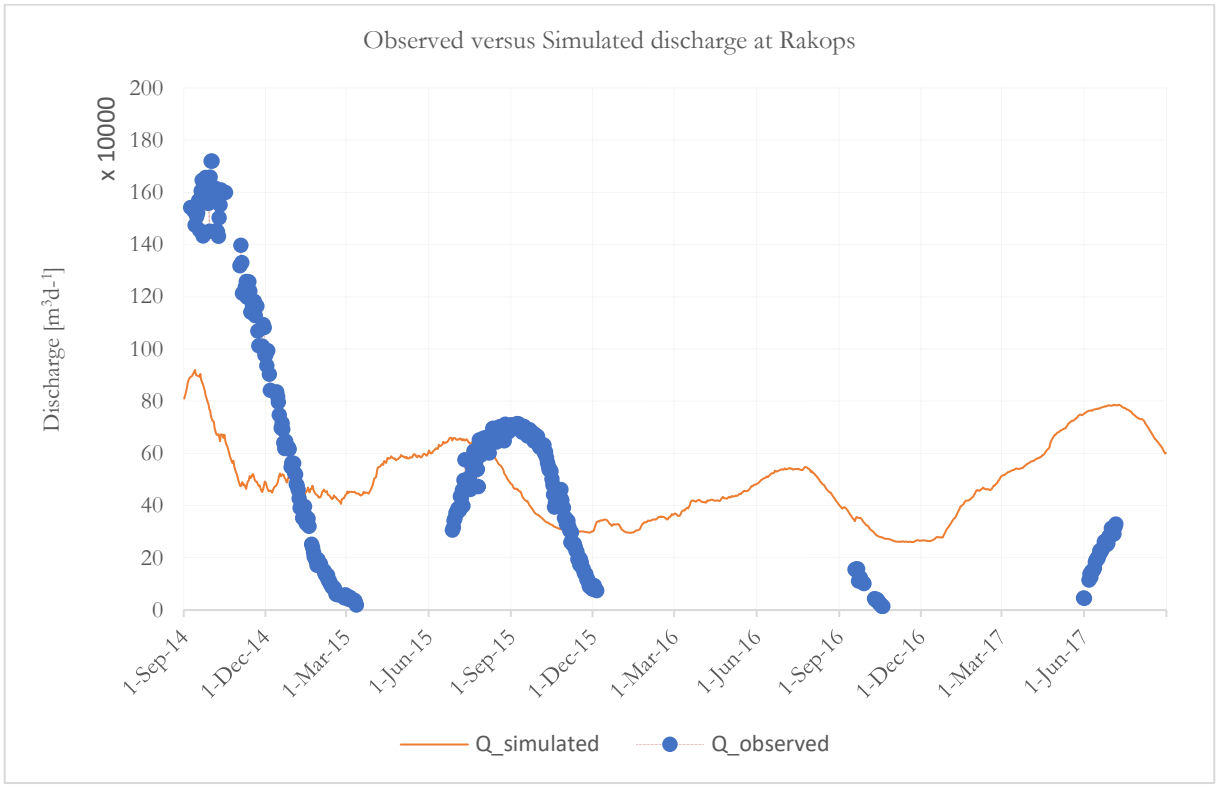
Observed versus Simulated discharge at Rakops
Discharge [m3d-1]
x 10000
200
180
160
140
120
100
80
60
40
20
0
1-Sep-14
1-Dec-14
1-Mar-15
1-Jun-15
1-Sep-15
1-Dec-15
1-Mar-16
1-Jun-16
1-Sep-16
1-Dec-16
1-Mar-17
1-Jun-17
Q_simulated
Q_observed

Appendix 3: Boreholes used for potentiometric surface development located within the modelled domain; (sourced form DWA, Botswana).

BH_ID	Easting	Northing	RWL_ masl_	DEM [m]	Heads_m asl
2104	171442.637	7799534.706	28.3	946	917.7
9541	254121.654	7662739.859	8.9	911	902.1
8004	245333.331	7674792.662	7.5	913	905.5
8045	259414.586	7708231.172	4	915	911
8272	162211.123	7800867.641	13.92	946	932.08
9737	245951.4321	7779822.652	14.75	928	913.25
9740	191813.7193	7772435.718	14.59	938	923.41
9844	237142.3	7767807.621	9.2	929	919.8
9845	228745.3127	7781092.351	25.4	939	913.6
10423	229502	7701659	12.44	925	912.56
10426	235168	7723324	12.45	926	913.55
10429	253071	7745327	14.53	937	922.47
10430	222035	7747579	16	928	912
10432	215220	7758644	17.6	932	914.4
10433	247030	7753092	15.87	926	910.13
9025	173413.503	7752380.287	19.94	931	911.06
9849	186516.326	7751066.642	20.41	932	911.59
1757	241681.413	7737846.35	12.5	927	914.5
10015	181938.67	7729082.137	31.48	946	914.52
10017	170912.652	7728841.943	32.35	945	912.65
Z1958	213171.153	7730775.211	25.3	947	921.7
Z1959	213171.153	7730775.211	16.46	947	930.54
8045	259414.586	7708231.172	4	915	911
Z8829	182068.687	7681559.404	45	945	900
8004	245333.331	7674792.662	7.5	913	905.5
Z8827	202355.223	7672504.143	43	946	903
Z8828	229655.787	7662125.374	18	913	895
Z3437	211015.729	7654224.155	13.41	950	936.59
Z3437	211015.729	7654224.155	15.24	950	934.76